Bales, Michelle

From: Angela Olpretean <angela.olpretean@antinternational.com>
Sent: Tuesday, September 08, 2015 7:55 AM
To: Bales, Michelle
Cc: 'Peter Rudling'; Rhodes, Bebbie
Subject: [External_Sender] SV: Permission Request

Good morning Ms. Bales,

Hereby, we confirm that ANT International grants permission for the U.S. Nuclear Regulatory Commission (NRC) to make an excerpt from the article, "Zr alloy corrosion and hydrogen pickup" available to the public in the NRC's ADAMS system.

The version of the excerpt that contains only material under ANT copyright will be sent to you by UPS.

Please let me know if you have any questions.

Best regards,
Angela Olpretean
On behalf of Peter Rudling

A.N.T. INTERNATIONAL®
ANGELA OLPRETEAN *Business Office Director*
Direct phone: +46 (0)70 263 13 77.
Analysvägen 5, SE-435 33 Mölnlycke, Sweden.
Phone: +46 (0)31-88 16 00. *Fax:* +46 (0)31-88 16 01.
www.antinternational.com

Från: Bales, Michelle [mailto:Michelle.Bales@nrc.gov]
Skickat: den 2 september 2015 22:17
Till: Angela Olpretean <angela.olpretean@antinternational.com>
Kopia: Peter Rudling (peter.rudling@antinternational.com) <peter.rudling@antinternational.com>; Rhodes, Bebbie <Bebbie.Rhodes@nrc.gov>
Ämne: Permission Request

Good morning Mrs. Olpretean,

I am writing to request permission for the U.S. Nuclear Regulatory Commission (NRC) to make an excerpt from the article, "Zr Alloy Corrosion and Hydrogen Pickup" available to the public in NRC's Agencywide Documents Access & Management System (ADAMS). The excerpt of interest is on the subject of hydrogen pickup data and models for Zircaloy-2 cladding material. The NRC staff used information in this article in the development of RG of Regulatory Guide 1.224, "Establishing Analytical Limits for Zirconium Cladding Material." By placing this document into ADAMS, the public will be able to freely access and print the document for their personal use. We will attach a cover letter to the file in ADAMS that indicates that any use or reproduction of the contents of the article are subject to the copyright conditions of ANT International.

Can you please provide a version of the excerpt that contains only material under ANT copyright?

Please let me know if you have any questions.

Best Regards,

- Michelle Bales

Zr Alloy Corrosion and Hydrogen Pickup

Author

Peter Rudling

Contributions from

Ron Adamson,
Friedrich Garzarolli
and, Brian Cox

ANT International, Mölnlycke, Sweden
December 2013

Contents

1 Design criteria

To ensure appropriate fuel performance the fuel rod oxide thickness, hydrogen pickup and CRUD build-up should be limited according to the NRC document NUREG-0800, Section 4.3 [NUREG, 2007].

The original rationale for specifying a maximum oxide (and CRUD) thickness for fuel claddings is based on the fact that the resulting temperature increase will lower the cladding mechanical strength. If the oxide and CRUD layer thickness become too large, the resistance to heat flux will become significant and a further increase in the thickness will raise the cladding temperature further. This increase in temperature will increase the cladding corrosion rate, thus increasing the oxide thickness further resulting in an even higher cladding temperature. Such a thermal feedback situation could increase the cladding temperature and lower the material strength to such an extent that the cladding may fail due to a tensile stress.

However, in reality, mechanical failure of the fuel cladding does not occur because the stresses involved are too small. Instead, the thermal feedback effect in PWRs may cause corrosion acceleration resulting in fuel clad failure by through wall oxidation. In high power experiments (140 W/cm²) in a PWR local perforations of the cladding wall occurred due to this phenomena at an oxide thickness of >50 µm, [Garzarolli et al, 1979]. Figure 1-1 summarizes the experience with thick oxide layers in a diagram showing oxide thickness and heat flux for each data point. A locus curve of constant corrosion rate (approximately a hyperbola) was drawn tentatively. The area above the locus curve indicates conditions that would lead to corrosion failures due to corrosion acceleration related to thermal feedback effects. The areas beneath this curve indicate conditions not leading to any thermal feedback corrosion acceleration.

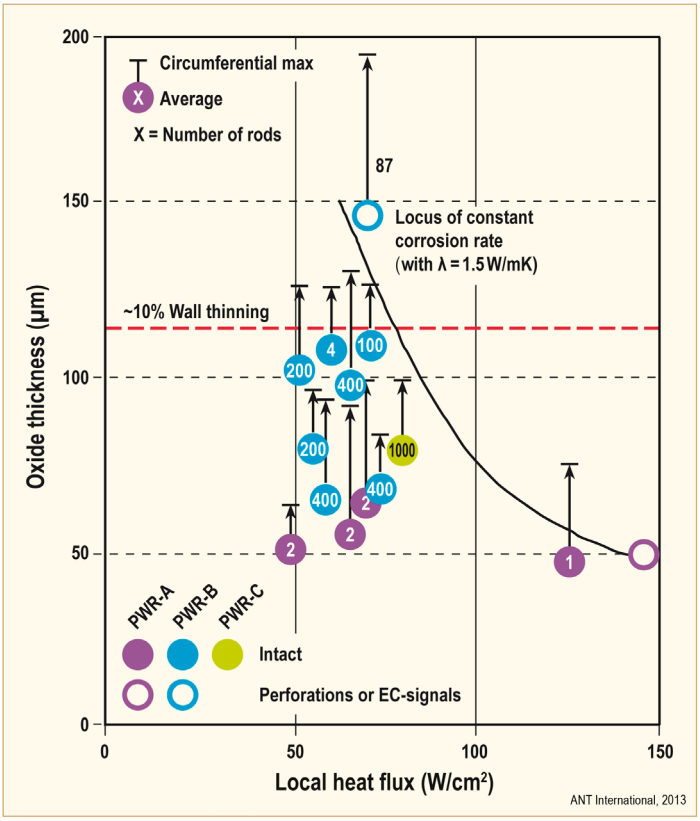

Figure 1-1: Maximum allowable uniform oxide layer thickness, after [Garzarolli & Stehle, 1987].

The maximum oxide thickness criterion used today by most regulators including the NRC for most PWR applications is 100 μm. The NRC has specified that this maximum oxide thickness is the average value along the cladding circumference in a transversal cross-section. Regulations on the uniformity of cladding oxide are also being imposed by the USNRC with the intent of constraining the formation of hydride blisters[1].

The hydrogen content of zirconium alloys must be limited to prevent brittle mechanical failures due to the formation of hydrides during normal operation, handling during outage and seismic events. However, because the impact of the hydrides on ductility is strongly dependent upon morphology and cladding texture, the NRC has not given a specific maximum allowable hydrogen content for zirconium alloy cladding materials. Instead, constraints on oxide thickness and uniformity appear to be emerging as a means for limiting hydrogen concentration. Such constraints seem to be based on a relatively linear relationship between oxide thickness and hydrogen concentration in Zry-4 cladding that operates in PWRs and on the ability to assess oxide thickness and uniformity via poolside inspections. However, other regulators are applying specific limits, for example:

- France - 600 ppm H
- Netherlands - 500 ppm H
- Germany - 2000 ppm H

[1] If there are large differences in the circumferential oxide thickness profile, e.g. due to local spallation of oxide, a large difference in fuel clad temperature at the outer surface may result. This situation will drive the soluble clad hydrogen to the colder spots in the cladding (where the oxide is thinnest) and when the solubility limit is exceeded form a hydride blister.

2 Introduction

The topic of Zr alloy corrosion and HPU has been covered in several ANT International published Reports. The interested reader is referred to the following Reports:

ZIRAT6[2]/IZNA1[3] STR Water Chemistry and CRUD Influence on Cladding Corrosion,

ZIRAT7/IZNA2 STR Corrosion of Zirconium Alloys,

ZIRAT8/IZNA3 STR The Effects of Zn Injection (PWRs and BWRs) and Noble Metal Chemistry (BWRs) on Fuel Performance,

ZIRAT9/IZNA4 STR Corrosion of Zr-Nb Alloys in PWRs,

ZIRAT12/IZNA7 STR Corrosion Mechanisms in Zirconium Alloys,

Section 6 in ZIRAT16/IZNA11 Annual Report,

ZIRAT16/IZNA11 STR Performance Evaluation of New Advanced Zr Alloys for PWRs/VVERs,

Sections 2 and 3.1 in Fuel Material Technology Report Vol. II,

PZAC PWR Zr Alloy Cladding Water Side Corrosion,

LCC2 STR CRUD in PWR/VVER and BWR Primary Circuits,

LCC6 STR Effect of Zink in BWR and PWR/ VVER on Activity Build-up, IGSCC and Fuel Performance,

LCC7 STR Introduction to Boiling Water Reactor Chemistry Volume I,

LCC8 STR Introduction to Boiling Water Reactor Chemistry Volume II,

LCC7 STR PWR/VVER Primary Side Coolant Chemistry, Volume I – Technical Basis and Recent Discussions,

LCC7 STR PWR/VVER Primary Side Coolant Chemistry, Volume II – Technical Basis and Recent Discussions, (give link to sample report on our web-site),

Corrosion of zirconium alloys is a thermodynamic and electrochemically based process affected by the following parameters, see Figure 2-1:

- The microstructure of the Zr alloy-metal surface.
- The water chemistry and the hydraulic conditions.
- The Zr alloy temperature (at the metal/oxide interface).

[2] Zirconium Alloy Technology
[3] Information on Zirconium Alloys

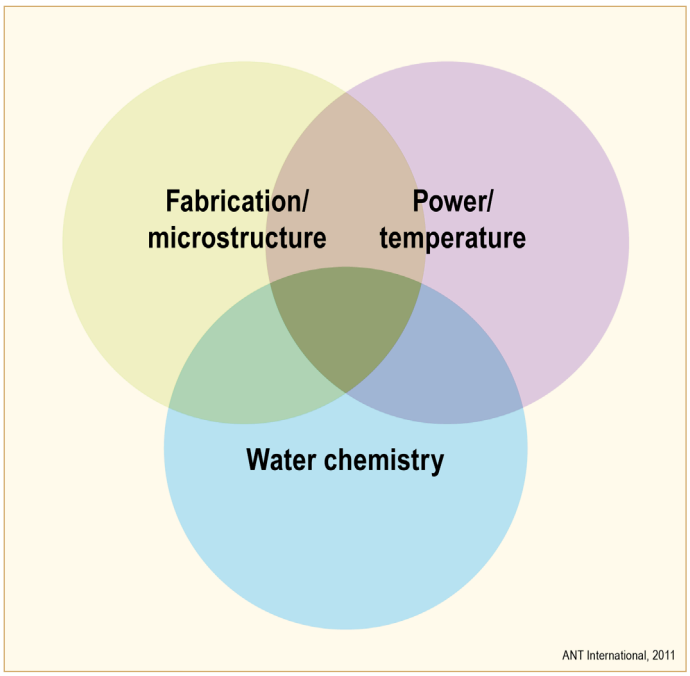

Figure 2-1: Parameters impacting corrosion performance of Zr Alloys.

During the initial oxidation/corrosion of zirconium alloys, a thin protective black oxide is formed. As the zirconium oxide grows in thickness the outer part of the oxide (facing the water/steam phase) is transformed into a greyish porous oxide. The oxide grows inwards into the zirconium alloy material.

In general there exists common understanding that only atomic hydrogen that is generated by cladding corrosion is picked-up by Zr alloys and not the dissolved molecular hydrogen that is added into the reactor coolant. In high temperature water Zr-based alloys build a thin, compact, black protective layer by early oxidation phase with water. Electrons released from Zr by oxidation are captured by hydrogen ions of the water that reduce them to hydrogen atoms. Some of these hydrogen atoms recombine to H_2 molecules and release from the Zr surface as hydrogen gas, whereas the other part can migrate into Zr matrix as soluble H atoms. When the solubility limit for picked-up hydrogen (about 100 mg/kg at 330°C) exceeds in the Zr-alloy, the excess hydrogen precipitates as Zr-Hydride. The ratio of the portion that is picked-up in the Zr alloy to total hydrogen formed by Zr oxidation (corrosion) is defined as Hydrogen Pick-Up Fraction (HPUF). This HPUF, depends on zirconium alloying content but also on temperature, water chemistry, and reactor start-up procedure. The total amount of hydrogen that is picked up by the Zirconium alloy, HPU is the product of the corrosion rate and the HPUF.

Enhanced Hydrogen Pickup (HPU) in the zirconium (Zr) alloy fuel cladding is one of the largest concerns regarding fuel cladding performance. This is because increased HPU could lead to

- Formation of dense hydride rim, which results in early increase in cladding corrosion (hydride rim corrodes faster than the Zr alloys) during normal reactor operation.
- Increased dimensional changes of Zr alloy fuel assembly components (Hydride has a 15% higher specific volume relative to the metallic Zr).
- Enhanced embrittlement of the Zr alloy components during accident conditions (LOCA, RIA and cask drop accident during interim dry storage (Zr-hydride is hard and brittle) [Garzarolli & Sabol, 2006].

The corrosion and hydriding process of Zirconium alloys is schematically shown in Figure 2-2.

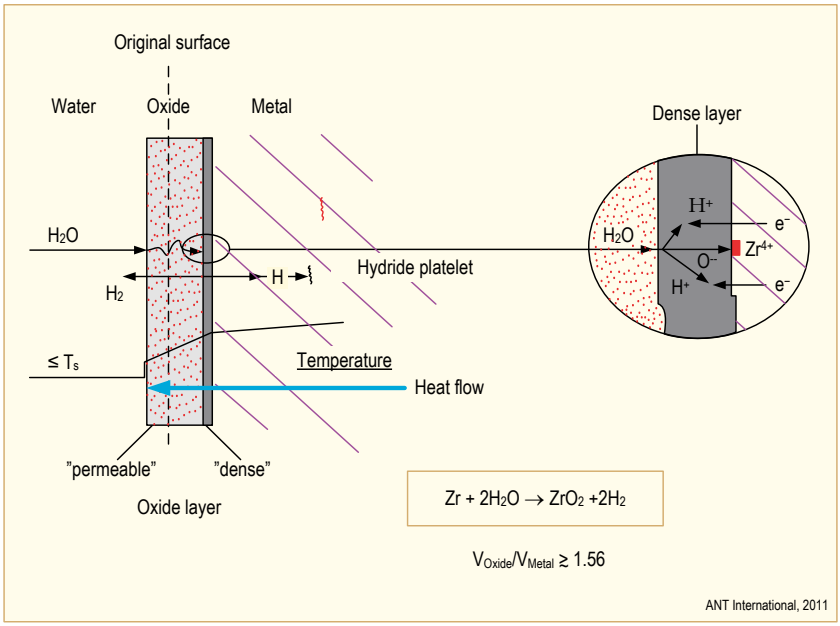

Figure 2-2: Schematic showing the corrosion and HPU process in zirconium alloys.

Due to the different fuel rod surface temperatures and water chemistry in the different types of power reactors, such as PWR, VVER, BWR, RBMK, CANDU, corrosion of the Zr-alloy claddings and structural components proceeds quite differently in the different reactor systems.

There are different types of corrosion mechanisms: uniform, nodular and shadow corrosion (Figure 2-3 to Figure 2-4).

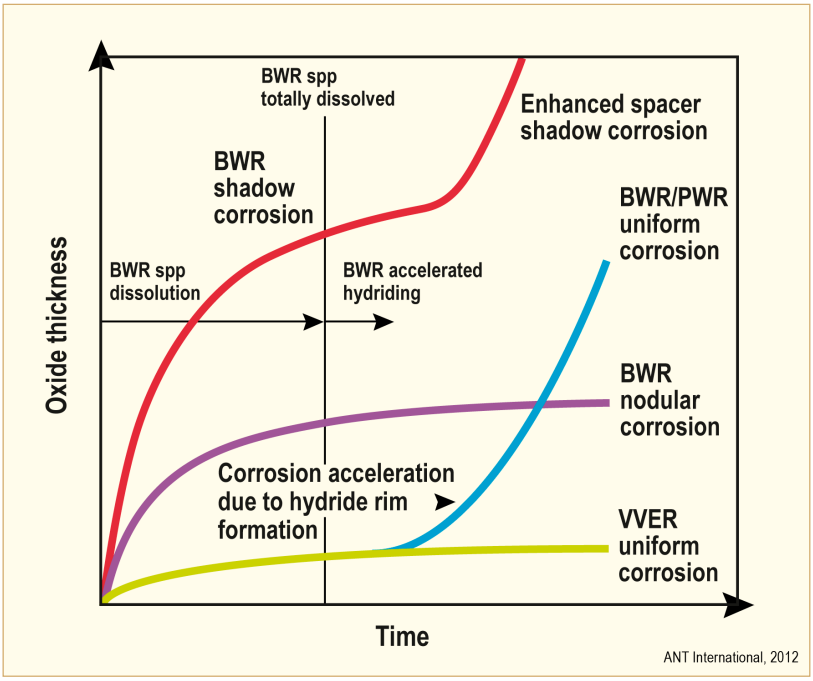

Figure 2-3: Oxide growth is schematically shown in BWRs, PWRs and VVERs. The uniform corrosion acceleration in BWRs and PWRs are due to the formation of a solid hydride at the Zr alloy metal/oxide interface. In BWRs the solid hydride formation is preceeded by the dissolution of the Second Phase Particles, SPPs in Zry-2, after [Rudling & Patterson, 2009].

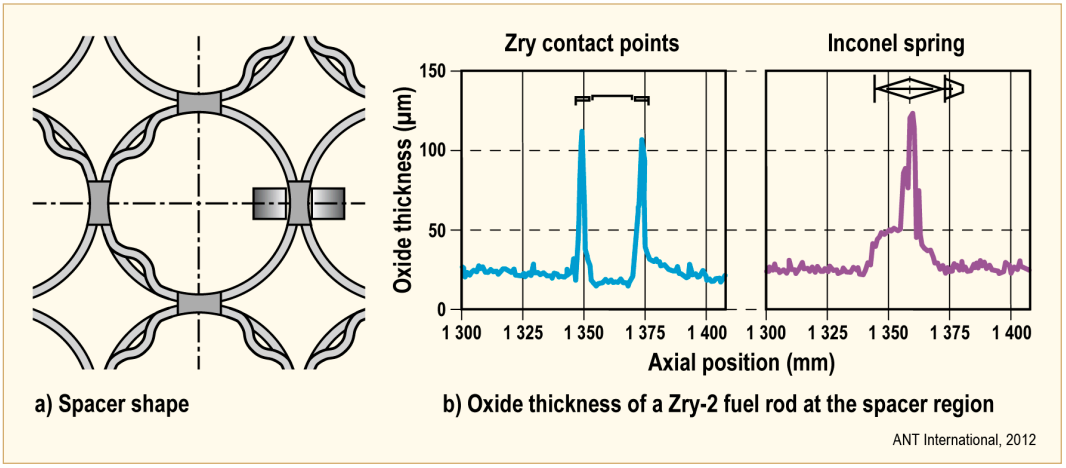

Figure 2-4: Oxide layer thickness profile of a BWR Zry-2 fuel rod opposite to Zry contact points (a) and Inconel contact point (b) after a burnup of 46 MWd/kgU, after [Garzarolli et al, 2001a].

- **Uniform corrosion** (PWRs/VVERs/CANDUs/BWRs) starts at the beginning of irradiation at a rapid rate and, slows quickly (Figure 2-3). With increasing oxidation and hydrogen absorption (pickup) at higher burnup, the concentration of hydrogen in Zr alloys can exceed it solubility limit and precipitate as hydrides. In components with heat transfer (e.g., fuel cladding), such hydrides tend to form in regions of lowest temperature. With the heat flux typical of LWR fuel rods, precipitation in regions of low temperature can lead to relatively high concentrations at the outer metal-oxide interface, which can, in turn, increase the oxidation rate. The corrosion mechanism is treated more in detail in LCC9 STR Effects of Coolant Chemistry on Fuel Performance, published by ANT International.

In PWRs, there is an increase in the oxide growth rate at about 20-30 microns because solid hydrides may form in the Zr alloy at this point, thus increasing the oxide growth rate. At oxide thicknesses of about 100 microns and a large surface heat flux, there may also be a thermal feedback effect, which then leads to a second oxidation acceleration step.

In VVERs, there is normally no acceleration of the uniform corrosion process due to the very low hydrogen pickup. The reason for the low hydrogen pickup is due both to the (normal) use of the Zr1Nb alloy E110 and different coolant chemistry.

In BWRs, the SPPs (nickel-bearing and chromium-bearing SPPs) in Zry-2 start to dissolve already at the start of irradiation due to the fast neutron flux. Dependent upon the initial size and type/chemistry of the SPP, the dissolution rate varies. At a certain fast fluence level (corresponding to a certain burnup) the SPP has completely dissolved in the matrix, the fluence level, when this complete dissolution occurs, increases with increased initial SPP size. When the SPPs have totally dissolved there is a dramatic increase in HPUF from 5-10% to over 100% (which means that part of the hydrogen must also come from the radiolytic hydrogen being produced) which eventually will lead to formation of a hydride rim at the metal/oxide interface. The hydride rim corrodes faster than the Zirconium alloy which means that at this point there is corrosion acceleration.

- **Nodular corrosion** (only occurs in oxidising environment such as in BWRs) starting after 10 to 100 days of irradiation in material with large Zircaloy Second Phase Particles (SPPs) (Figure 2-3). Nodular corrosion is characterized by locally a much thicker oxide patches appearing as white spots. The corrosion rate is initially very large but levels of at high burnups. Due to the low oxidation potential in a PWR/VVER only uniform corrosion normally exists. However, if for some reason there would be an increase in the coolant oxidation potential, nodular corrosion may also occur in PWRs/VVERs. The corrosion mechanism is treated more in detail in Section 3.3

- **Shadow corrosion** (almost only in BWRs since it requires an oxidising environment) starting after a few days of irradiation (Figure 2-3), which may accelerate at higher burnups. Although agreement does not exist regarding the underlying mechanism, shadow corrosion is frequently postulated to be a galvanic type of corrosion. Shadow corrosion has "always" been present in BWRs, but not in PWRs, primarily related to the high PWR hydrogen concentration which reduces or eliminates galvanic potentials between dissimilar alloy components. Shadow corrosion occurs in areas where a Zr alloy is in contact with or in close proximity to a dissimilar material such as nickel-based alloys (Inconel) or stainless steel, e.g. spacers in case of fuel rods (Figure 2-4) and control rods in case of BWR fuel outer channels. The corrosion mechanism is treated more in detail in LCC9 STR Effects of Coolant Chemistry on Fuel Performance, published by ANT International.

  There is one case when a late in life oxidation acceleration occurred; viz., Enhanced Spacer Shadow Corrosion, (ESSC)[4] in KernKraftwerk Leibstadt (KKL), see ZIRAT5/IZNA1 Annual Reports (AR) [Adamson et al, 2000/2001] for more details. The mechanism for this acceleration on oxide growth is not clear, but it may have to do with that the SPPs were dissolved at this burnup level. The KKL corrosion failures are treated more in detail in LCC9 STR Effects of Coolant Chemistry on Fuel Performance, published by ANT International.

[4] This corrosion phenomenon resulted in a few failed rods. This accelerated type of corrosion occurred on the fuel cladding material at spacer locations (the spacer springs in BWR fuel assemblies are made of a Ni-alloy such as X750). Water chemistry seems also to play a role. Specifically coolant chemistry with low Fe/(Ni-Zn) ratio seems to be aggressive provided that the cladding material shows poor corrosion performance. A fuel cladding material with good corrosion resistance (i.e. larger SPPs) does not result in ESSC, enhanced spacer shadow corrosion, even in aggressive water chemistry.

3 Corrosion and Hydrogen Pickup (HPU) mechanisms

3.1 Introduction

The corrosion and hydrogen pickup mechanisms are dealt with in Sections 3.2, 3.3 and, 3.4 and the most influential variables impacting corrosion and HPU are provided in Section 4

In the subsequent sections it will be shown that the oxide microstructure formed on the Zr alloys is mostly porous but have dense part, barrier layer, at the metal/oxide interface – it is the thickness and quality of this barrier layer that determines the corrosion rate and HPUF. The barrier layer thickness depends on the tendency to form either equiaxed or columnar grains, where the latter provide better corrosion resistance. The tendency to form either equiaxed or columnar grains depends in turn of the environment, e.g. the water chemistry and the Zr alloy microstructure (which depends on chemical composition and manufacturing history of the Zr alloy material).

3.2 Uniform corrosion

Corrosion of zirconium alloys at elevated temperatures is basically an electrochemical process involving a galvanic cell (Figure 3-1) [Cox, 2003] and [Cox, 2005]. The growth of the oxide film by oxygen vacancy diffusion is the anodic process and reduction of hydrogen ions from the water by electrons diffusing through the oxide film is the cathodic process.

Anodic half-cell reaction at the oxide/metal interface:

$$Zr + 2O^{2-} \rightarrow ZrO_2 + 2\square^{\circ} + 4e^{-} \quad \text{(Eq. 2)}$$

Cathodic half-cell reaction at the oxide/metal interface is:

$$2\square^{\circ} + 2H_2O + 4e^{-} \rightarrow 2O^{2-} + 4H^{\bullet} \quad \text{(Eq. 3)}$$

Since the oxygen vacancies ($\square^{\circ}$) will migrate out through the oxide via the zirconia crystallite boundaries, and the electrons will migrate via a few electrical conducting sites (perhaps associated with cracks in the oxide triggered by second phase particles), the cathodic half-cell reaction should be considered in two parts.

A water dissociation step:

$$2\square^{\circ} + 2H_2O \rightarrow 2O^{2-} + 4H^{+} \quad \text{(Eq. 4)}$$

and a proton discharge step:

$$4H^{+} + 4e^{-} \rightarrow 4H^{\bullet} \quad \text{(Eq. 5)}$$

Figure 3-1: "Corrosion as an electrochemical process".

The oxygen vacancies will diffuse out from the oxide/metal interface in the opposite direction to the oxygen ions, which have been shown to diffuse preferentially via the oxide-crystallite boundaries, [Cox & Roy, 1966] and [Cox & Pemsler, 1968].

The initial "air-formed" oxide is dense and protective and present on all Zr alloy surfaces exposed to an oxygen-containing environment, consists of very fine equiaxed nano-crystals of ZrO_2, with a certain orientations relative to the orientation of the Zr grains on which they form, [Ploc, 1970]. Some of these grains with preferred orientations will grow into columnar grains to about 2 µm, e.g., [Godlewski et al, 1991], [Anada & Takeda, 1996], [Une et al, 2010]. The preferential crystallite orientations are those that will minimise stress due to the volume change on going from Zr to ZrO_2 (the Pilling-Bedworth ratio of ~1.56[5]). According to [Motta et al, 2005] small mismatches in crystalline orientation relative to the preferred orientation cause stresses to accumulate. [Preuss et al, 2010] estimated the highest compressive stresses to be about 1200 MPa near the metal/oxide interface and about zero close to the outer surface in an 80 µm thick oxide layer, formed on ZIRLO.

The stress buildup causes the columnar grains to stop growing at a certain point and requires re-nucleation of equiaxed grains at the oxide/metal interface e.g. [Garzarolli et al, 1991], [Preuss et al, 2010], (Figure 3-2). The formation of equiaxed grains are also associated with microporosity at the equiaxed grain boundaries.

Immediately after transition an equiaxed ZrO_2 structure is seen at the metal/oxide interface and again, some of the equiaxed grains will grow into columnar grains. Thus, the oxide will be layered with equiaxed grains and columnar grains in-between (Figure 3-3).

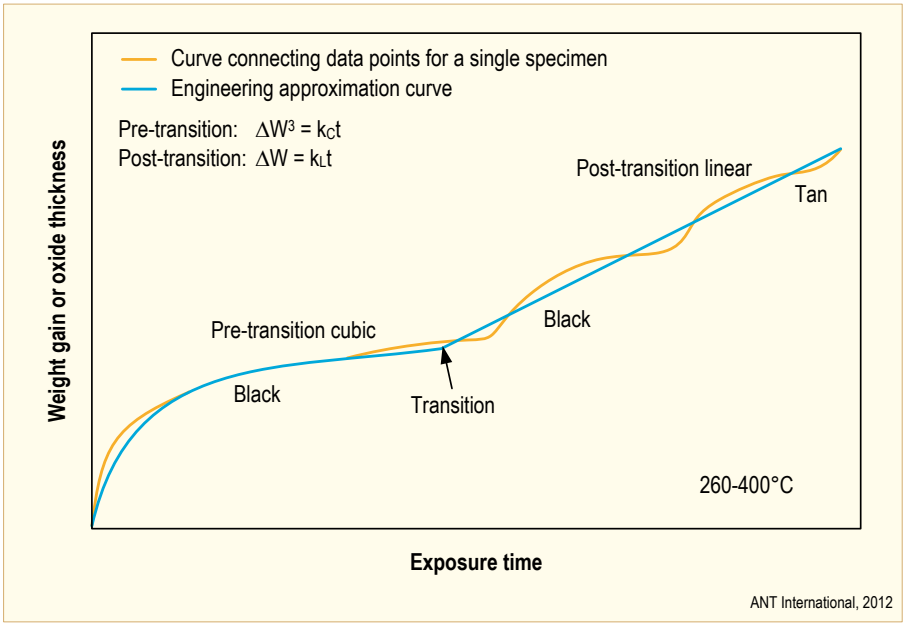

Figure 3-2: Schematic representation of the corrosion behaviour of Zircaloy (Zry)-4 in the temperature range 260-400°C. The figure presents a simplified view of the corrosion kinetics in pressurized water, an approximately cubic pre-transition growth law followed by a sharp transition, when an oxide thickness of 1.5-3 µm has been reached to an approximately linear post-transition corrosion rate, after [Hillner, 1977].

[5] The ratio of ZrO_2/Zr metal volumes

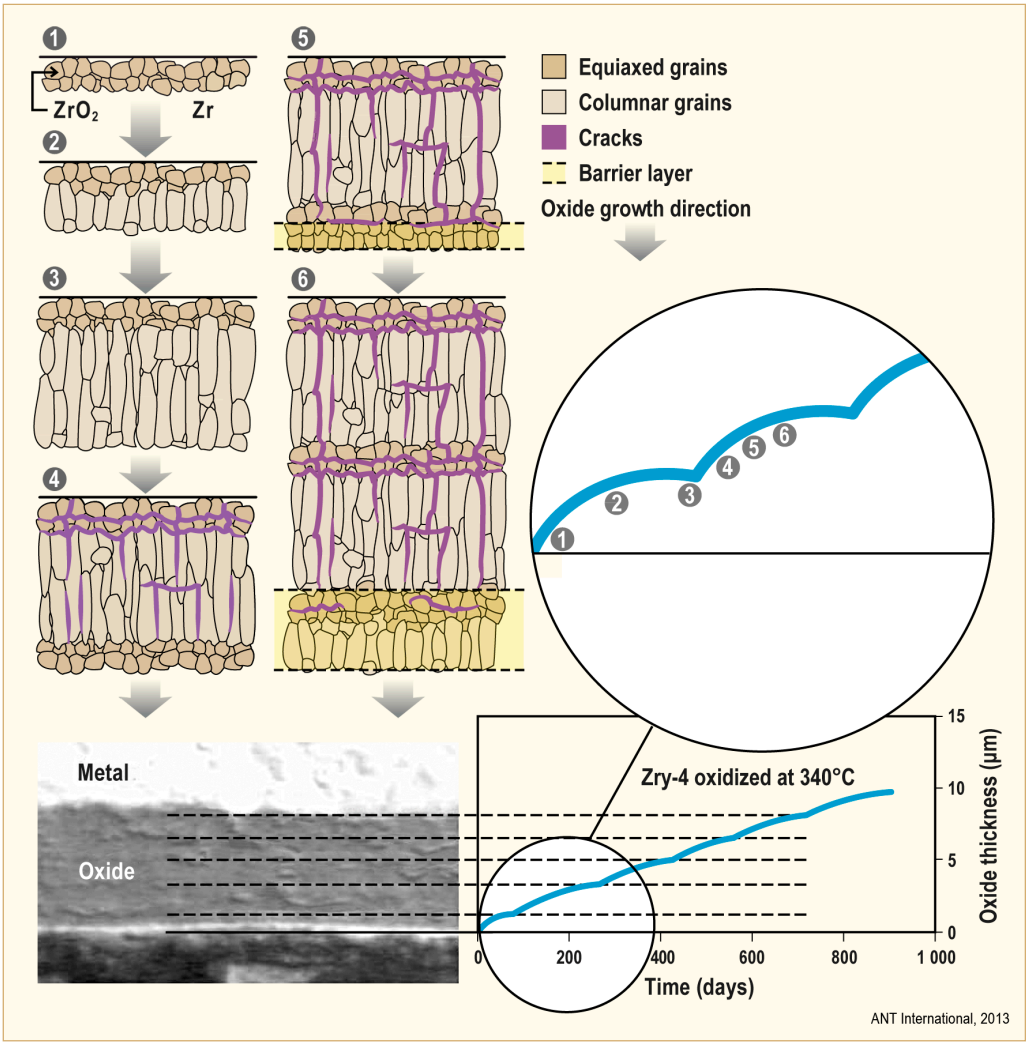

Figure 3-3: Relation between schematic oxide structure and oxidation kinetics. Corrosion of Zry-4 in autoclave at 340-360°C, after [Bouineau et al, 2007].

Several examinations have shown that an obvious correlation exist between the post transition corrosion rate and the cyclic oxide spacing (i.e., the oxide thickness between the equiaxed oxide layers – which often can be seen as lateral oxide cracks in the equiaxed oxide layers) (Figure 3-4). The extent to which these columnar crystallites grow without breaking down is a function of the alloy composition and the oxidation environment and correlates with the oxidation rate, i.e., frequent breakdowns correlates with higher corrosion rates.

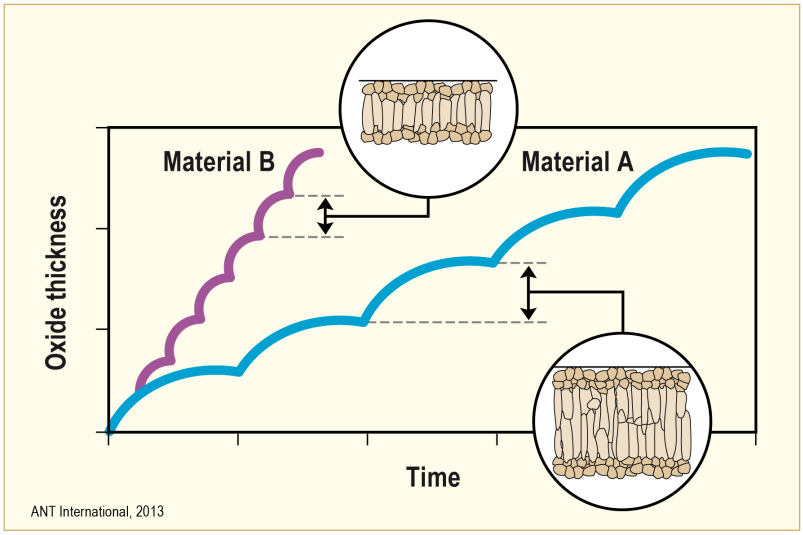

Figure 3-4: Schematic showing the difference in oxide characteristics between two different materials with different oxidation rates.

The difference in corrosion rate between different materials is related to the frequency with which the periodic corrosion cycle is repeating the pretransition stage of oxide growth, more frequent cycles for less corrosion resistant materials (Figure 3-5).

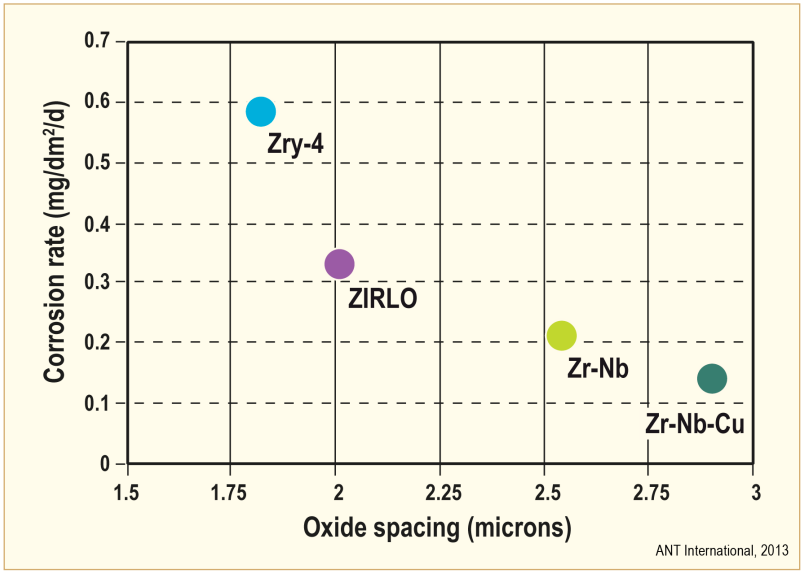

Figure 3-5: Corrosion behaviour of different Zr alloys in 360°C water, after [Yilmazbayhan et al, 2004].

It is well-known that LiOH in high concentrations may increase corrosion rate and the effect of LiOH solutions on the oxidation process is related to the breakdown of the columnar oxide structure. All oxides grown in LiOH solutions are completely equiaxed microcrystalline oxides. This failure to produce columnar oxide crystallites seems to derive from two factors: Firstly the small solubility of ZrO_2 in LiOH probably attacks the film that allows a large increase in post-transition corrosion rates, [Cox et al, 1996].

Columnar grains are associated with good corrosion resistance while equiaxed grains with poor corrosion performance [Yilmazbayhan et al, 2006].

In the range of normal reactor operating conditions there are only two mobile species in the ZrO_2 lattice: - oxygen ions/vacancies and electrons/holes. Although oxygen diffusion is a slow process, it is the essential mechanism by which the oxide thickens. The outer part of the oxide layer has some microporosity and microcracks that allow H_2O as well as other molecules to penetrate this part of the oxide. The inner part of this oxide layer, the barrier layer, that cannot be penetrated by e.g. H_2O is limiting the oxygen anion diffusion and thereby the corrosion rate. Figure 3-6 shows the correlation of the corrosion rate and the barrier layer thickness. The average thickness and the quality of the barrier govern the corrosion rate in cases when oxygen anion diffusion limits corrosion rate. The average thickness can be between <0.1 µm and >2 µm depending on environment and material. Whereas a rather thick barrier layer is built up by columnar grains, thin barrier layers exist in equiaxed grains. Pores and tangential cracks may exist in the barrier layer but without any connection to the water-oxide interface at the outer side of the barrier layer, which means that oxygen anions have to diffuse through this part of the oxide.

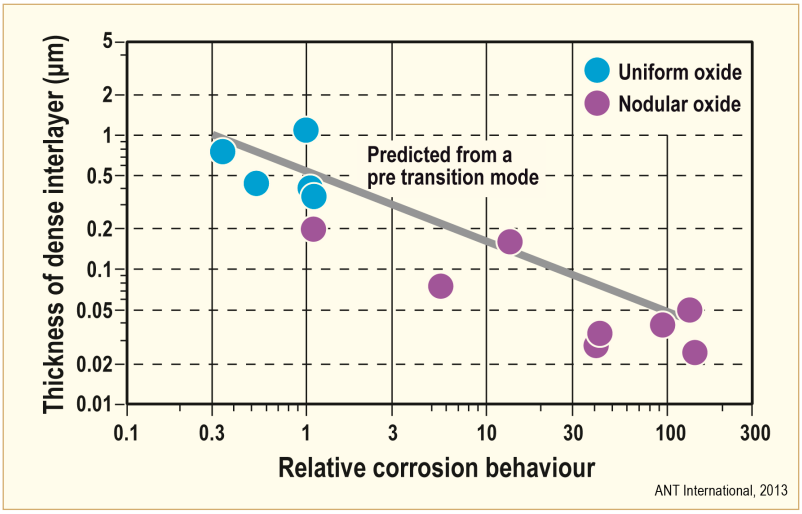

Figure 3-6: Thickness of barrier layer (from impedance measurements in H_2SO_4 of a variety of unirradiated Zry-4/2 oxide samples formed with widely differing corrosion rates (uniform, accelerated, and nodular)) versus relative corrosion behaviour of Zircaloy. It is noteworthy that nodular oxide, See section 3.3, characterized with a high corrosion rate has a thin barrier layer thickness, after [Garzarolli et al, 1991].

It must be pointed out that several examination have shown that the thickness of the pretransition oxide layer and the average thickness of the oxide between periodic oxidation rate transitions does not correspond to the barrier layer thickness (Figure 3-3), although instantaneous corrosion rate calculations are performed using these thickness values. For instance [Une et al, 2010] obtained deuterium profiles measured by NRA of pretransition oxide layers developed in 400°C D_2O steam on 3 different Zr alloys (with varying alloying chemistry). The pre-transition oxide layer was about 1.6 µm, while the barrier layer was only about 0.7-0.8 µm and the rest of the pre-transition oxide, 0.8-0.9 µm is porous. [Bossis et al, 2000] concluded from impedance measurements of Zry-4 samples containing oxide layers formed in 415°C steam (Figure 3-7) a barrier layer of 0.4 to 1.6 µm. [Göhr et al, 1996] found a somewhat thicker barrier layer from in-situ impedance tests after corrosion in 350°C water.

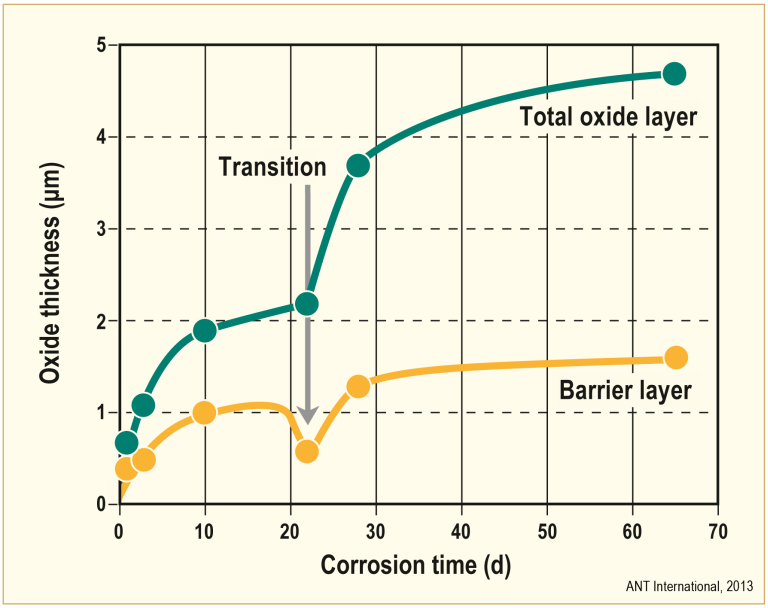

Figure 3-7: Development of total and barrier layer thickness, as deduced from impedance analysis, during corrosion of Zry-4 in 415°C 100 bar steam, after [Bossis et al, 2000].

3.3 Nodular corrosion

Nodular corrosion is a non-uniform type of corrosion that can form after some incubation time in BWRs on FRs and structural components or in out-of-reactor high pressure steam tests at 450-550°C. Nodule nucleation occurs in BWR usually after 10 to 20 days for Zry-2 and after 30-100 days for Zry-4. This type of corrosion is characterized by the formation of irregularly shaped patches of thick oxide, which increase in depth and grow laterally with increasing time (t) and fast fluence (φt).

The tendency for nodular corrosion depends largely on the microstructure of Zry, and increases with the size of the SPPs and oxidation potential in the coolant (Figure 3-8 and Figure 3-9).

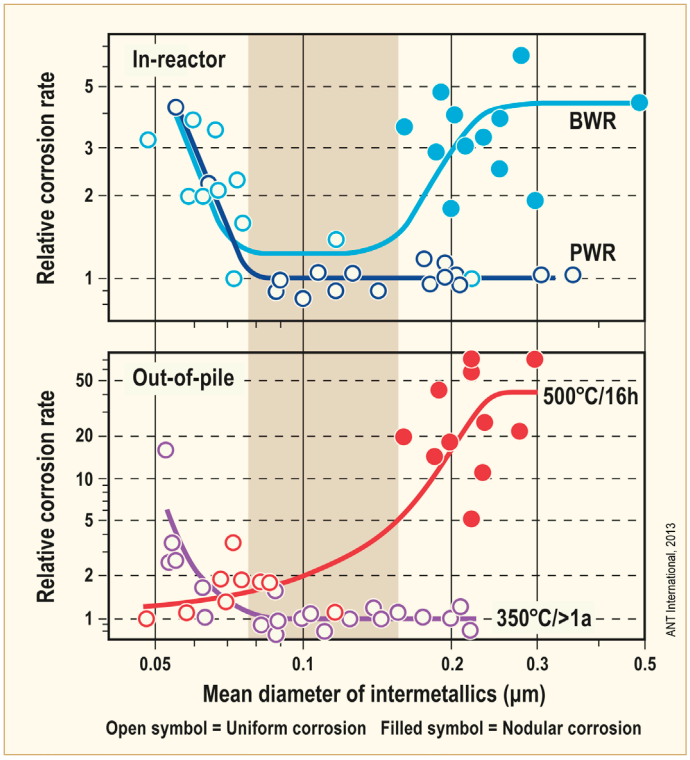

Figure 3-8: Corrosion of Zircaloy versus size of intermetallic precipitates, after [Garzarolli et al, 1996a].

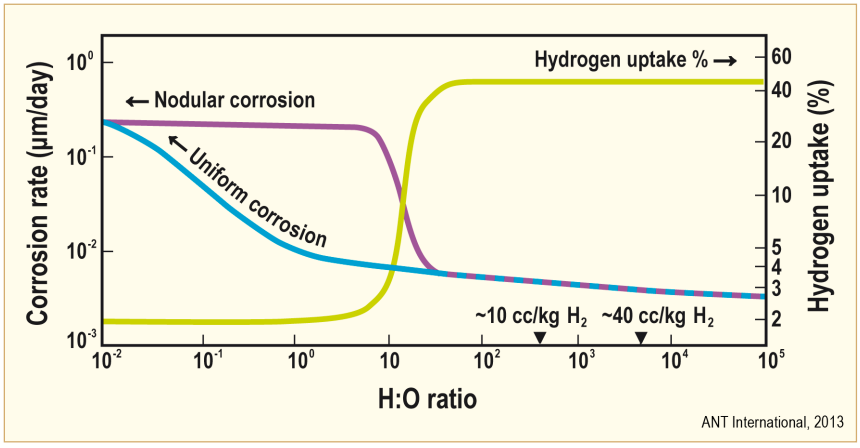

Figure 3-9: Effect of water chemistry on in-reactor oxidation and hydrogen uptake rates, after [Cox, 1985b].

Microstructure examinations of oxide layers with nodular oxide formed out-of-pile at High Temperatures (HTs) [Beie et al, 1994] and [Garzarolli et al, 1991], have shown that nodular oxide has an equiaxed structure, whereas uniform oxide a columnar (Figure 3-10). In one sample with nodular oxide, which was fast cooled after the 500°C steam test, an amorphous oxide interlayer was seen at the metal oxide interface. Fine grains nucleated and grew in this interlayer, forming an equiaxed crystal structure with grain boundary cracks. In other nodular oxide samples, which were furnace cooled from 500°C, a thin interlayer with columnar grains was seen at the interface below the equiaxed grains. This thin interlayer with uniform oxide characteristics was probably formed during cooling at temperatures <450°C.

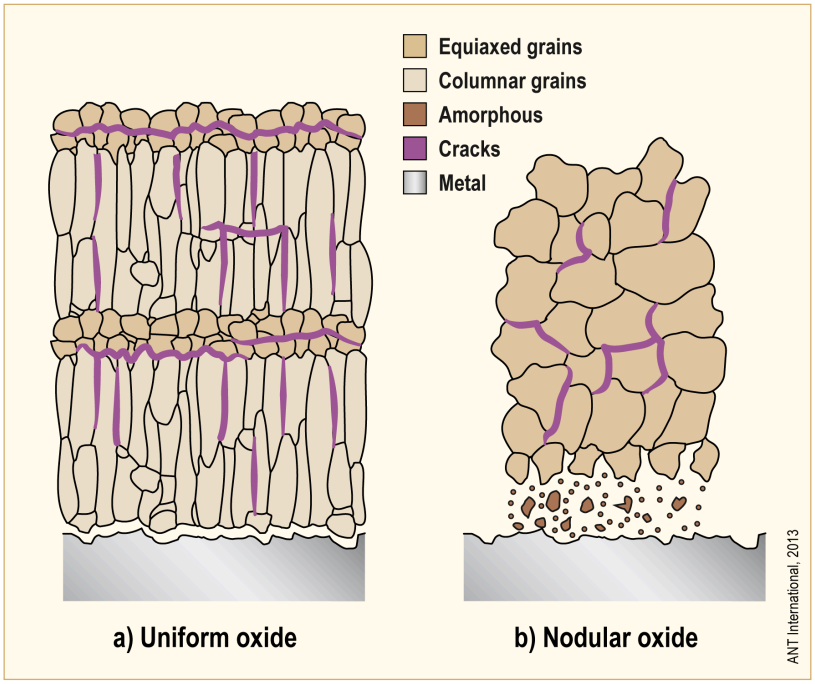

Figure 3-10: Structural differences of uniform and nodular oxide, after [Garzarolli & Sell, 2006].

No widely accepted mechanism exists for nodular corrosion. Most of the existing hypotheses deals with nucleation of nodular corrosion, for more details see Sections 3 and 4 by Garzarolli in [Adamson et al, 2007/2008].

It is a fallacy that PWRs are immune to nodular corrosion; see Cox in [Adamson et al, 2007/2008]. Provided the dissolved hydrogen in the reactor water is high enough to ensure that all metals in the PWR structure are operating at the reversible hydrogen potential there will be no galvanic potential available between any of the metals present to drive a galvanic cell and to create nodular corrosion between dissimilar metals. That this is the case is shown by at least three observations:

i) No H_2 was added to the water during the first cycle of the Obrigheim reactor and severe nodular corrosion was observed.

ii) The Chinese did not add H_2 to the water in their reactor loop test of the fuel for their indigenous PWR (Chinshan) and again serious nodular corrosion was observed.

iii) CANDU reactors operate with low dissolved H_2 in the water and this is near the borderline for eliminating nodular corrosion. As a result, a number of fuel tests have shown incipient nodular corrosion [Urbanic et al, 1979].

3.4 Shadow corrosion

3.4.1 Introduction

Enhanced corrosion of zirconium alloys may occur - under oxidising conditions - when the corroding surface is close to, or in contact with, certain other metallic components. The shape of the component is often reproduced in the shape of an area of enhanced corrosion, suggestive of a shadow cast by the component on the zirconium alloy surface. The term "shadow corrosion" is therefore often used to describe the phenomena. Observations of shadow corrosion on water reactor components have been noted for many years. In 1974, [Johnson et al, 1974], reported enhanced corrosion in Zircaloy coupons located near, but not touching, small pieces of platinum in the Advanced Test Reactor (ATR). Also, [Trowse et al, 1977], reported enhanced fuel rod corrosion beneath steel spacers in the Steam Generating Heavy Water Reactor (SGHWR). Details available in 2002 are given in ZIRAT7 STR Corrosion of Zirconium Alloys, [Adamson et al, 2002], for more details see Section 4.2 in ZIRAT12 STR on Corrosion Mechanisms.

3.4.2 BWR fuel channels

Most commonly observed are the control blade shadows on BWR channel surfaces adjacent to the control blade handles. It was shown, [Chen & Adamson, 1994], that the handle image is faithfully reproduced on the channel surface, but is larger than the actual handle, shown schematically in Figure 3-11.

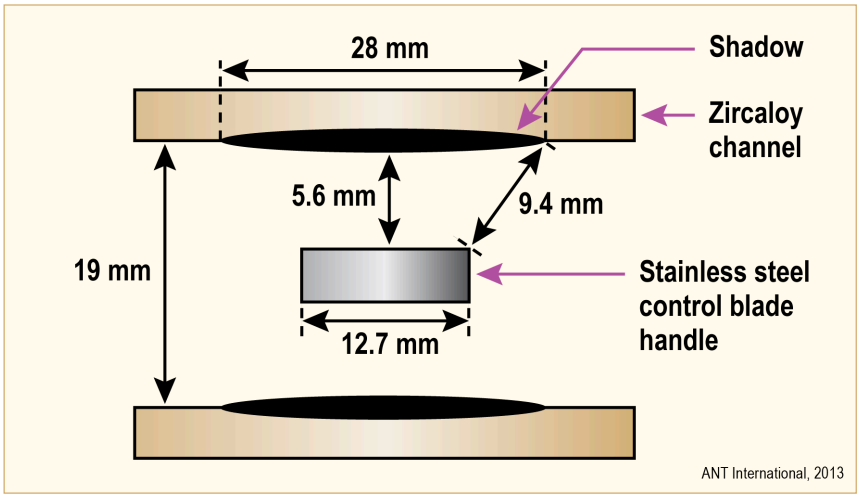

Figure 3-11: Geometrical relationships between control blade handle and channel for the shadow, after [Chen & Adamson, 1994].

Hot cell examination of a similar channel shows that oxide thickness within the shadow area can be much higher than outside the shadow, [Adamson et al, 2000]. Since temperature gradients are small in a channel wall, re-distribution of hydrogen by thermal-gradient-driven diffusion is also small, indicating in this case a much reduced hydrogen pick-up rate in the shadow.

It is also observed that control blade shadows preferentially form during the first cycle of operation and that the thickness tends to saturate with burn-up, as shown in Figure 3-12 [Fukuya et al, 1994].

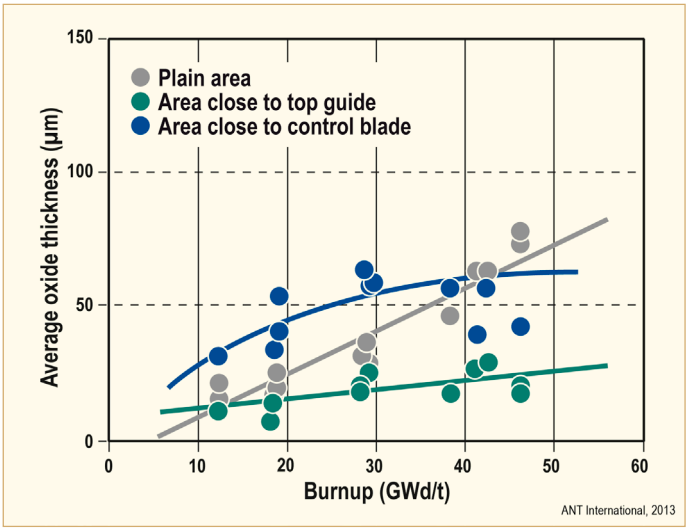

Figure 3-12: Oxide thickness in BWR channels as function of burn-up. Shadows form close to the control blade and close to the top guide plate, after [Fukuya et al, 1994].

3.4.3 BWR fuel rods

Shadows on fuelled or non-fuelled rods have been observed under Zircaloy spacers with Inconel springs or under all-Inconel spacers (Figure 3-13). Again, this illustrates the trend for saturation of the oxide thickness with fluence or burn-up. In most cases, shadows have not caused fuel performance problems. The upper curve in Figure 3-13 for a specific cladding condition is an exception.

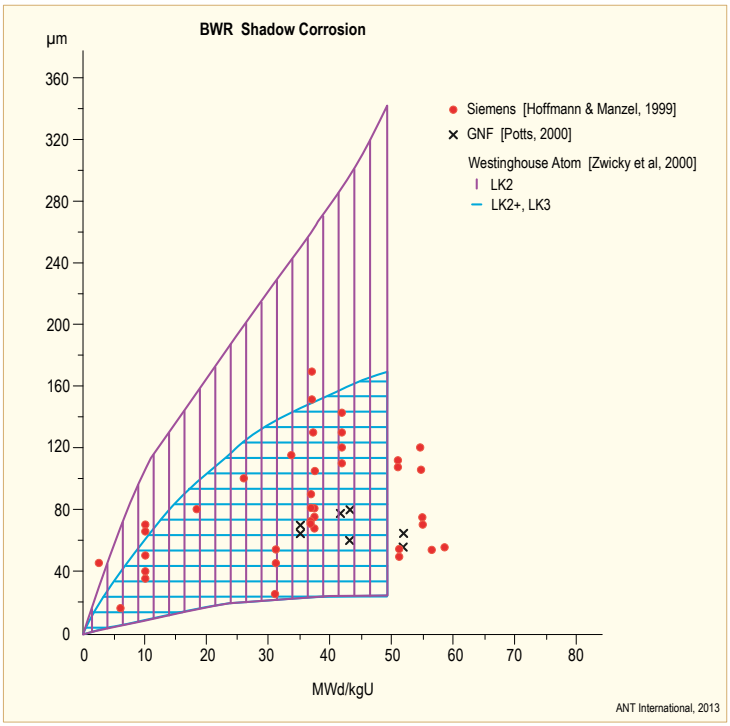

Figure 3-13: Shadow corrosion data of various BWR fuel vendors claddings, after [Hoffmann & Manzel, 1999]; [Potts, 2000a], and [Zwicky et al, 2000].

3.4.4 Mechanism

Most researches believe that shadow corrosion is a galvanic corrosion phenomenon.

The root cause of shadow corrosion is very likely the rather large potential difference between fresh Zry surface and stainless steel or Inconel. For galvanic corrosion, a path for electron transfer between the cathodic shadower (SS, Inconel, Pt) and the anodic Zry as well as a conductive path through the water separating the two parts is required.

Electrochemical measurements out-of-pile (no irradiation) at 290°C in a simulated BWR environment exhibited quite large potential differences between Inconel and fresh Zry whereas the potential difference in simulated PWR environment was small – which would explain why shadow corrosion is not seen in PWRs. Figure 3-14 shows the ECP behaviour of Zry-2, 304 SS, Alloy X-750, and Pt electrodes as a function of immersion under various water chemistry conditions. It is clearly seen that the ECP difference between Zry-2 and other alloys becomes smaller in the presence of hydrogen. When no oxygen is available, no significant ECP differences among alloys is observed.

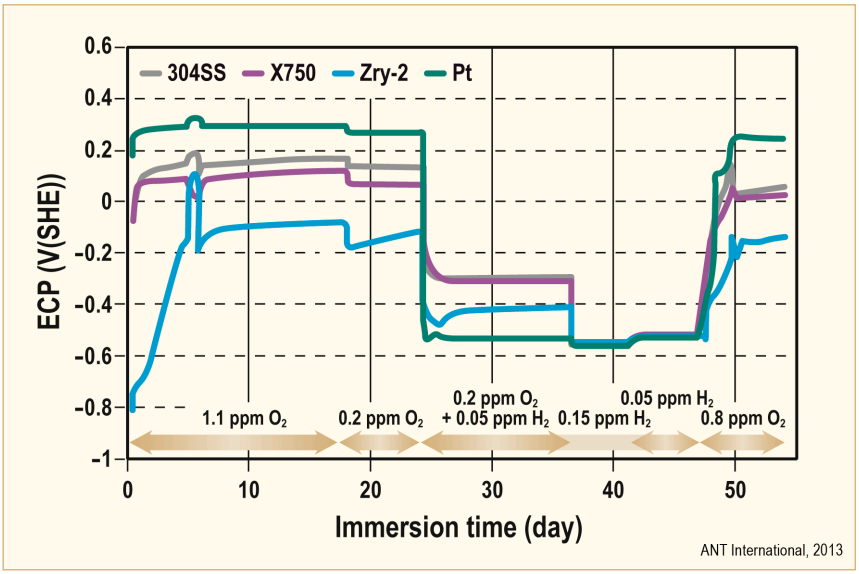

Figure 3-14: Electro Chemical Potential of Zry-2, 304SS, Alloy X-750, and Pt electrodes in 300°C water containing various concentrations of hydrogen and oxygen, after [Kim et al, 2010].

Radiolysis in-BWR, leading to significant H_2O_2 concentrations, further increases very likely the potential difference between dissimilar metals by increasing the redox potential of the coolant (by radiolytic oxidation products) and an increased corrosion of Zry (reducing the corrosion potential). This was experimentally shown by at least at lower coolant temperatures [Lysell et al, 2001]. [Kim et al, 2010] used photoelectrochemical investigation on radiation-enhanced phenomena of shadow corrosion to emphasize the potential difference between the two alloys. They measured the electrochemical potential of Zry-2, Zry-4, Ziron, NSF, stainless steel (SS), Inc-750, and Pt in 300°C water and confirmed that a significant potential difference between the Zr-alloys and SS/Inc-750/Pt) only exists in oxygenated water. They furthermore showed that this potential difference increases as consequence of an UV illumination, imitating the Cherenkov-ray radiation in a BWR (Figure 3-15).

For such a galvanic corrosion mechanism, one would expect an increased growth rate of shadow corrosion with increased potential differences. The potential differences can increase with increasing red/ox potential of the coolant. The species most affecting the red/ox potential of the coolant are O_2, Cr^{6+}, and $NO^{3+}$and H_2O_2. The potential difference is furthermore enhanced in reactor, [Lysell et al, 2001] and by UV light (Figure 3-15), [Kim et al, 2010].

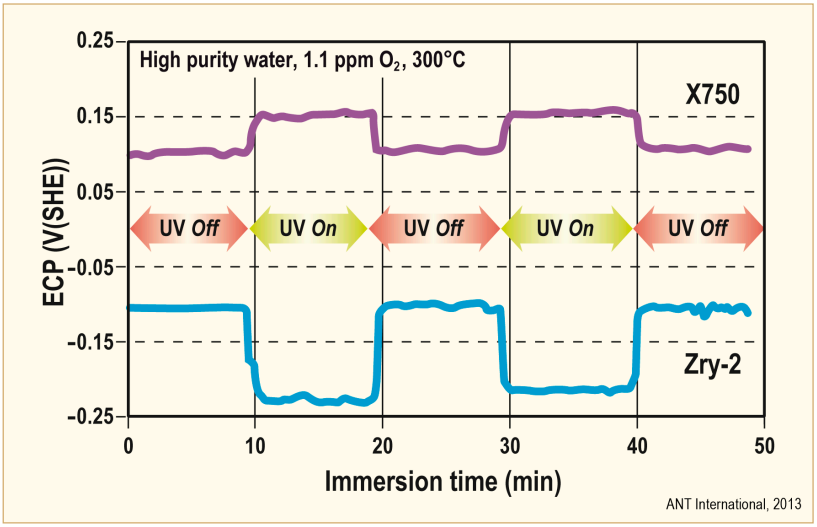

Figure 3-15: Electrochemical Corrosion Potential of Inconel X750 and Zry 2 electrodes in 300°C water containing 1.1 ppm O_2 with and without UV illumination, [Kim et al, 2010].

Figure 3-16 gives a schematic of the processes which occur in irradiation-assisted galvanically-driven shadow corrosion. Given is an Inconel component (cathode, shadower, counter) at a corrosion potential E1 and a zirconium alloy (anode, shadow former) at a potential E2, with E2>E1. The two pieces are connected by (F) either an insulating rod (as in many in-reactor experiments) or some sort of circuitous electrical connection path (as proposed for real reactor components). All are sitting in BWR-type reactor water and in an intense radiation field. Irradiation plays three important roles: 1) causes the normal insulating oxides (ZrO_2) to become conductors, likely due to a photoconductivity effect, 2) increases the conductivity of the water through radiolysis, and 3) assists in initiating reaction (A). Role (1) is very important because without it the transfer of electrons (e-) between the Inconel and the zirconium alloy would be difficult or impossible, particularly in reported test reactor experiments. Reaction (A) produces OH- ions and reaction (B) produces H+ (protons) and O^{2-}. The potential difference drives H+ toward the Inconel (cathode) and O^{2-} toward the zirconium surface (anode), where at (C) it forms ZrO_2 and electrons (e^-). Since the potential difference falls off with separation distance, the oxide that thickens has the general shape of the Inconel but is slightly larger. After reaction (C) the electron (e^-) is driven by the potential difference back to the Inconel (cathode), where it combines (D) with H^+ to form H^0 and H_2 gas. This reaction is different from a non-galvanic corrosion process whereby hydrogen would form near the ZrO_2/water interface, and part of it would evolve as H_2 gas and part would form hydride in the zirconium alloy matrix.

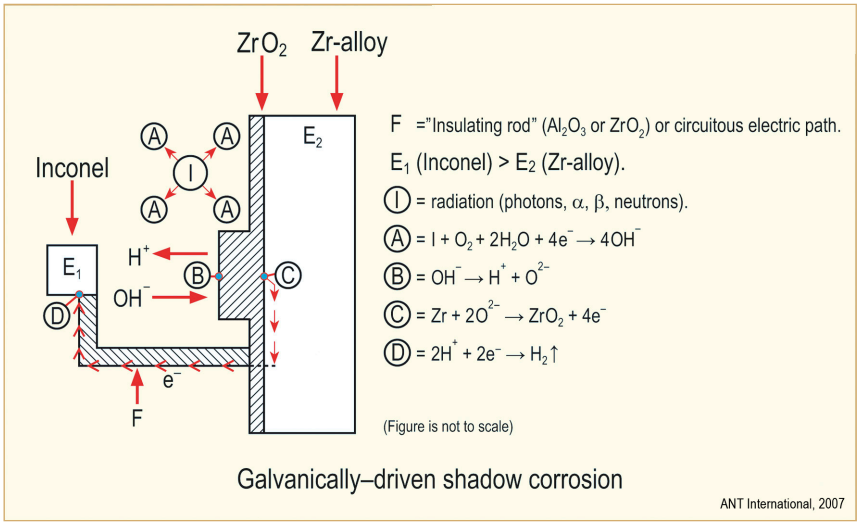

Figure 3-16: Schematic of processes involved in irradiation–assisted, galvanically -driven shadow corrosion. In this case Inconel at potential E_1 is the cathode and a zirconium alloy at potential E_2 is the anode, Adamson in [Adamson et al, 2007/2008].

3.5 Conclusions on corrosion mechanism

- The corrosion rate is governed by the oxygen anion diffusivity through a barrier layer, the thicker the layer the lower the corrosion rate. The barrier layer thickness varies in time by repeated transition building-up and breaking down the barrier layer thickness (cyclic oxide layer thickness).
- Higher corrosion rates are correlated to larger fractions of equiaxed grains while better corrosion resistance is associated with columnar grains. The equiaxed grains are often associated with cracks/porous at its grain boundaries making this type of oxide structure less protective.
- The effects of LiOH are two-fold:
  - Pore formation due to preferential cubic or tetragonal ZrO_2 dissolution [Cox & Wu, 1993] and consequently a drastic reduction of the barrier layer thickness at the metal/oxide interface
  - Formation of equiaxed grains (instead of columnar grains) which are less protective, i.e., results in a thinner barrier layer.
- Especially in BWRs, Zr alloy corrosion depends on water chemistry. Probably all impurities that affect the oxidation potential at the oxide water surface, such as O_2, Cr^{6+}, H_2O_2, etc., may have a significant effect on shadow corrosion, nodular corrosion, and corrosion of Nb containing alloys.

3.6 Hydrogen uptake mechanism

The hydrogen atoms released at the oxide/environment interface by reduction by the electrons can recombine to form hydrogen molecules (which will dissolve in the water) or can diffuse inwards to the oxide/metal interface if they can find a suitable path through the oxide film. Just how this does occur is to this date not known.

It has been speculated that the hydrogen may pass through the barrier layer by:

- Migration of the hydrogen down via local imperfections (cracks and pores) in the barrier oxide film,
- Transport of hydrogen through non-oxidized SPP (e.g. containing Ni or Cu), acting as windows,
- Diffusion of hydrogen in the oxide grain boundaries if a metallic Ni band (from irradiation induced dissolution of Nickel-bearing SPPs e.g. in Zry-2) exists in the grain boundaries of the barrier layer.

The oxidation reaction of Zr alloys with H_2O leads to the release of hydrogen. Oxygen ion vacancies (V_O^{2+}) and electrons (e^-) from the Zr oxidation reaction

Eq. 3-1: $$2O_2^- + Zr \rightarrow ZrO_2 + 4e^-,$$

that diffuses out to the oxide-water interface of the barrier layer will react with water molecules and release two hydrogen atoms:

Eq. 3-2: $$V_O^{2+} + H_2O \rightarrow O^{2-} + 2H^+ \text{ and}$$

Eq. 3-3: $$2e^- + 2H^+ \rightarrow 2H^0 \text{ or}$$

Eq. 3-4: $$2e^- + H_2O \rightarrow O^{2-} + 2H^0$$

Most of these hydrogen atoms will usually then recombine to give H_2 molecules, which can diffuse into the coolant environment. Some H atoms, however, may migrate into the Zr matrix. It is these H atoms that represent the "Hydrogen Uptake" of the Zr alloy (Figure 2-2).

In reactor radiolysis may create additional hydrogen at the barrier layer surface according:

Eq. 3-5: $$2H_2O \rightarrow 2OH^0 + 2H^0$$

The HPUF is not a physical property but results from a competition between two kinetic processes:

- H atom recombination and diffusion into the environment and
- H atom migration into the Zr matrix.

The HPUF vary as a result of a number of factors such as the temperature and pressure of the environment, the oxide thickness and morphology, the potential gradient over the barrier layer, as well as the redox potential of the environment.

Since proton discharge process (Eq. 3-3) and the water dissociation process (Eq. 3-5) takes place at a site on the oxide-water interface the electrons from the Zr oxidation reaction (Eq. 3-2) must be conducted through an oxide which is a very good insulator (except in-reactor), the most probable sites for the electrons to discharge the protons will be those where the conduction path for the electrons is a minimum. The direct diffusion route through the oxide film is not available to them, since all claims to measure such diffusion coefficients have been shown to be due to OH^- ions migrating down cracks or pores in the oxide and were not H^O diffusion through the ZrO_2 lattice [Ramasubramanian, 1996] and [Elmoselhi et al, 1994].

The uptake of hydrogen by the zirconium alloy matrix during its corrosion, arising from the reduction of protons by the electrons from the Zr cathodic-half-cell reaction is considered by e.g. [Elmoselhi et al, 1994], [Cox & Wong, 1999] and [Ramasubramanian et al, 2000], to be a function of the number of through-wall flaws present in the ZrO_2 barrier film that penetrate right through to the oxide/metal interface. These flaws seem not to be perpetual features of a particular site in the oxide, but are regularly healing up and new flaws are being generated. The frequency of such sites in alloys such as Zry-2 and Zr-2.5 % Nb seems to be in the same ratio as the H-uptake percentages for the different alloys [Cox & Wong, 1999]. Since the "barrier" oxide films are usually imperfect to the extent of containing at least a few flaws that penetrate right through to the oxide/metal interface, these oxide flaws are the most probable route for H uptake.

However, if the hydrogen is being liberated at the bottoms of a few small pores or cracks – not fully reaching the metal, then the hydrogen could build up at these sites until an almost 100% H_2 atmosphere is generated in the pore, which would soon lead to a breakdown of any oxide barrier at the bottom of the pore and to an uptake of hydrogen [Cox, 1985a]. [Ploc, 1999] concluded from TEM examined of oxide layers on Zr2.5Nb, that the deuterium uptake in CANDU reactors is primarily via the ribbon porosity, which is along the boundary between the oxidized α-Zr and β-Zr phases.

4 Parameters impacting corrosion and HPU

4.1 Microstructure

4.1.1 Effect on corrosion rate

The major material parameters that can affect corrosion are:

- Alloying additions and impurities
- Solute content
- SPP characteristics (the influence being their size and composition)
- Degree of cold-work/recrystallisation

The effect of all these parameters on corrosion rate differs in different environments, such as hydrogenated, oxygenated, and LiOH-containing coolants. The effect also varies with temperature and system pressure.

The alloying elements and impurities of modern zirconium alloys, such as Sn, Nb, Fe, Cr, Ni, O, Si, C are either fully dissolved in the alloy matrix (Sn, O) or dissolved to a large extent (Nb) or almost fully precipitated in small intermetallic second phase particles (Fe, Cr, Ni, Si, C). The effect of the alloying element on the corrosion rate depends on the corrosive environment itself, as can be seen from Table 4-1, and are discussed in the following:

- Sn
  - hydrogenated environments such as in PWRs and VVERs:
    - increases uniform corrosion rate
    - reduces corrosion rate in diluted LiOH (e.g. PWRs)
  - oxidising environments such as in BWRs
    - decreases nodular corrosion tendency
- Nb
  - hydrogenated water and steam
    - reduces corrosion rate in, in the concentration range up to 0.5%, where Nb is in solid solution in the α-Zr matrix.
  - BWRs
    - Nb-containing alloys can suffer from increased corrosion rate under oxygenated coolant conditions
- Transition Metals (TM) alloying elements Fe, Cr, Ni, V, and Cu, all have a very low solubility in the α-Zr, and impacts corrosion rate at concentrations far above their solubility limit in the α-Zr matrix. Thus, corrosion rate of Zr-TM alloys is governed by the intermetallics (SPP).
  - PWRs and out of pile with and without LiOH-containing water

- The transition elements (TM) Fe, Cr, Ni, V, Cu reduce uniform corrosion rate in Nb-free alloys. Zr-Sn-TM alloys with a low TM content usually show a significant corrosion acceleration at longer exposure times, whereas higher TM contents reduce this late corrosion acceleration, [Broy et al, 2000]. In this respect, Fe and Ni are more beneficial than Cr, V, and Cu, at least in PWRs and out of pile. Cr and V can even, under certain conditions, increase corrosion out of pile and in-PWR.

– In BWRs, the effect of transition elements on corrosion rate is not so clear.

Table 4-1: Effect of alloying elements on corrosion of zirconium alloys [Adamson et al, 2005], [Adamson et al, 2006/2007] and [Adamson & Cox, 2005].

Element	Solubil. (%)	Best alloy content (%)	Out-pile corrosion	In-PWR corr.	LiOH corr.	In-BWR corr.	HPUF
Sn	2	0/>1	—	=	+ +	+	0
Nb	0.5	0.5/>2	+ +	+ +	0	—/+	+/**0**
Fe	<0.01	≥0.3	+ +	+ +	+ +	+	0/+
Cr	<0.01	≥0.15	+/—	+	+ +	+	+ (>0.15)
Ni	<0.01	0.05	+ +	+		+	=/0
V	<0.01	≥0.15	+/—	+	+ +	+	+
Cu	<0.1	≥0. 5	+				0
0: no effect, — increase, = strong increase, + reduction, ++ strong reduction, 0/+ effect differs in different environments.							
ANT International, 2013							

The effect of impurities on corrosion of zirconium alloys is given in Table 4-2.

- Nitrogen in solid solution in the concentration range of >30 to 120 ppm, increases corrosion rate significantly (depending on the alloy composition).
- Oxygen, which is also soluble in the studied range, increases corrosion slightly.
- Carbon increases corrosion above about 100 ppm, when it precipitates as carbides.
- Si, in the range of 80 and 120 ppm, can reduce the corrosion rate if the β-quenching step during the alloy manufacturing was not perfect. Fine silicides can act as nucleation sites for Zr-FeCrNi SPPs, making the SPP distribution more homogeneous thereby reducing corrosion rate for lots not subjected to fast beta quenching. At higher concentrations of Si (>150 ppm) the corrosion rate is increased and probably the hydrogen pick-up fraction is decreased.
- P increases nodular corrosion rate at >10 ppm but has no effect on uniform corrosion rate in the studied range.
- Mn increases corrosion rate if it exceeds the solubility limit in α-Zr.
- Al, which is fully soluble in α-Zr, increases corrosion rate if the content is above 80 ppm.
- S has no effect on the uniform corrosion rate in the studied range.

Table 4-2: Effect of impurities on corrosion of zirconium alloys [Adamson et al, 2005], [Adamson et al, 2006/2007] and [Adamson & Cox, 2005].

Element	Conc. studied (ppm)	Out-pile	In-PWR	In-BWR
O	600-2000	—/0	0	—
N	20-2000	=	=	=
Si	<120/>120-	+/—	+	+
C	<100/>100-300	0/—	—	0
Al	<80/>80-400	0/—		
Mn	<300/>300-5000	0/—		
P	3-25	0		—
S	1-40	0		
0: no effect, — increase, = strong increase, + reduction, ++ strong reduction, 0/+ sometimes				
ANT International, 2013				

In zirconium alloys, different types of SPPs can appear. The type and characteristics of various SPPs and their dependence on manufacturing heat treatments are described in Table 4-3.

In Zr-Fe alloys the orthorhombic Zr_3Fe phase appears whereas in Zr-Cr alloys the hexagonal Laves phase $ZrCr_2$ exists. In zirconium alloys that contain Fe and Cr, such as Zry-4, the type of SPP depends on the Fe/Cr ratio. If the Fe/Cr alloying ratio is <4 the only phase formed is the Laves phase, $Zr(Cr,Fe)_2$. At a Fe/Cr alloying ratio of >4 Zr_3Fe or Zr_2Fe is also formed. The size of the Laves phase precipitates is smaller than the size of the Zr_2Fe precipitates and the Zr_3Fe precipitates are generally significantly larger than the other two precipitate types. One of the most important zirconium alloys, Zry-2, contains Ni in addition to Sn, Fe and Cr. In this system, two different types of SPP are formed. These are the hexagonal Laves phase –Zr $(FeCr)_2$ and the body-centred tetragonal Zintel phase - $Zr_2(FeNi)$. The size of the Zintel phase precipitates is somewhat larger than that of the Laves phase precipitates.

Zr-Nb alloys usually contain fine precipitates of β-Nb (80%Nb20%Zr) or β-Zr (20%Nb80%Zr) depending on fabrication route. Several modern Zr-Sn-Nb alloys, such as ZIRLO or E635, contain about 0.7- 1 wt% Nb as well as 0.1 to 0.5 wt% Fe. Furthermore, most binary Zr-Nb alloys, such as M5 or Zr-2.5Nb, contain some Fe as an impurity (several 100 wtppm). At high Nb and moderate Fe concentrations, a hexagonal $Zr(NbFe)_2$ phase, with Nb/Fe=1-1.5, is often found besides the fine β-Nb precipitates. At medium Fe and not too high Nb contents all SPPs are of the Laves phase $Zr(NbFe)_2$ type. At high Fe and rather lower Nb concentrations a cubic $(ZrNb)_2Fe$ phase may be formed in addition to the Laves phase or even replacing the Laves phase. The size of the $Zr(NbFe)_2$ precipitates in fully α-processed Zr-Nb alloys with some iron is, even in low-temperature-processed material, quite large (100-200 nm) and larger than the size of the β-Nb precipitates (~50 nm). The $(ZrNb)_2Fe$ phase is the largest (500 nm).

C or Si impurities form binary SPPs with zirconium only during processing in the β-Zr range if their content is above 150 and 50 ppm, respectively. In the α-Zr range, Si usually forms, together with Fe, the bct $Zr_2(FeSi)$ phase. The size of the $Zr_2(FeSi)$ phase is generally very fine and much finer than that of the usual Laves SPP in Zry-4.

Table 4-3: Type and characteristics of SPP in zirconium alloys. Information from [Adamson et al, 2002].

Alloying elements	Solubility in α (%)	Trans. Temp. α/ (α+β) (°C)	Type of SPP	Structure of SPP	Max existing temp. (°C)	SPP size (μm)/distribution after heat treatment in low α–Zr phase range	high α–Zr phase range	(α+β)–Zr phase range
Fe	0.01	795	Zr_3Fe or Zr_2Fe	Orthorhombic bct	885 998	0.5/uniform	1/uniform	
Cr	0.01	830	$ZrCr_2$	Laves, fcc	1560	0.02/uniform	0.15/uniform	
Fe+Cr	0.01	800	$Zr(Fe,Cr)_2$	Laves, usually hex.		0.04/uniform	0.2/uniform	0.4/at GB*
Fe+Ni	0.01	800	$Zr_2(Fe,Ni)$	Zintel, tetrag		0.2/uniform	0.7/uniform	
Nb	0.5	620	β-Nb or β-Zr	bcc	2000 1740	0.03/uniform	0.05/uniform	>0.1/at GB*
Nb+Fe	0.3/0.01	600	$Zr(Fe,Nb)_2$ or $(Zr,Nb)_2Fe$	Laves, hex tetrag/fcc	~700 ~750		0.15/uniform 0.5/uniform	0.7/at GB*
Nb+Fe+Cr	0.3/0.01	600	$Zr(Fe,Cr,Nb)_2$	Laves, hex			0.15/uniform	
Impurities								
C	3	800	ZrC		3427			at>150 ppm >0.1 μm
Si	0.01	860	Zr_3Si		1650		0.05/uniform	at>150 ppm >0.1 μm
Si+Fe	0.01	800	$Zr_2(Fe,Si)$					
H	0.06	550	Zr_2H					
* Grain Boundaries								
ANT International, 2013								

At normal light water reactor temperatures (270-370°C (543-643K)) the SPPs change under irradiation in a combination of two ways – amorphisation and dissolution. The amorphisation process begins at the outside surface of the SPP, is connected with a significant decrease of the Fe/Cr ratio, and works its way inward with increasing fluence. At typical Light Water Reactor (LWR) operating temperatures, SPP amorphisation and dissolution occurs relentlessly until the SPP essentially disappears. As SPPs dissolve, the zirconium matrix becomes enriched (well beyond the normal solubility limit) in the dissolving elements. Figure 4-1 shows the decrease of the relative $Zr(Fe,Cr)_2$ SPP volume and the oxide layer build up for Zry-4 samples irradiated in a PWR at 290°C. The figure shows that the oxide thickness increases with decreasing volume fraction of SPPs - *it may be speculated that the SPPs in Zry-2 and -4 forms the barrier layer and when the SPPs are lost due to dissolution, the barrier layer cannot form resulting in a corrosion rate increase.* A critical material temperature exists above which the recrystallisation processes are fast enough to prevent the SPP irradiation damage accumulation needed for transformation or dissolution of the SPPs. For moderate burn-up at <330°C, the SPP would become partially amorphous and partially dissolved, depending on its initial size. At >330°C it would remain crystalline and would partially dissolve, the extent of which depending on initial size. At >380°C the SPPs of Zry-4 do not dissolve any more but grow under irradiation, [Adamson & Cox, 2005] and [Garzarolli et al, 1996b].

As far as the Zr-Nb alloys are concerned, neither the β-Nb, $Zr(Nb,Fe)_2$, nor $(Zr,Nb)_2Fe$ SPPs become amorphous during irradiation at >330°C, ß-Nb precipitates only change their Zr/(Nb+Zr) ratio (from 0.1 to 0.45), $Zr(Nb,Fe)_2$ SPPs lose most of the Fe and become ß-Nb and the large $(Zr,Nb)_2Fe$ SPPs remain their original size and composition.

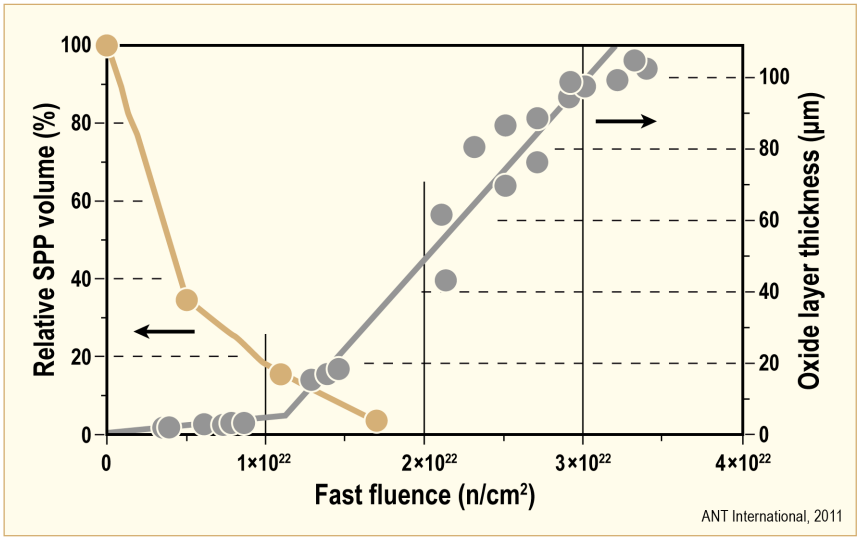

Figure 4-1: Influence of irradiation to very high fluences at 290°C on corrosion in PWR and SPP dissolution of Zry-4 with large SPP, after [Garzarolli et al, 2002a].

The size, distribution and kind of SPP can play a significant role in out-of-pile corrosion in oxygen-free water and steam, in PWRs and in BWRs. However, the effect is different for different alloys, as can be seen from Table 4-4.

Table 4-4: Effect of SPP size on corrosion of zirconium alloys [Adamson et al, 2007/2008].

Alloy type	Effect of SPP size on corrosion in			
	350°C water	500°C steam	In-PWR	In-BWR
Zr-Sn-Fe, Cr	Increases <70 nm	Increases <150 nm	Increases < 80 nm	Increases <80 nm and at >150 nm
Zr-Nb-Sn	Slightly lower at very fine size	Slightly lower at very fine size	Significantly lower at very fine size	Slightly lower at very fine size
Zr-Nb-(Sn)-Fe,Cr	Slightly lower at very fine size	Slightly lower at very fine size	Significantly lower at very fine size	Slightly lower at very fine size

ANT International, 2013

As shown in Figure 4-2 in the case of Zircaloy, SPP size has a very pronounced effect on corrosion in 350°C water, 500°C steam, as well as in PWRs and BWRs. Uniform corrosion rate increases out of pile in 350°C water and in pile at a SPP size below 70-80 nm and nodular corrosion appears in-BWR and in 500°C steam in lots with a SPP size larger than 150 nm.

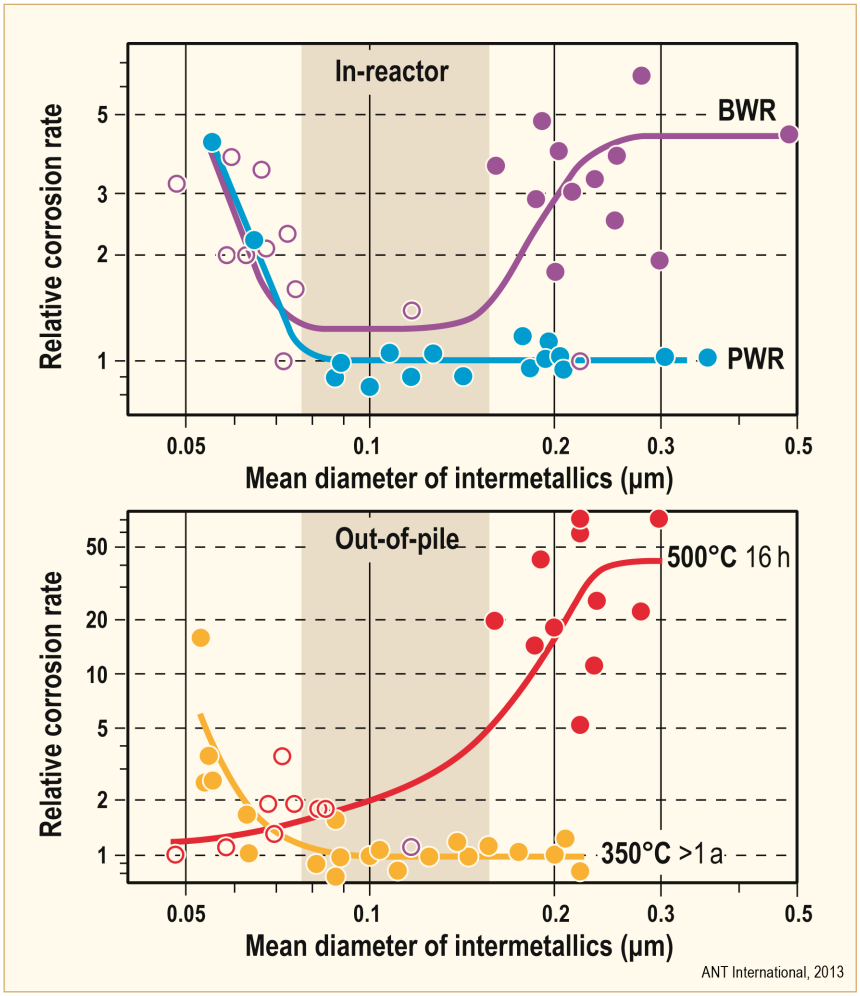

Figure 4-2: Corrosion of Zircaloy versus size of intermetallic precipitates, after [Garzarolli et al, 1996a].

However, it has to be mentioned that it is not fully clear whether these effects are primarily due the SPP characteristics or due to the solute content. Some scientists consider the solute content of Fe and Cr as the real root cause for the observed differences, e.g. [Cheng & Adamson, 1987]. The α-Zr solute content increases with decreasing SPP size and annealing (A)-parameter[6]. The solute content can affect the stoichiometric structure of the zirconium oxide layer, by replacing Zr^{+4} by subvalent atoms, such as Fe^{+3}, Cr^{+3}, Ni^{+}, thereby increasing the oxygen vacancy concentration and affecting the oxide electrical conductivity. The solute content in the matrix depends on the SPP size as can be concluded from Figure 4-3. Fine SPPs with a high surface energy are in equilibrium with an increased solute content. Furthermore, fine SPPs become dissolved after rather low neutron fluences in BWRs. The often-observed late-accelerated corrosion in BWRs, that starts earlier the finer the SPPs are, might well be initiated by the super-saturation of the transition elements in α-Zr metal. Ex-reactor corrosion tests on irradiated material have shown increased corrosion rates, which depend upon fast fluence and initial SPP size, [Cheng et al, 1994]. However, the observed increased out-of-pile or in-PWR corrosion rate of Zry-4 with a low A–parameter (SPP size) does not require an irradiation-induced dissolution of the SPP. It arises if the SPP size is below a threshold value which depends on a particular exposure time.

[6] The annealing (A) parameter is a measure of the heat input after the last beta-quenching peformed during the manufacturing process. A large value indicate employment of higher annealing temperatures/longer

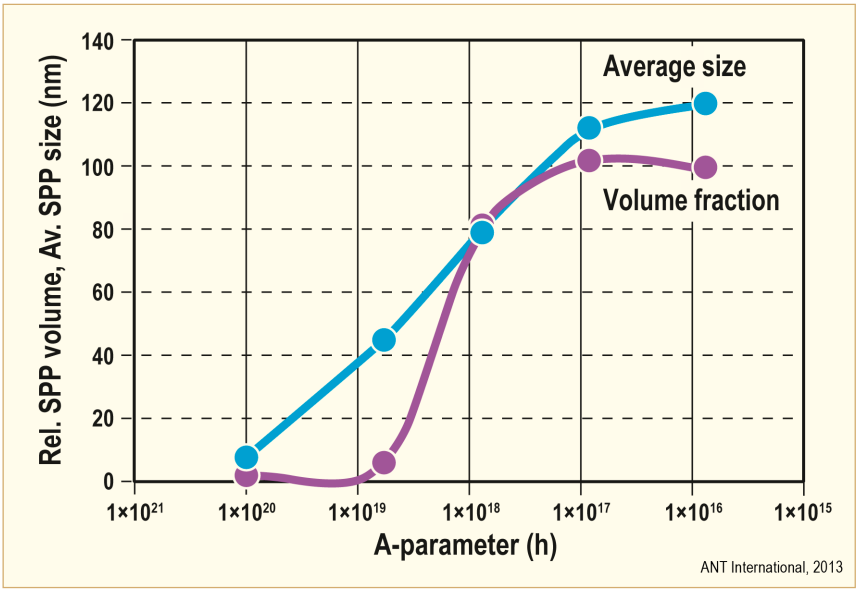

Figure 4-3: Precipitate size and volume, estimated with Synchrotron radiation, in Zry-4 versus Annealing (A)-parameter, after [Motta et al, 2002].

In-BWRs, an increase in hydrogen pick-up is observed before the onset of increased corrosion rate, at least in Zry-2. Increased corrosion rate in Zry-4 lots with a SPP size of >80 nm is seen out of pile only in hydrogenated, oxygen-free 350°C water and 400°C steam. The influence of the SPP size in oxygen-free water is reduced if no hydrogen is added. [Garzarolli et al, 1989a], reported on an out-of-pile corrosion test with a set of Zry-4 materials which showed variations in the corrosion rate of more than a factor of 2, that correlated with the Zry-4 yield strength, in the first thousand days. However, in the same study it was found that when hydrogen was added in the next thousand days the corrosion rate of the Zry-4 materials changed significantly. The corrosion resistance ranking did not correlate to the yield strength anymore but correlated to the SPP size. They also reported on steam test results for two Zry-4 lots with a low A-parameter (3E-19 h) and a high A-parameter (3E-17 h). The low A-parameter material showed a significantly accelerated corrosion rate. After 15 days H_2O_2 was added for a 3 day period. As consequence of this, the corrosion rate of the low A-parameter material reduced almost to normal rate but increased later on under normal ASTM conditions to the same significantly increased corrosion rate after a three 3-days interval. No increased corrosion rate is seen under oxidizing water conditions out-of-pile. The late-increased corrosion rate observed in Zry-2 at high burn-ups starts earlier for smaller initial SPP sizes, which is probably initiated by a different corrosion phenomenon from that that which leads to the increased corrosion of Zry-4 with fine SPP, discussed before. Figure 4-4 shows the existence ranges for accelerated and nodular corrosion in pile and out of pile in hydrogenated water, oxygenated water and high-pressure steam environments for Zry-4. Accelerated corrosion appears only under hydrogenated conditions in Zry-4 with an A-parameter of <3E-18 h at temperatures ≤420°C. Nodular corrosion is observed in-BWR in Zry-4 lots with an A-parameter of >1E-18 h and can be simulated out-of-pile only under oxygen-free conditions in high-pressure steam at 450-550°C.

---

annealing times while smaller annealing parameter indicates usage of lower annealing temperatures/shorter annealing times after the last beta-quenching. Increased annealing (A) parameter will allow the SPPs in the microstructure to grow to larger sizes.

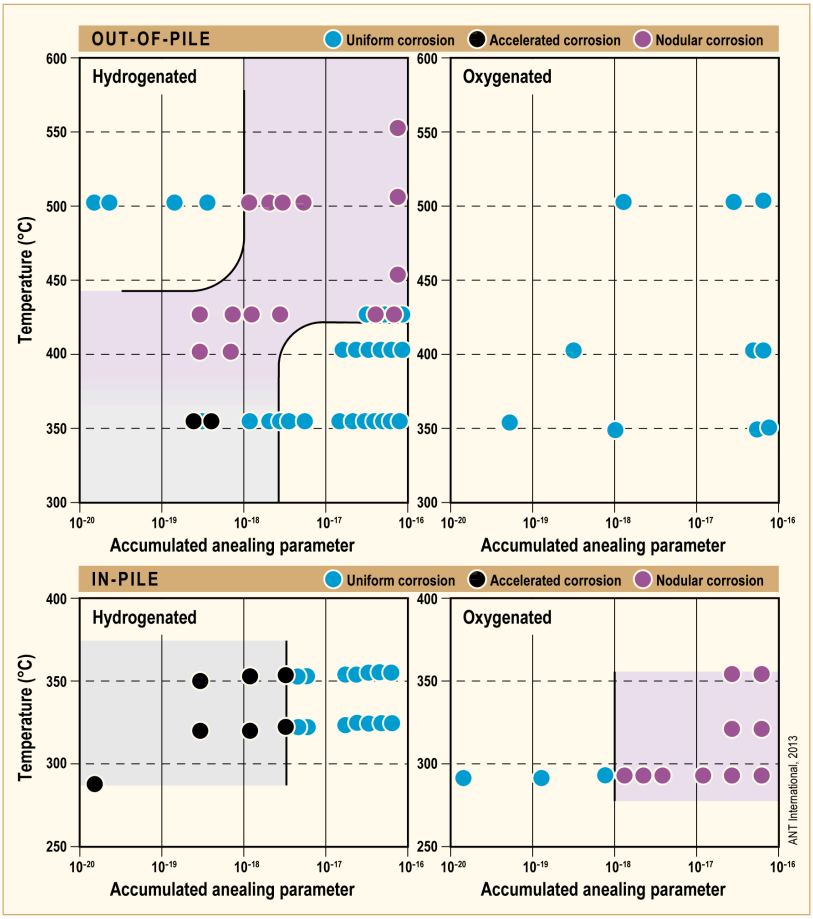

Figure 4-4: Appearance map for nodular and accelerated corrosion for Zry-4 in water and steam; after [Garzarolli et al, 1989a].

Nevertheless, the experience with Zr-Nb-Fe alloys in-PWR raises some questions regarding the possible effects of the Fe solute content on corrosion. In these alloys the Fe-containing SPP have been found to lose their Fe content during irradiation, increasing the supersaturated solute content, but no increase of corrosion has been observed at high fluences. β-quenched as well as pre-irradiated Zr-alloys, having a large fraction of the transition elements (Fe, Cr, Ni etc.) in supersaturated solution, generally show rather high corrosion, probably mostly due to their influence on yield and creep strength.

It was pointed out earlier in this section that the increased corrosion rate with a non-optimized size of SPP does not start from the early beginning, but only after some time after formation of a certain oxide thickness. Also nodular corrosion, which appears in high-pressure steam at ≥500°C and in-BWR on Zircaloy with large SPP, starts after an initiation period, which is in-BWR several 10s to more than 100 days corresponding to a oxide thickness between 2 and 3 µm. Out of pile at 500°C, nodular corrosion starts earlier at an oxide thickness of about 1 µm and can be suppressed by preoxidation in H_2O_2 to oxide thickness values of >4 µm. A H_2O_2 preoxidation to lower oxide thickness values than this still reduces the nodule density significantly.

Corrosion tests in water, steam and in-reactor experience have shown that an addition of >0.3-0.5% Nb to the Zr-alloy blurs the above described SPP size dependency on corrosion.

Improved corrosion resistance of zirconium alloys in water can be either achieved by the addition of >0.3 % Fe+Cr+Ni, which primarily is located in SPPs, or by a Nb content of ≥0.3%. Nb is distributed in the metal uniformly as a solute up to a concentration of 0.3-0.5%. Only at higher concentrations do β-Nb or Zr-Nb-Fe, Cr SPPs arise in such alloys. Obviously, in alloys which have a good corrosion resistance due to sufficient Nb solute content, SPPs do not play an important role, whereas in alloys which have good corrosion resistance, primarily due to Fe, Cr, Ni, and V present in SPPs, an optimum SPP size is needed.

As far as the microstructure is concerned, besides the distribution of SPP and the SPP crystallographic phases, a marked corrosion influence has been observed from final cold deformation and final annealing. These two process steps affect dislocation density, grain size and shape and, as a consequence of these parameters, yield strength and creep strength. Out-of-pile corrosion tests have often shown a decreasing corrosion rate with decreasing yield strength (lower cold deformation and higher final annealing temperatures) for a certain material, e.g. as shown in Figure 4-5. In PWR the effect of these parameters has exactly the contrary effect on corrosion rate. Figure 4-6 reveals that in-PWR corrosion rate is increased with decreasing amount of final cold work and increasing final annealing temperature. It was pointed out earlier in this section that this difference in out-of-pile and in-PWR behaviour probably correlate with the stresses in the oxide. Out-of-pile, these stresses are governed by the yield strength, that decreases with decreasing degree of final cold deformation and increasing degree of recrystallisation. On the other hand, in PWRs these stresses are a result of the irradiation creep strength that increases with decreasing yield strength and increasing degree of recrystallisation, e.g. [Seibold & Garzarolli, 2002].

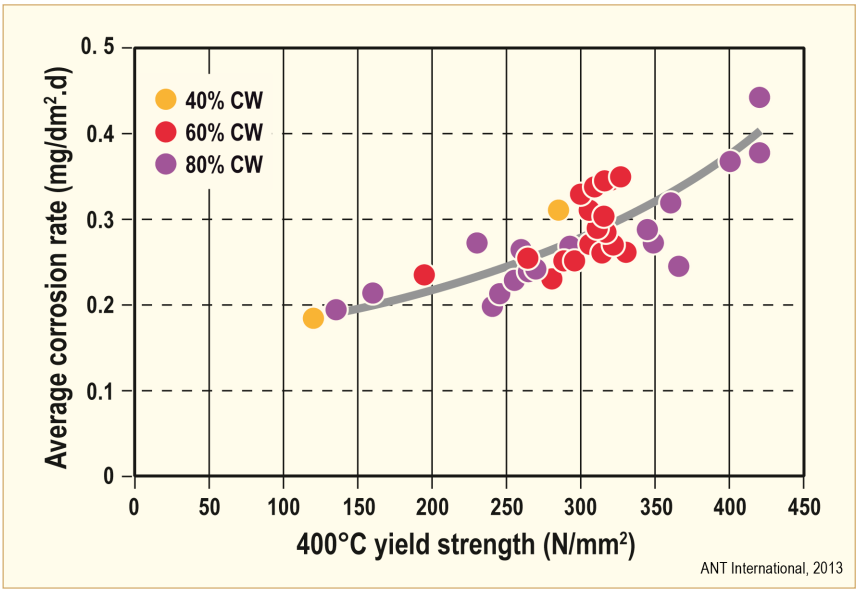

Figure 4-5: Effect of yield strength and final cold deformation on post-transition corrosion in 350°C water, e.g. after [Garzarolli et al, 1985].

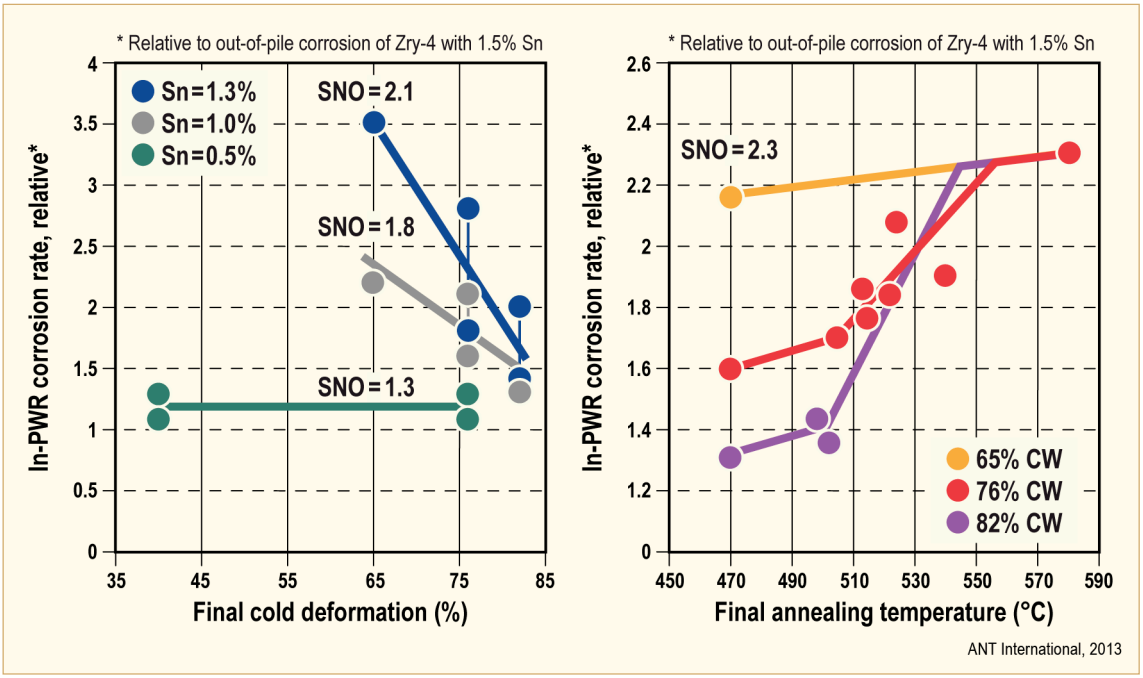

Figure 4-6: Effect of Cold Work and Final Annealing on In-PWR Corrosion, after [Seibold & Garzarolli, 2002].

4.1.2 Effect on HPUF

4.1.2.1 No irradiation

The effects of alloying elements in Zr on HPUF in steam and degassed water (the dissolved oxygen and hydrogen in water has been removed by a degassing procedure) out-of-reactor are as follows (Figure 4-7 to Figure 4-9):

- Sn - being in solid solution within the Zr metal matrix - was found in the early tests to have little effect on the HPUF,
- Nickel-bearing SPPs – increased HPUF,
- V, Cr-contained in SPPs-, and Nb– to a large extent (0.5%) in solid solution - reduce the HPUF:
  - The beneficial effect of Nb is explained by the observed surface segregation of Nb^{5+}, which should enhance the cathodic water reduction ($H^+ + e^- \rightarrow H^0$), [Bossis et al, 2002] and [Ramasubramanian et al, 2002].

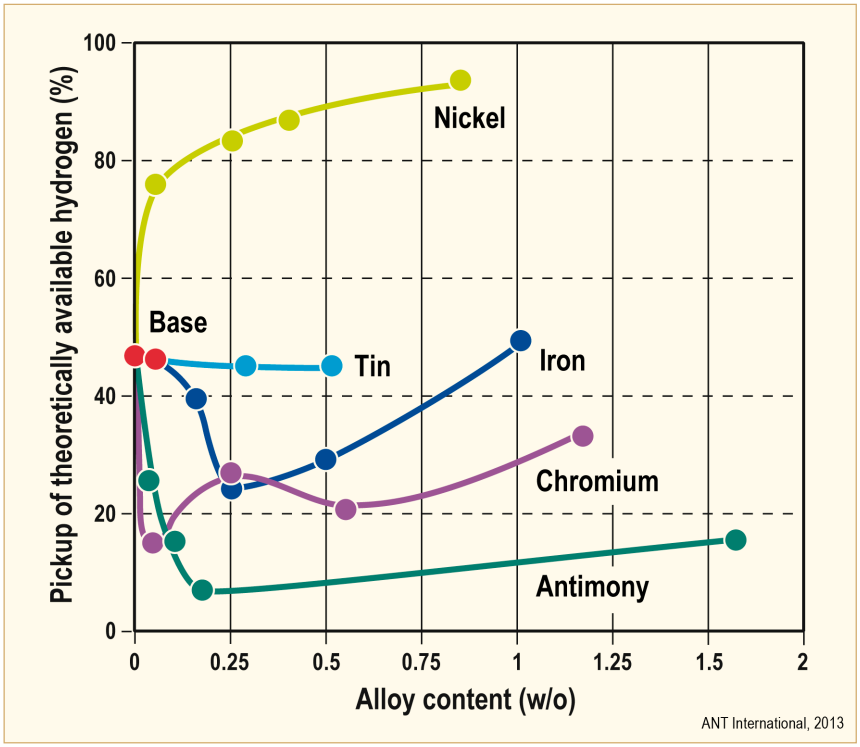

Figure 4-7: HPU in different Zr alloys exposed in 650°F (343°C) degassed water under static conditions for 575 days, after [Berry et al, 1961].

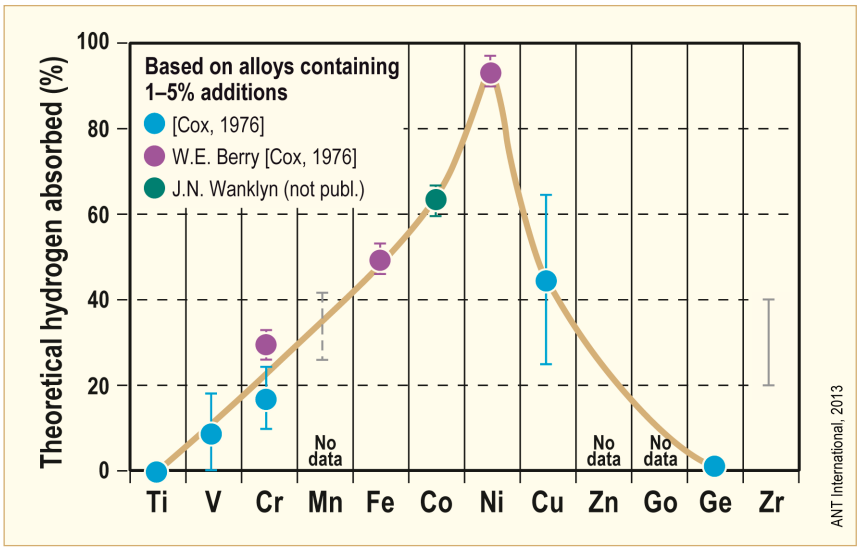

Figure 4-8: Effect of some alloying elements forming intermetallic precipitates on hydrogen uptake percentage, after [Cox, 1976].

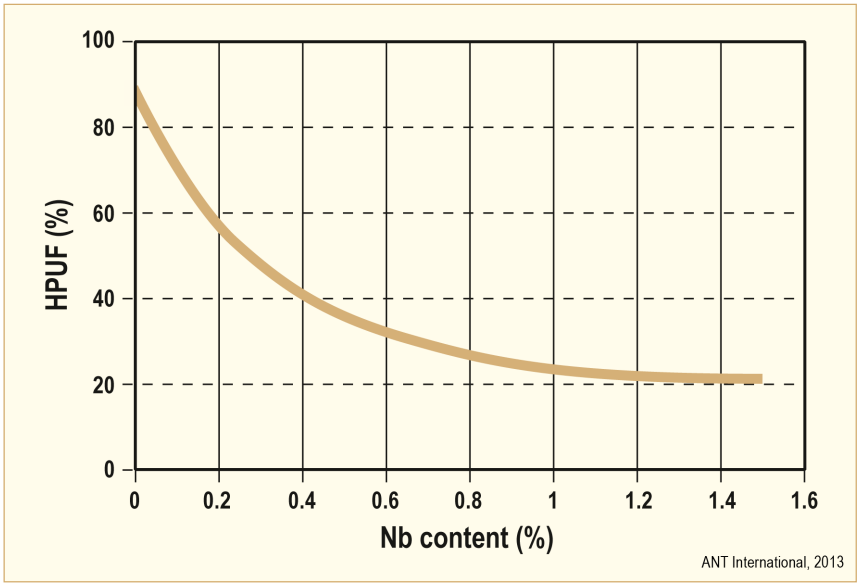

Figure 4-9: Effect of Niobium on the HPUF of binary Zr-Nb alloys degassed water under static conditions at 350°C after 750 days, after [Kiselev et al, 1962].

Comparing HPUF of different alloys in degassed water and steam, Zry-2 shows generally the largest HPUF (due to its Ni-content) while Zr alloys containing Nb exhibit generally low HPUF values (Table 4-5). The lowest values were reported for binary Zr-Nb alloys (Zr1Nb and Zr2.5Nb). The HPUF in steam is generally higher than in degassed water except for Zry-2, which shows quite similar HPUF values in both environments.

Table 4-5: HPUF observed in degassed water and steam - out-of-reactor - for different Zr-alloys.

Material	HPUF (%) in ≤360°C water	HPUF (%) in ≥400°C steam	References
Zry-2	17-47	17-47	[Kass, 1962]
	23-35	23-32	[Richter & Tverberg, 1962]
	39-66	55-63	[Tyzack et al, 1977]
	59-83	55-73	[Harada et al, 1991]
	69-91	113-160	[Hoffmann & Sell, 2011]
Zry-4	10-26	22-34	[Kass, 1962]
	18	66	[Sabol et al, 1989]
	24-31	26-51	[Harada et al, 1991]
	26-30		[Garde et al, 1994]
	9-34	45-57	[Hoffmann & Sell, 2011]
Low-Sn-Zry-4	26	16	[Garde et al, 1994] & [Garde et al, 2002]
DXELS		45	[Garde et al, 2002]
	9-39	25-54	[Hoffmann & Sell, 2011]
ZrSnFeV	18-47	28-50	[Hoffmann & Sell, 2011]
ZIRLO	7	25	[Sabol et al, 1989]
Zr3Nb1Sn	8-12	11-19	[Richter & Tverberg, 1962]
ZrSnNbFeCrV	11-45	19-34	[Hoffmann & Sell, 2011]
Zr1Nb	22		[Kiselev et al, 1962]
	5-6	16-22	[Tyzack et al, 1977]
			[Hoffmann & Sell, 2011]
Zr2.5Nb	5-6	18-33	[Tyzack et al, 1977]
	4	16	[Sabol et al,1989]
	1-5		[Elmoselhi et al, 1994]
			ANT International, 2011

Analysis of the results shows that:

- Increased ingot Fe/Ni alloying ratio (which also correlates with the chemical composition of the SPPs) decreases HPUF in water (with our without LiOH) and steam (Figure 4-10). *A possible explanation for the effect could be that, provided that the $Zr_2(FeNi)$ SPP are large enough to bridge the very thin barrier layer, a decrease in Fe/Ni ratio increases the possibility to keep the Ni in metallic phase in the oxide grain boundaries and act as a freeway for hydrogen ingress into the material*, see Section 4.1

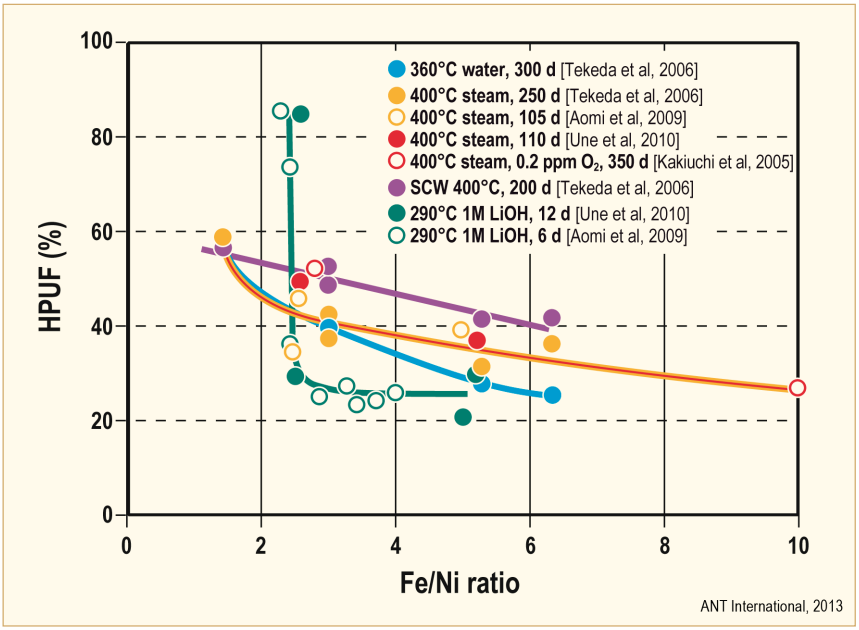

Figure 4-10: Effect of the Fe to Ni alloy ratio and the type of corrosion tests on the HPUF, Supercritical Water (SCW), after [Adamson et al, 2011], [Takeda et al, 2006] and [Aomi et al, 2009].

As far as the out reactor HPUF is considered the following conclusions can be drawn:

- The HPUF increases with increasing H content of O-free water and decreases to rather low values above a certain O content in the water.
- Boric acid additions with or without LiOH decrease the HPUF significantly.
- HPUF of Ni containing alloys in O-free environments is much larger than that of similar alloys free of Ni.
- For Zr-Sn-FeCrNi alloys (similar as Zry-2) the HPUF decreases with increasing Fe/Ni ratio of the alloy.
- Binary Zr-Nb alloys have the lowest HPUF in O-free water and steam. The HPUF decreases with increasing Nb in the alloying range of 0-0.8 % and remains rather constant at higher Nb contents.
- The HPUF of ZrSnFeCr alloys increases with decreasing corrosion rate e.g. [Rudling & Vesterlund, 1993], (Figure 4-11). Similar results were later presented by [Charquet et al, 1994] Figure 4-12 and [Broy et al, 2000].*Thus, if an alloy is modified so its corrosion rate is decreased, the HPUF will increase. In many cases it may be difficult to separate the effect of corrosion rate and alloying addition on HPUF since also the alloying addition may impact the corrosion rate.*

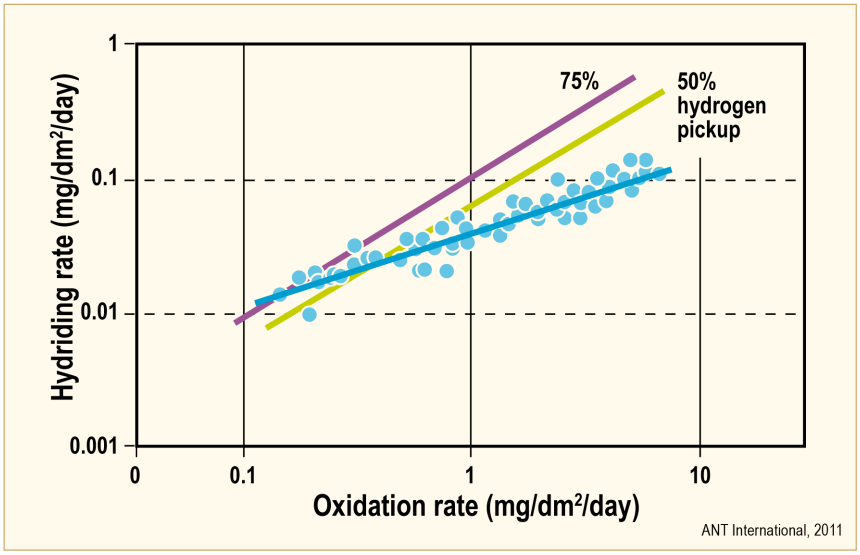

Figure 4-11: HPU vs. oxidation rate for Zry-4 materials with varying Sn and Fe content and A-parameter in 400°C/105 bar steam tests, after [Rudling & Vesterlund, 1993].

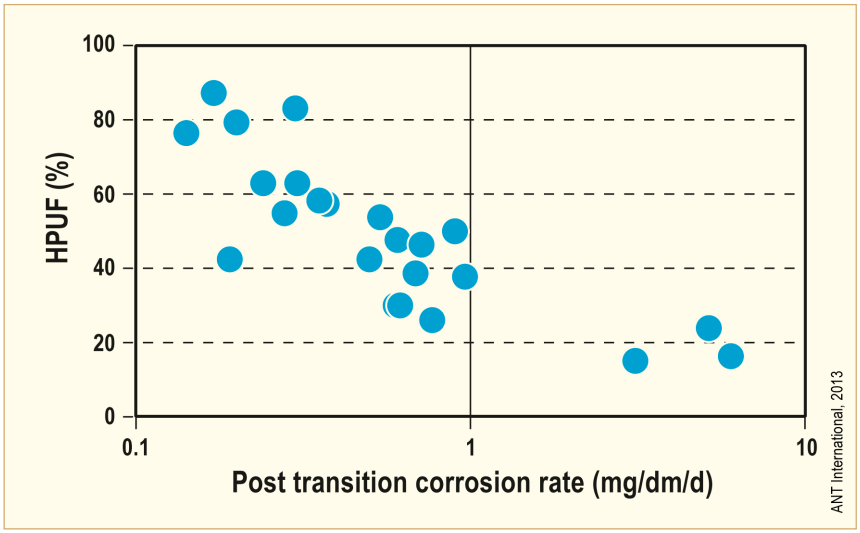

Figure 4-12: HPUF versus post-transition corrosion rate of Zry-4 type alloys with different condition, after [Charquet et al, 1994].

4.1.2.2 Irradiation

Large variations of the HPUF between different alloys and different material conditions have also been found in tests carried out in the G7 loop in ETR in a O_2-free water with about 30 cm²/kg H_2 and NH_4OH addition with a RT pH of 10, [Johnson, 1968]. The results can be summarized as follows:

- The lowest HPUF values (3-5%) were seen for Zr2.5Nb,

- The highest values were seen for Zr1.2Cu0.28Fe (67-146%). *The very high HPUF of Zr1.2Cu0.28Fe out of flux and in flux is an indication that the Cu and Fe have formed large Zr-Cu-Fe SPPs that could bridge the barrier layer. Cu is rather noble and stays metallic at the barrier layer outer surface in the tested environment. Large SPPs could therefore act as windows for H and allow even uptake of hydrogen from the water.*

- Zry-2 showed a higher HPUF (19-43%) than that of Zry-4 and Zr1.2Cr0.08Fe (7-18%) and Zr3Sn1Nb showed values of (21-25%).

Another series of in reactor loop tests was reported by [Amaev et al, 1971]. The tests were performed in the BW loop of the MR reactor in oxygenated water at 280°C and lasted 146 days. The following results were obtained:

- The hydrogen absorption was:
  - Very low for Zr1Nb (5%),
  - moderate for Zr2.5Nb (30%), Zr2.5Nb0.5Cu (12-24%), and Zr1Sn1Nb0.5Fe (28%),
  - significantly higher HPUF were found for Zr0.7Fe0.7Ni with very likely large SPP (high annealing temperatures) (39%). *Probably the Zr-Fe-Ni SPP bridged the barrier layer and contributed to the HPU.*

4.2 Massive hydrides

4.2.1 Introduction

Once hydrogen contents exceed the solubility limit (80-150 ppm, depending on temperature) hydrides precipitate more or less uniformly throughout the fuel rod cladding wall. At still higher concentrations, however, at more than 300 ppm under high heat fluxes, hydrides tend to concentrate at the colder outer rim of the cladding and may even form a more or less dense ZrH_2 layer. This concentration at the OD is due to the diffusion of hydrogen down the temperature gradient.

It was first suggested by [Shewmon, 1958] that under a steep thermal gradient like that from the inside to outside of a fuel cladding tube hydrogen will be redistributed rapidly to the colder outer surface. The hydrogen equilibrium pressure and the heat of solution, that depends on the H-content and temperature, cause hydrogen to diffuse down a temperature gradient. The heat flux through the FR cladding creates a radial temperature difference across the cladding wall with the lower temperature at the Outer Diameter (OD) in contact with the coolant. The relationship of the hydrogen Terminal Solid Solubility (TSS) and the hydrogen distribution in the material is shown in Figure 4-13. The TSS will be reached first at the colder outer surface and thus all the hydrogen absorbed above the TSS will precipitate at this surface, at least at high temperature gradients (heat flux).

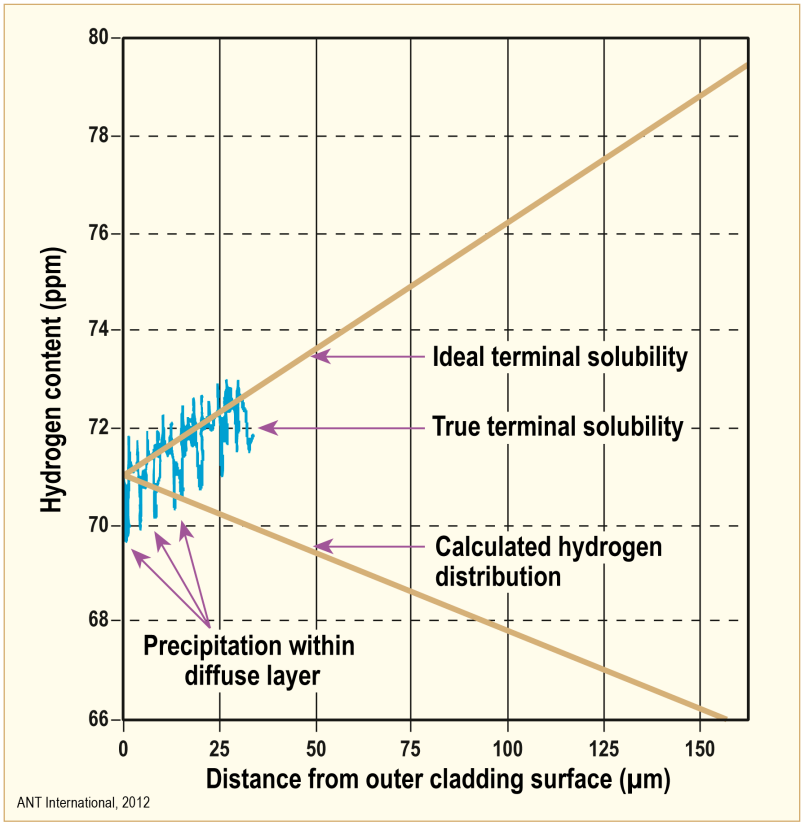

Figure 4-13: The effect of the temperature dependent TSS on hydrogen distribution in cladding wall, after [Asher & Trowse, 1970].

The hydrogen absorbed by the zirconium alloys during the corrosion reaction is redistributed by the temperature gradients in materials with a surface heat flux (i.e. fuel rods). A significant portion of the hydrogen diffuses from the cladding bulk to the cooler cladding OD and forms a rim of hydride on the OD that can approach a near 100% solid hydride structure.

For structural components (which are not subjected to a heat flux), hydrogen can still concentrate at the metal/oxide interface if the hydrogen ingress rate (due to e.g. high corrosion rate) is larger than the hydrogen diffusion rate away from the metal/oxide interface location.

Several studies have shown that oxide layer thickness is increased at regions of high hydride concentration, indicating that Zr-hydrides corrode faster than zirconium-alloy metal, see subsequent subsections.

Figure 4-14 shows that tendency for hydride rim formation depends on heat flux and hydrogen content (which increases with burnup).

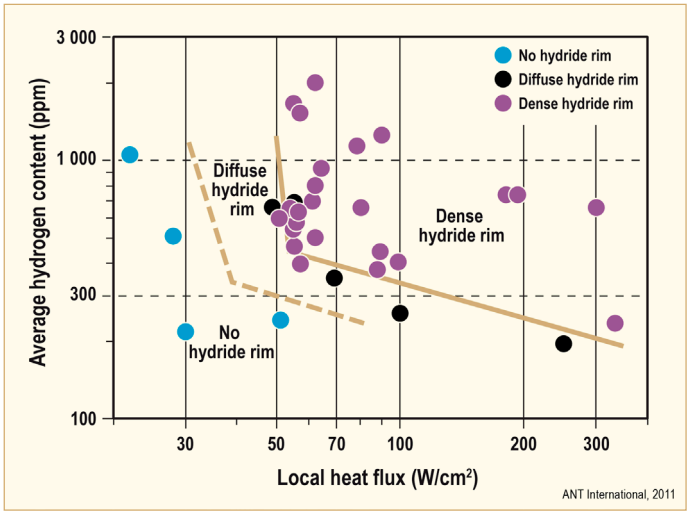

Figure 4-14: Critical conditions for the formation of a hydride rim from H-redistribution tests, after [Garzarolli et al, 2001b].

4.2.2 Out-of-reactor

A possible acceleration of corrosion when hydrides precipitate at the metal oxide interface was proposed already in the early sixties, e.g. [Cox & Johnston, 1962]. In the early nineties [Garde, 1991] proposed that the observed acceleration of in-PWR fuel cladding corrosion at high BUs (>50 MWd/kgU) might be due to a high hydride density at the metal oxide interface. [Garde, 1991] also speculated that the corrosion rate transition usually observed in out of pile tests might be associated with the onset of hydride precipitation at the metal-oxide interface.

[Kido, 1993] reported on corrosion tests in 360°C water with Zry-4 samples, pre-charged in a hydrogen/argon gas mixtures to an average content of 100 to 3300 ppm H. The tests showed a definite acceleration of the post transition corrosion rate for samples with an average hydrogen content exceeding 1000 ppm (Figure 4-15). However, no effect of hydrogen is seen for the pre-transition corrosion rate. No information was given on the distribution of hydrogen/hydrides in the samples but increased hydrogen concentration at the surface was likely, especially for the samples with a high average H-content. The charging method used in these tests tends to form hydride rims.

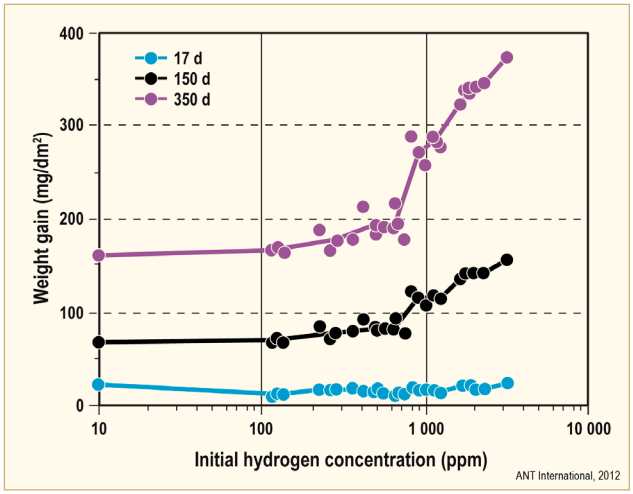

Figure 4-15: Weight gain at 17, 150, and 350 days at 360°C as a function of initial average hydrogen concentration, after [Kido, 1993].

The detrimental role of hydrogen/hydrides was later confirmed by [Blat & Noel, 1995] and [Blat et al, 1998]. Tests with high Sn (1.5%) Cold Work (CW) and SR Zry-4 cladding samples were made after pre-hydriding by both cathodic and gaseous charging. Their experiments showed a large corrosion rate increase only for cathodic charged samples, which exhibited an almost massive hydride rim at the surface.

Later, it was confirmed, that a significant increase in post-transition corrosion rate only occurs if the hydrogen concentration at the surface is very large (Figure 4-16), ≥8000 ppm [Garzarolli et al, 2001b]. A hydrogen concentration of 8000 ppm correlates to a 50% dense hydride rim. The samples used for the long term (900 days) corrosion tests in water at 350°C had different surface hydrogen contents used in simulated start-up tests in PWRs, as described by [Pettersson et al, 2007].

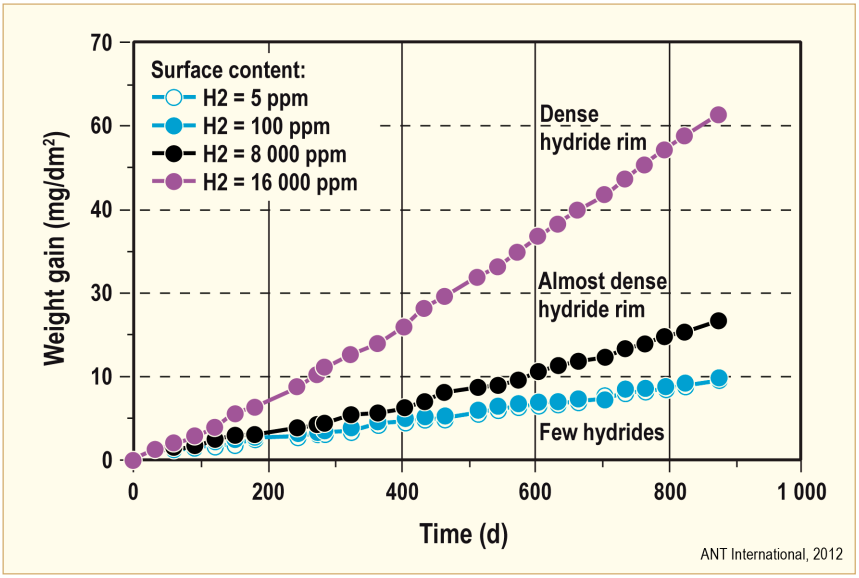

Figure 4-16: Out of pile corrosion of Zry-4 cladding samples with hydride rims in 350°C water, after [Garzarolli et al, 2001b].

4.2.3 BWRs

4.2.3.1 BWR fuel rods

This section will show that at a certain fluence level, there is a dramatic increase in HPUF in Zry-2 (but not in Zry-4) that is correlated with an increase in Zry-2 corrosion rate later on. It is speculated that the increase in HPU/HPUF is due to dissolution of the Ni-bearing SPPs in Zry-2 which may increase the hydrogen transport rate through the oxide barrier layer. Once a solid hydride rim is formed at the oxide/metal interface the corrosion rate increases. Zry-4 which does not contain the Ni-bearing SPPs does not show any increase in HPUF at higher fluence levels.

Figure 4-17 shows how the HPU increases with burnup for various Zry-2 BWR fuel rod designs.

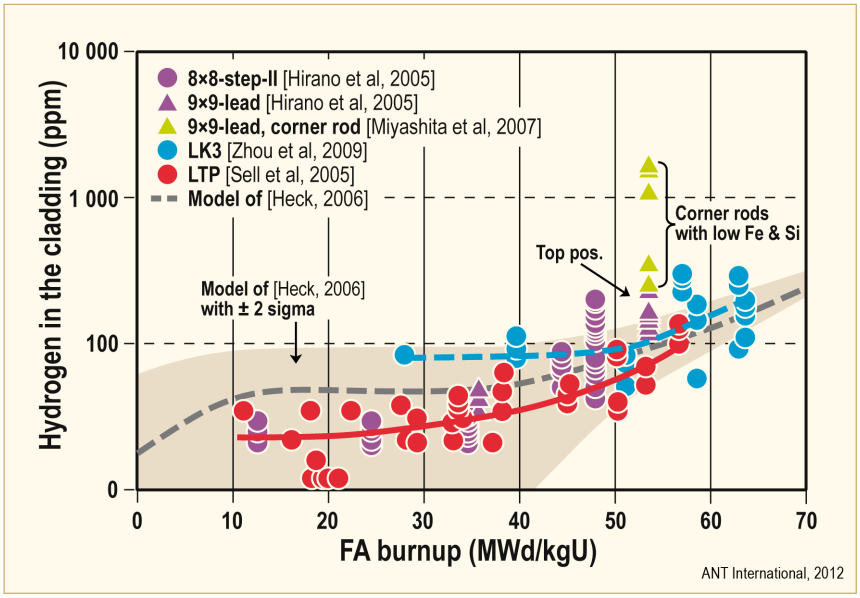

Figure 4-17: Hydrogen pickup of Zry-2 fuel rod claddings in BWR at high burnups, after [Hayashi et al, 2003], [Ledergerber et al, 2005], [Hirano et al, 2005], [Miyashita et al, 2007], [Zhou et al, 2009], [Sell et al, 2005], and [Heck, 2006].

High burnup BWR 9×9 lead use fuel assemblies (LUAs), designed for the maximum assembly burnup of 55 MWd/kgU, were irradiated in Fukushima Dai-ni Nuclear Power Station in 1996. Two different types of designs were tested, Type-A and -B. The chemical compositions of the Zry-2 cladding materials used in this program are shown in Table 4-6.

Table 4-6: Chemical composition of cladding materials, after [Miyashita et al, 2007].

	Sn (wt%)	Fe (wt%)	Cr (wt%)	Ni (wt%)	Si (ppm)
Type – a1	1.32	0.18	0.10	0.07	95
Type – a2	1.33	0.17	0.11	0.07	42
Type – b1	1.31	0.18	0.10	0.07	95
Type – b2	1.32	0.16	0.10	0.06	45
ANT International, 2013					

Some of the LUAs, each from Type-A and Type-B, were taken out of the reactor after 3 cycle (1171 days) and 5 cycle (1957 days) irradiations for the PIEs. The examined Type-A LUAs achieved 35.0 MWd/kgU and 53.0 MWd/kgU, the Type-B ones 35.6 MWd/kgU and 53.5 MWd/kgU.

The oxide thickness profile of one of the corner rods (in the corner of the fuel assembly) with type-b2 is shown in Figure 4-18. The peaks represented by the red curve are shadow corrosion at the spacer locations.

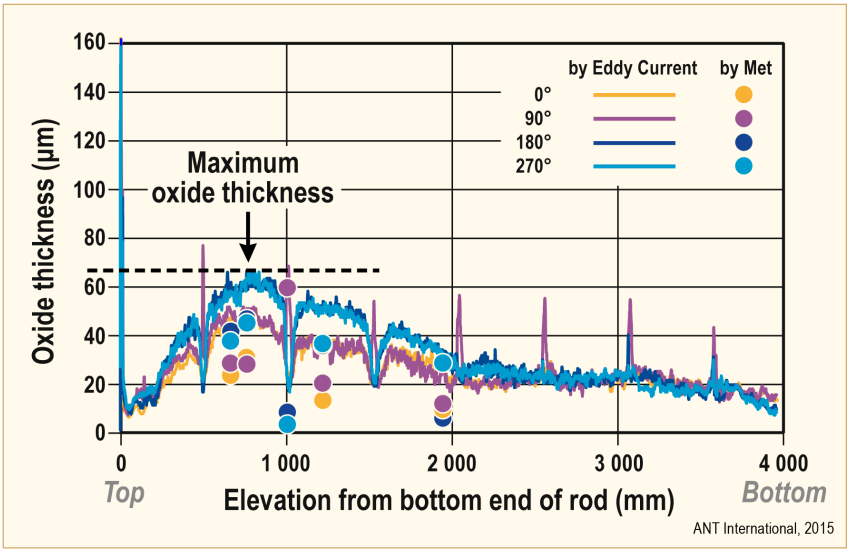

Figure 4-18: EC oxide thickness profile of a type-b2 corner rod after 5 cycles, 53.5 MWd/kgU. The four curves are eddy current lift-off traces from the bottom to the top of the fuel rod along 4 different generatrices (separated 90 degrees). The data points are oxide thickness data measured by metallography [Miyashita et al, 2007].

Metallographic examinations showed a massive hydride rim at the "Maximum oxide thickness position". The axial distribution of hydrogen in fuel rods at the assembly corners and non-corners are shown in Figure 4-19.

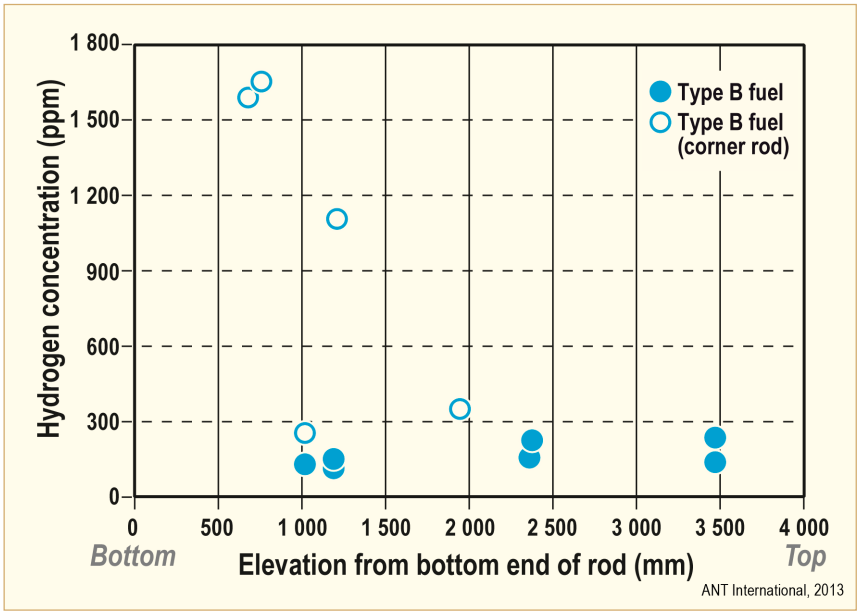

Figure 4-19: Hydrogen concentration in type-b2 fuel rod claddings after 5 irradiation cycles, 53.5 MWd/kgU, after [Miyashita et al, 2007].

In Figure 4-20 the HPUF is shown for all examined high burnup fuel rods versus the oxide layer thickness. The figure shows a strong increase with increasing oxide thickness. At an oxide thickness of > 25 µm HPUF values are > 100%, *indicating that not only corrosion hydrogen is taken up by the fuel clad material but that also other processes, such as a catalytic hydrogen uptake may contribute*. However, no examinations were done to assess the SPP size distribution. *From the data here it is impossible to say whether the increased corrosion rate (manifested by increased oxide thickness) is due to increased HPUF or results in increased HPUF.*

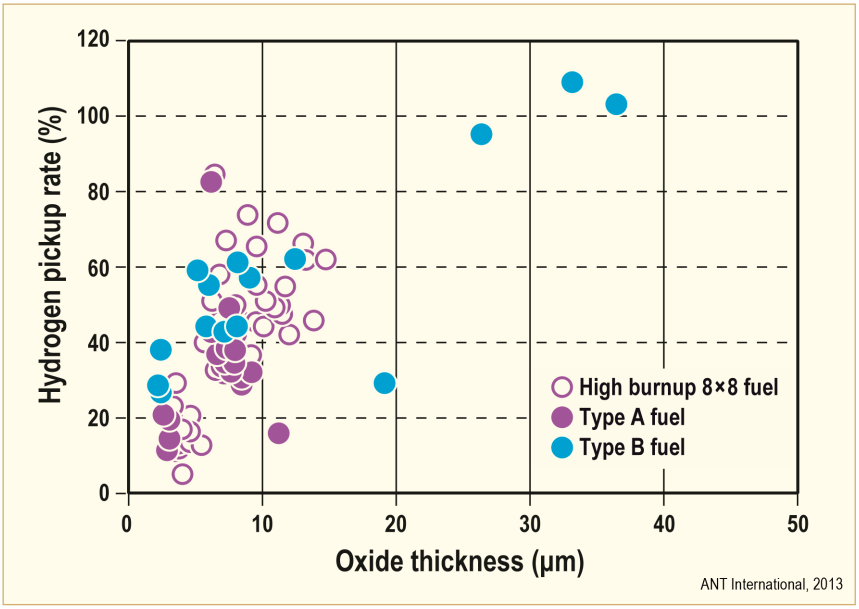

Figure 4-20: HPUF of all examined high burnup fuel rods, after [Miyashita et al, 2007].

In the late 1990s [Sihver & Hallstadius, 1999], [Limbäck et al, 2001] and [Tägtström et al, 1999] reported that uniform oxide formation and Hydrogen Pickup, HPU of LK2 and LK2+ fuel cladding of ABB (today Westinghouse) accelerated at higher burnups while the LK3 material was much less affected (Figure 4-21). The reason for the different behaviour of three different materials was proposed to be the initial SPP size, which is very small for LK2 (low A-parameter) and largest for LK3. The authors argued that a minimum SPP size is necessary to form a protective barrier layer and if the SPPs are too small e.g. due to fast dissolution of initially small SPPs, the barrier layer protectiveness will deteriorate resulting in increased corrosion rate. In addition the Fe content of LK2 was rather low (about 0.11%) and has been increased for LK2+ and LK3 to about 0.18%. This Fe content increase may also play a role in delaying the accelerated corrosion and HPUF since increased Fe content increases SPP size with constant manufacturing process. *The data shows that increased HPUF occurs at lower burnups than the corrosion rate acceleration, which suggest that increased HPUF results in increased corrosion rate – instead of vice versa.*

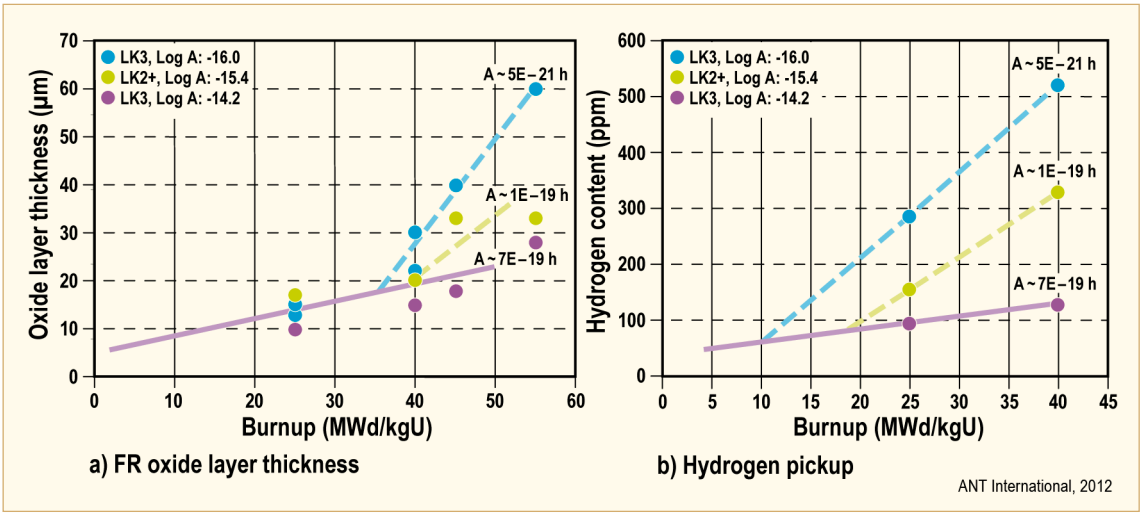

Figure 4-21: Late Increased Corrosion of LK Zry-2 claddings in Forsmark-3, after [Sihver & Hallstadius, 1999], [Limbäck et al, 2001] and [Tägtström et al, 1999].

4.2.3.2 BWR structural components

A summary of *HPU in Zry-2 FA structural components* indicated hydrogen levels up to 2000 ppm at burnups equivalent to 85 GWD/MT (Figure 4-22), [Cheng et al, 2009]. The components include components without surface heat flux such as spacers, water rods and unfuelled coupons, Figure 4-22. Fuel channel materials show a similar trend, Figure 4-23.

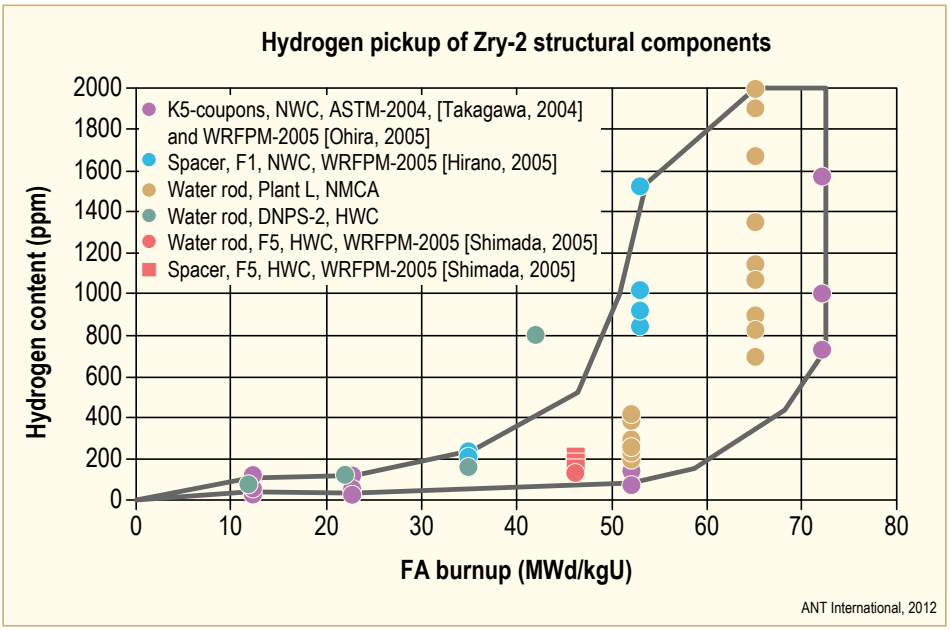

Figure 4-22: Trend of accelerated hydriding of Zry-2 water rods, spacers, and irradiated coupons with increasing FA burnup or fluence, after [Cheng et al, 2009].

The material hydrogen content is a product of corrosion rate and HPUF. The reason for the dramatic increase in HPU in Figure 4-22 is due to the large increase in HPUF at a burnup of about 35 MWd/kgU for Zry-2 only (Figure 4-23). It is believed that the increase in corrosion rate of Zry-2 at a burnup of 50 MWd/kgU (Figure 4-24), may be a function of the increased HPU in the Zry-2 material – it is well-known that hydrides may accelerate Zr alloy corrosion rate. Zry-4 materials usually show some nodular corrosion under isothermal conditions and this is the reason for the higher corrosion rate of Zry-4compared to that of Zry-2 in Figure 4-24.

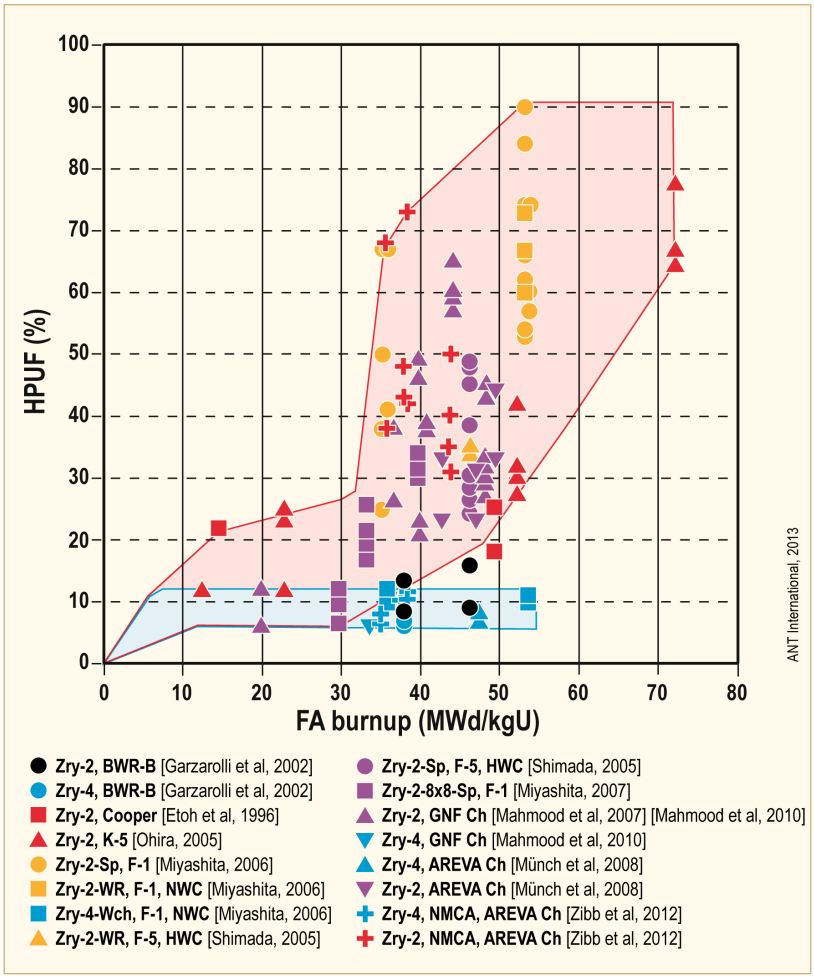

Figure 4-23: Hydrogen pickup fraction (HPUF) of Zry-2 and -4 structural components in BWR, after [Rudling et al, 2012].

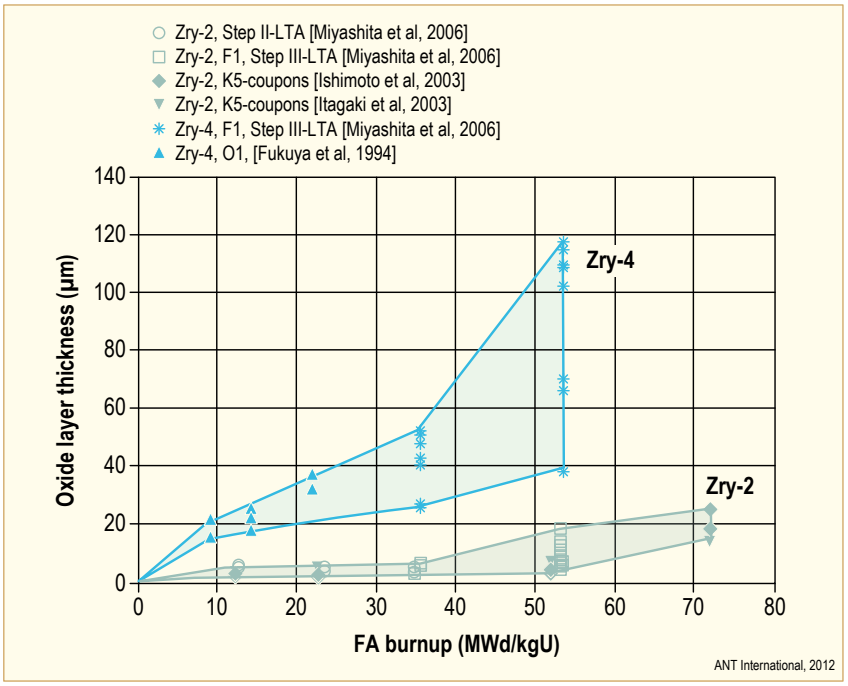

Figure 4-24: Oxide growth behaviour of Zry-2 and Zry-4 under isothermal conditions according different Japanese studies. The higher oxidation rate for Zry-4 is due to nodular corrosion compared to Zry-2 with uniform corrosion, after [Miyashita et al, 2006], [Ishimoto et al, 2003], [Itagaki et al, 2003] and [Fukuya et al, 1994].

The reason for the dramatic increase in HPUF for the Zry-2 materials is the result of the irradiation induced dissolution of the nickel-bearing second phase particles (SPPs) which does not exist in Zry-4. In 1995 [Huang et al, 1996] reported that after irradiation of Zry-2 coupons with fine SPP in a commercial BWR HPUF as well as the corrosion rate increased at high BUs due to the irradiation induced SPP dissolution. The authors showed that when SPPs virtually "disappeared", within the resolution of Scanning Transmission Electron Microscopy (STEM) at that time, HPU and corrosion increased. Figure 4-25, Table 4-7 and Table 4-8 illustrate that trend, especially for specimen 1R, whose SPPs disappeared between fluences of 2.5 and 8.5 x 10^{25} n/m^2 (E>1 MeV).

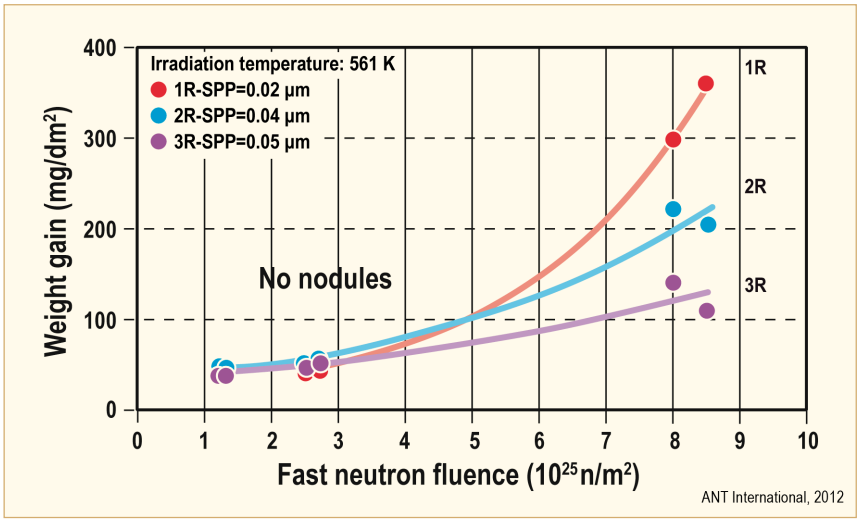

Figure 4-25: Corrosion as a function of fluence for Zry-2 for non-heat transfer surface specimens having different SPP sizes. An oxide weight gain of 15 mg/dm^2 corresponds to 1 micron of oxide, after [Huang et al, 1996].

Table 4-7: Acceleration of corrosion and HPU after irradiation of Zry-2 with fine SPP sizes to high fluences, after [Huang et al, 1996].

Specimen	A-parameter (h)	Fluence (n/cm²)	Med. SPP size (nm)	Weight gain (mg/dm²)	HPUF (%)
3R	1.45E-19	0	25		
2R	7.40E-20	0	32		
1R	3.46E-21	0	42		
3R	1.45E-19	2.5E21		40	2
2R	7.40E-20	2.5E21		53	3
1R	3.46E-21	2.5E21		45	2
3R	1.45E-19	8.5E21		112	26
2R	7.40E-20	8.5E21		204	35
1R	3.46E-21	8.5E21		294	25

ANT International, 2012

Table 4-8: STEM characterisation on SPPs of archive and irradiated non-heat transfer surfaces Zry-2, after [Huang et al, 1996].

Fluence 10^{25} n/m²	Sample	Median of size distribution, (µm)	$\overline{X}_{Fe}$	Y_{Fe}	Number density of precipitates, 10^7/cm²
0	1R	0.025	0.45 ± 0.02	0.53 ± 0.03	3.6
	2R	0.032	0.46 ± 0.04	0.55 ± 0.04	2.1
	3R	0.042	0.44 ± 0.03	0.52 ± 0.03	1.6
2.5	1R	0.016	0.32 ± 0.04	0.48 ± 0.05	1.9
	2R	0.063	0.33 ± 0.04	0.49 ± 0.04	1.3
	3R	0.082	0.32 ± 0.03	0.48 ± 0.04	1.3
8.5	1R	~0	…	…	~0
	2R	0.038	0.17 ± 0.06	N/A	0.1
	3R	0.112	0.17 ± 0.05	0.40 ± 0.08	0.5

$$Y_{Fe} = \frac{Fe}{Fe + Ni}$$

$$\overline{X}_{Fe} \frac{(X_{Fe,initial})(V_{crystalline}) + (X_{Fe,min})(V_{amorphous})}{V_{crystalline} + V_{amorphous}}$$

ANT International, 2011

4.2.3.3 Proposed mechanism for accelerated HPU in Zry-2 in BWRs,

According to Section 3.6, there is no reliable evidence for H atom diffusion through the ZrO_2 lattice [Elmoselhi et al, 1994] and [Ramasubramanian, 1996]. Since the barrier layer of the oxide films is usually imperfect and probably contains a few flaws that penetrate right through to the oxide/metal interface, these oxide flaws are the probable route for H uptake [Cox & Wong, 1999]. However, there are cases when is believed that SPPs – through alloying and high annealing temperatures/long annealing times resulting in large SPPs – may bridge the barrier layer and form an additional rapid path of hydrogen ingress into the Zr alloy material provided that the SPPs are noble enough and the environment is reducing enough to keep the SPPs in metallic form. In one reported case accelerated HPU was noted in PWR guide tubes that contained stainless steel particles embedded in the Zry-4 guide tube material bridging the oxide barrier layer resulting in excessive HPU, see LCC9 STR Effects of Coolant Chemistry on Fuel Performance, published by ANT International for more details.

In the following a mechanism by [Garzarolli et al, 2010] is proposed why there is an increase in HPUF at a high fluence level in Zry-2.

Acceleration of the HPUF in BWRs at high burnups is seen only for Zry-2 and not for Zry-4. This indicates that Ni may play an important role for the HPUF acceleration (since Ni is contained in Zry-2 but not in Zry-4). In out of pile tests, high HPUF was only reported for oxygen free hydrogenated environments and again only for Zry-2, as can be seen from Figure 4-26. An acceleration of HPUF of Zry-2 is reported in-pile at high burnups in hydrogenated environments without boric acid additions and rather low temperatures when oxide thickness exceeds 10-15 µm, e.g. [Urbanic et al, 1987], and when the SPPs are largely dissolved by neutron irradiation. No acceleration of HPU is observed for Zry-2 in PWRs, which operate with Boric acid (Boric acid, has contrary to LiOH, too large molecules to enter into the porous Zr oxide layer).

Furthermore, PWR cladding temperatures are so high that a significant SPP dissolution may not occur.

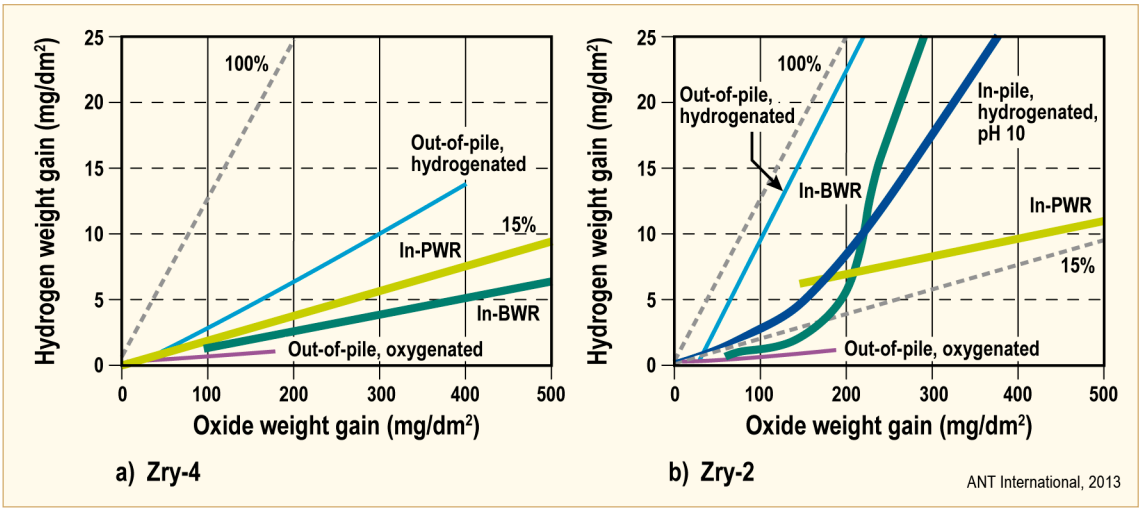

Figure 4-26: Time Averaged HPUF of Zry-2 and Zry-4 in Different Environments, after [Hillner,1964], [Urbanic et al, 1987] and [Limbäck et al, 1994].

Figure 4-27 shows how HPUF of Zircaloy varies with the corrosion conditions and the REDOX potential. From this figure the following key conclusions can be obtained:

- In out-of-pile oxygen free hydrogenated water (REDOX potential about -800 mV), Zry-2 HPUF is increased at medium oxide thickness values (after rate transition, >2 µm). In this environment the Ni-bearing SPP should not be oxidized (the REDOX is below the oxidation potential of Ni, see arrow in Figure 4-27) and may bridge the barrier layer and form a path for the corrosion hydrogen to enter the Zr-2 material.

- If oxygen is contained in the water, even in very small quantities, the REDOX potential increases, the Ni-bearing SPPs becomes oxidised and HPUF of Zry-2 coupons decreases significantly and becomes similar to that of Zry-4.

- Ni could only remain metallic on the surface of the barrier layer in BWR conditions if the REDOX potential in the outer porous oxide would be significantly reduced, e.g. by corrosion hydrogen, radiolysis, and other processes. This reduction of corrosion potential could only occur if the bulk coolant (with high REDOX potential) cannot mix with the local environment at the barrier layer oxide/water interface (with low REDOX potential). Such a situation can occur if the outer porous part of the oxide layer is thick enough, which may happen at high burnups.

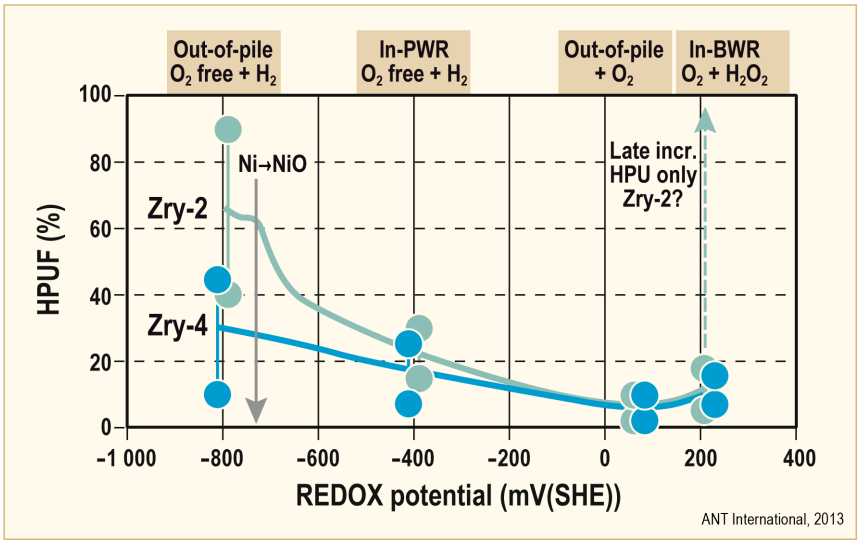

Figure 4-27: Hydrogen pick up fraction (in %), and effect of SPP size on increased corrosion phenomena in different high temperature water environments as a function of varying REDOX potential, after [Garzarolli et al, 2010].

The location, where alloying elements oxidize in the Zr oxide layer is determined by the oxygen partial pressure within the oxide. Oxidation is expected when the equilibrium oxygen pressure for the metal/oxide reaction of the alloying element is exceeded (Figure 4-28). Cr should remain metallic only in the innermost part of the oxide barrier layer. Fe, Sn, and Ni should remain metallic over a major part of the barrier layer. Ni under oxygen-free hydrogenated conditions may remain metallic even at the outer surface of the barrier layer. The oxygen potential at the outer surface is lowest under oxygen free out-reactor conditions, low in-PWR and highest under oxygenated water conditions in-BWR. Thus the fraction of the oxide layer in which the alloying elements exist still in metallic form should be different in the different environments.

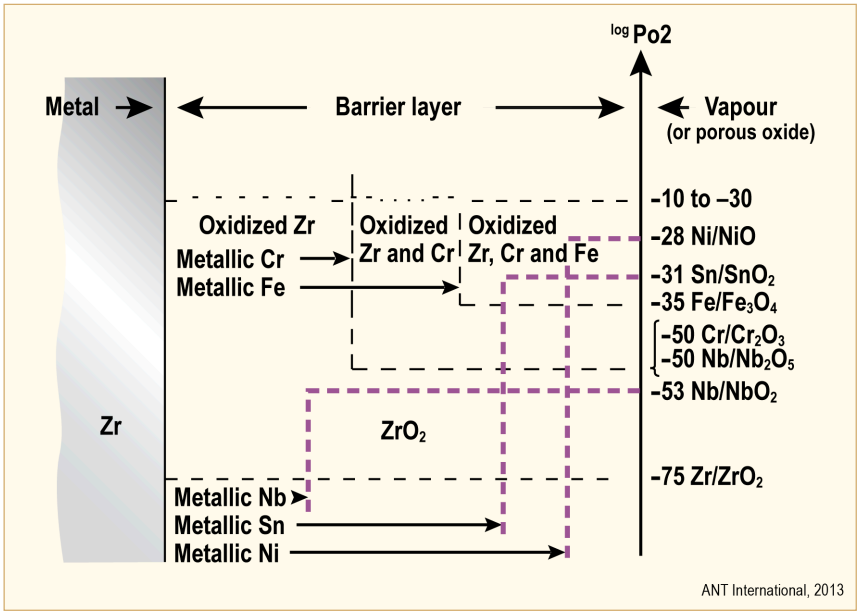

Figure 4-28: Stability domain of Zr, Fe, Cr, Ni, and Sn at the metallic state in the dense oxide layer versus the distance from the metal-oxide interface and corresponding value of the oxygen partial pressure, after [Pêcheur et al, 1994].

It is well-known that alloying elements and impurities often concentration in grain boundaries Thus, due to SPP dissolution Fe and Ni are in forced Zr-alloy metal solution, both elements will very likely also concentrate at the oxide crystallite boundaries in the ZrO_2 film. Consequently, metallic Fe-Ni bands should exist at oxide grain boundaries at least in the inner part of the barrier layer, when a highly irradiated Zry-2 matrix oxidizes. These metallic bands may oxidize or remain at least to some fraction metallic at the outer surface of the oxide barrier layer, depending on the REDOX potential at this position. Fe will always oxidize in a water environment but Ni may stay metallic if the environment is hydrogenated and free of oxygen.

As already mentioned, a much higher HPUF was found for Zry-2 than for the Ni free Zry-2 and Zry-4 in out of pile tests in oxygen free hydrogenated water and steam, and under certain conditions HPUF values close or even above 100% could be reached, e.g. [Hillner, 1964]. The high HPUF very likely needs Ni-bearing SPPs that are large enough to bridge the barrier layer. In case of the reported out-of-pile tests, e.g. [Hillner, 1964], the size of the SPP was very likely rather large. Unfortunately no HPUF data from out of pile corrosion tests in fully oxygen free environments have been published for Zry-2 lots with widely varying SPP sizes. But it can be suggested that small SPPs typical for modern BWR claddings may not bridge the barrier layer and may thus not lead to an increased HPUF in out-of-pile tests. However, Ni rich metallic bands at the oxide grain boundaries of highly irradiated Zry-2 could well act as a path for hydrogen to enter the metal, as long as they are not fully oxidized at the outer surface of the barrier layer.

The microstructural differences in the oxide layer of BWR claddings with rather fine SPP are schematically shown in Figure 4-29 for low and high burnups.

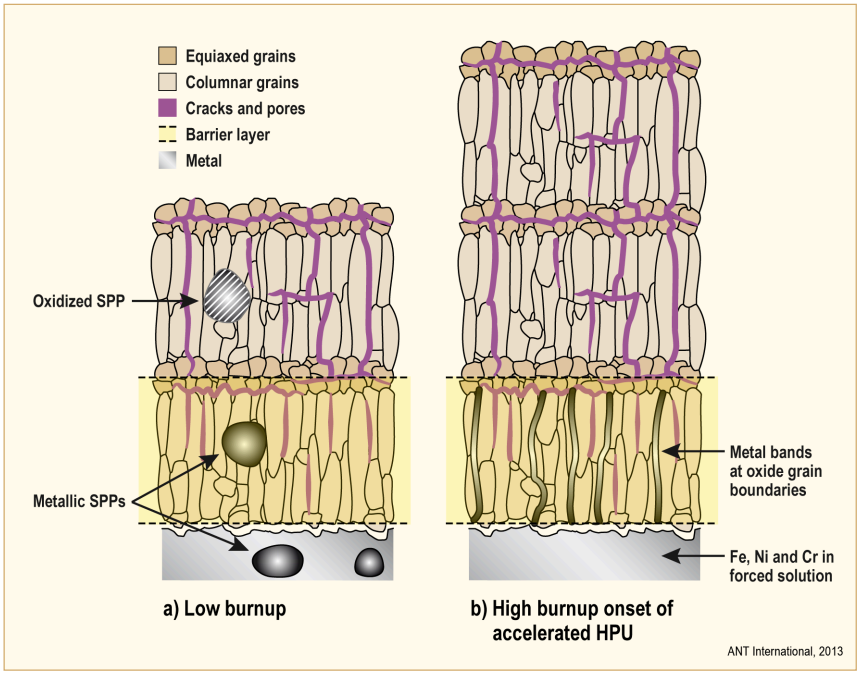

Figure 4-29: Schematics showing the material microstructure at a) low burnup with low HPUF and b) high burnup with high HPUF.

Figure 4-29a shows schematically the situation at low burnup with low corrosion rate and low HPUF. All SPPs in the Zry-2 matrix are in metallic form and essentially no dissolution of the SPPs in the Zry-2 matrix has occurred. However, the SPPs incorporated in the growing oxide are slowly oxidized. The inner part of the columnar oxide at the metal/oxide interface constitutes the "barrier layer". The corrosion process is limited by the O^{2-} diffusion through the "barrier layer". The small fraction of corrosion hydrogen is suggested to be picked up by the Zry-2 material through tiny defects in the "barrier layer", or other imperfections.

Figure 4-29b shows the situation at higher burnup, when all the SPPs have been dissolved. Water molecules can easily penetrate the outer part of the oxide arriving at the "barrier layer" at which it dissociates into O^{2-} and H^{+}. The O^{2-} diffusion still occurs through the "barrier layer" with significant thickness resulting in a moderate corrosion rate. The H^{+} is reduced at the outer part of the barrier layer by the electrons released from the ionization of the Zr atoms into Zr^{4+} at the metal/oxide interface. Due to the dissolution of the SPPs it is hypothesized that Ni and Fe in solution is concentrated at the oxide grain boundaries, (shown in the Figure 4-29b as grey bands in the barrier layers). If the Ni/Fe ratio is high enough in the grain boundary and the oxidation potential at the outer part of the barrier layer is low enough, the Ni/Fe band may be metallic up to the interface to the porous layer and form a freeway of hydrogen transport into the Zry-2 matrix thus resulting in a dramatic increase in HPUF.

As already pointed out, Ni could remain metallic on the surface of the barrier layer in case of BWR conditions only at high burnups, if the outer porous part of the oxide layer has reached a significant thickness and the pores are very fine. At such conditions an environment with high hydrogen concentration from the corrosion process can build up in the oxide. Under such circumstances a potential gradient must exist over the porous outer part of the oxide (more positive at the outer part of the porous oxide) which should reduce the concentration of negatively charged ions, such as e.g. the radiolytic product HO_2^-, at the inner part of the porous oxide layer. At the same time the potential gradient will favour migration of H^+ to the inner oxide surface. Furthermore, in the outer porous part of the oxide layer corrosion hydrogen will react with the oxygen from the BWR coolant by radiolysis, which may result in such a low REDOX potential at the barrier oxide layer/water interface that Ni remains metallic. [Rishel et al, 2007] reported that tetragonal Zr oxide (which is more abundant in the inner part of the oxide) increases the heterogeneous radiolysis significantly, which may increase the radiolysis in the inner part of the oxide.

The observation that acceleration of HPU at high burnup starts under isothermal condition much earlier than under a high heat flux (fuel cladding) can be explained by the increased mixing of the coolant within the oxide (with low REDOX potential) with that of the bulk coolant (with high REDOX potential) in the latter case. With such an increased mixing occurring in fuel rods the higher REDOX potential in the outer porous oxide will delay the HPUF acceleration compared to the situation with structural components without surface heat flux.

Furthermore, the beneficial effect of Cu in the water on lowering the HPU at high burnup fits well with the observation that Cu makes the radiolysis more sluggish (Figure 4-30). Cu should thus reduce the radiolytic reaction of oxygen from the coolant with the corrosion hydrogen in the oxide pores and therefore increase the oxidation potential in the oxide. Cu, in addition, may cause nodular corrosion with large pores, which favour coolant mixing and increase the potential at the metal/oxide interface and as consequence delay the increased hydrogen pick up.

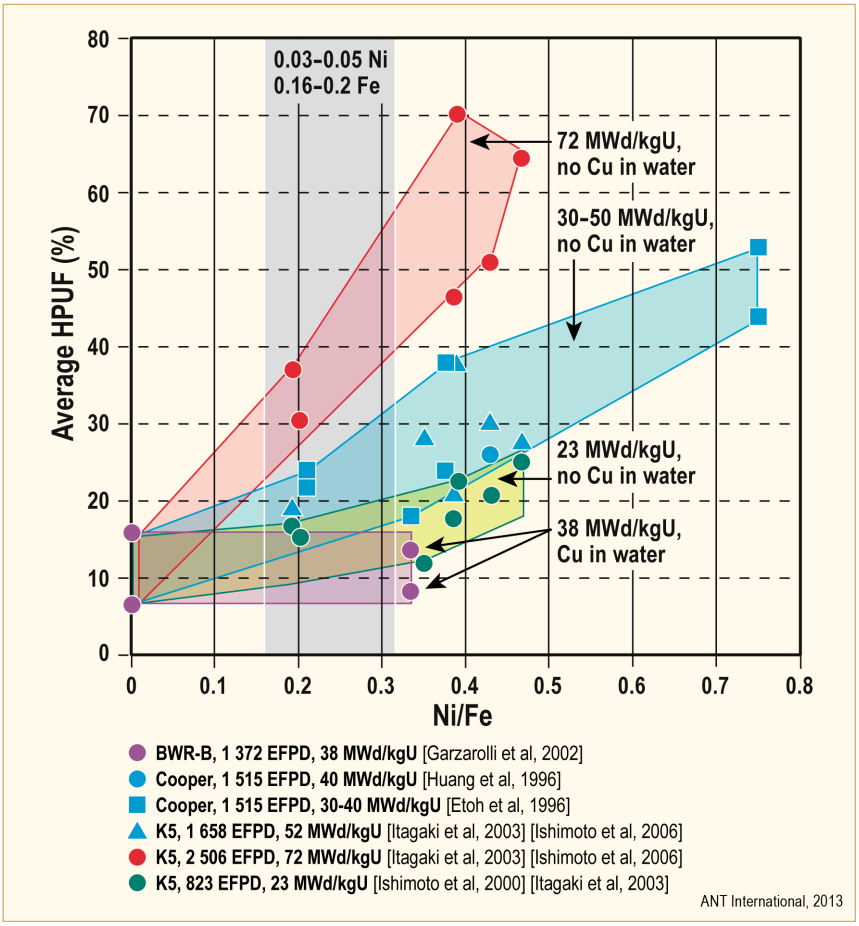

Figure 4-30: Correlation between the Ni/Fe content ratio of Zry and the time averaged HPUF at high burnups under isothermal conditions. The ASTM specification for Zry-2 allows a Ni/Fe ratio of 0.15-1.14, after [Garzarolli et al, 2002a], [Huang et al, 1996], [Etoh et al, 1996], [Ishimoto et al, 2000], [Ishimoto et al, 2006] and [Itagaki et al, 2003].

4.2.4 PWR and VVERs

4.2.4.1 Fuel rods

Figure 4-31 shows that the oxide thickness increases due to:

1) Increased temperature with increasing elevation above the bottom of the rod (0-2100 mm above the bottom of the rod) and,

2) Hydride rim formation according to [Fuketa et al, 2001].

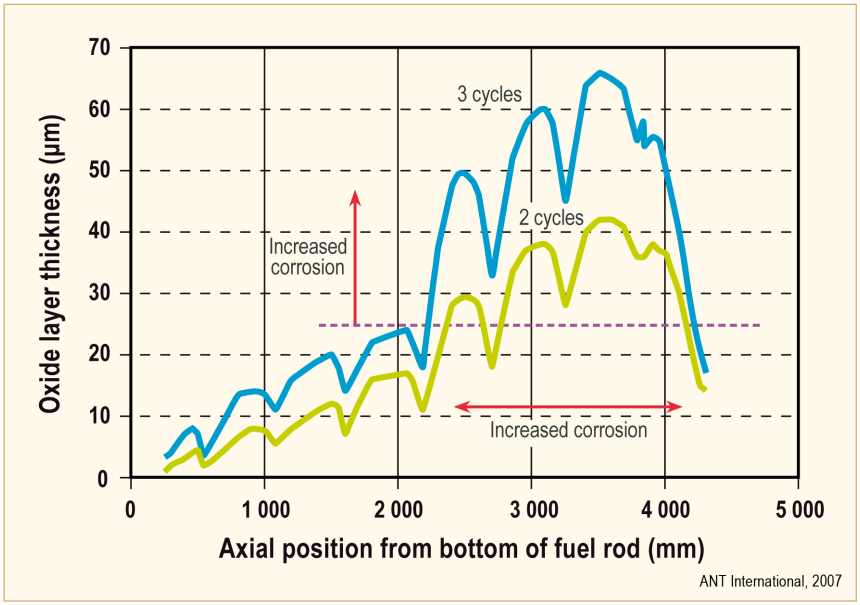

Figure 4-31: Oxide thickness profile of fuel rod H4 after 2 and 3 exposure cycles, after [Seibold et al, 1995].

The measured peak oxide thickness values versus burnup are shown for Zry-4 and ZIRLO-type alloys in Figure 4-32. It is clear that at higher burnups there is an acceleration of the corrosion rate *and it is suggested that this acceleration is due to formation of a solid hydride rim at the oxide/metal interface*.

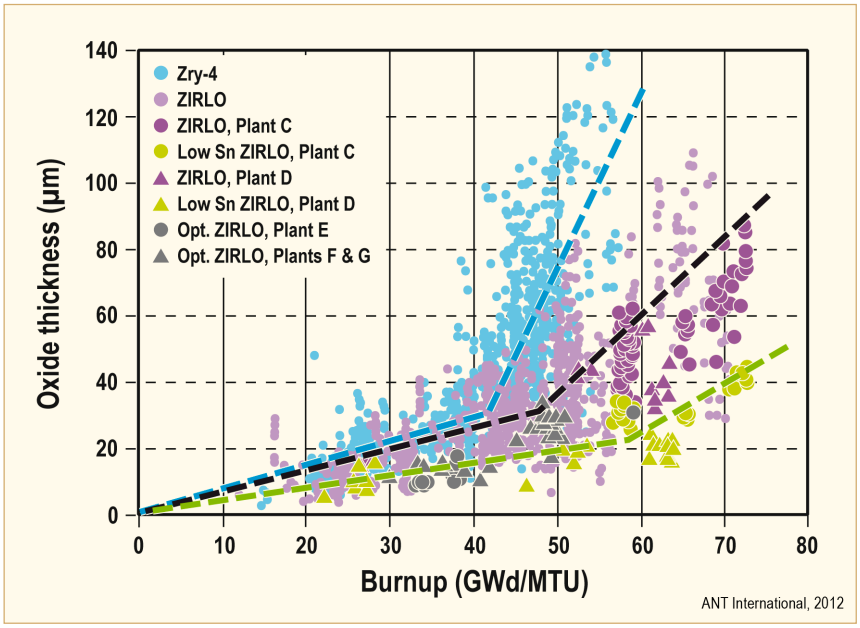

Figure 4-32: Oxide thickness of Optimized ZIRLO versus burnup. The increase in slope of the dashed curves is believed to be due to hydride rim formation, after [Mitchell et al, 2010].

The peak oxide thickness values of MDA as measured up to 4 cycles in Vandellos II are shown in Figure 4-33 together with data from FRs with ZIRLO and Low-Sn Zry-4 irradiated in the same FAs. After the 4th cycle, several reference low tin Zry-4 FRs showed an accelerated increase of the oxide thickness. The maximum oxide thickness values after the 4th cycle were between 40 and 100 µm for the reference low tin Zry-4 rods and between 40 and 60 µm for the MDA and ZIRLO rods. PIE indicated that the accelerated increase of oxide layer of low Sn Zry rods was due to formation of a dense hydride rim at the outer surface; see encircled area in Figure 4-33 [Tsukuda et al, 2003].

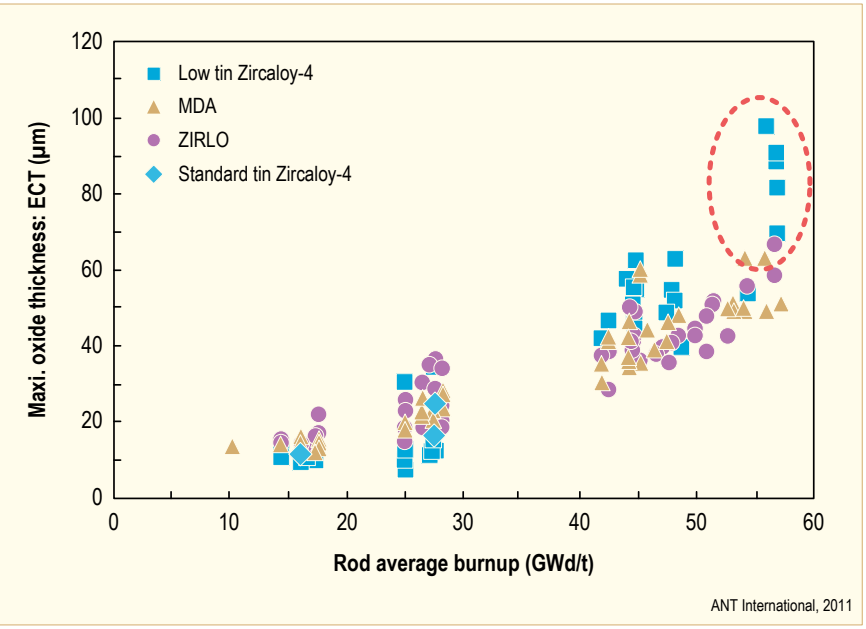

Figure 4-33: Comparison of the corrosion behaviour on low-Sn-Zry-4, MDA, and ZIRLO FRs in the PWR Vandellos II, after [Tsukuda et al, 2003].

Extended irradiations were performed after transfer of ten MDA and ZIRLO FRs with a burnup of about 55 MWd/kgU to inner positions of a two cycle assembly. These rods were then operated for an additional cycle to burnups between 67 and 75 MWd/kgU [Watanabe et al, 2005]. The MDA and ZIRLO-clad FRs operated at a relatively high Linear Heat Generation Rate (LHGR) and heat flux during the 5th cycle. The FA average LHGR value was about 200 W/cm (67 W/cm²). PIE of the 5 cycle rods was performed in the Studsvik hot cell laboratory and showed a strong acceleration of corrosion in the fifth cycle (Figure 4-34). The reason for this increase of the enhancement factor is probably due to the formation of hydride rims at the metal/oxide interface early in the 5th cycle.

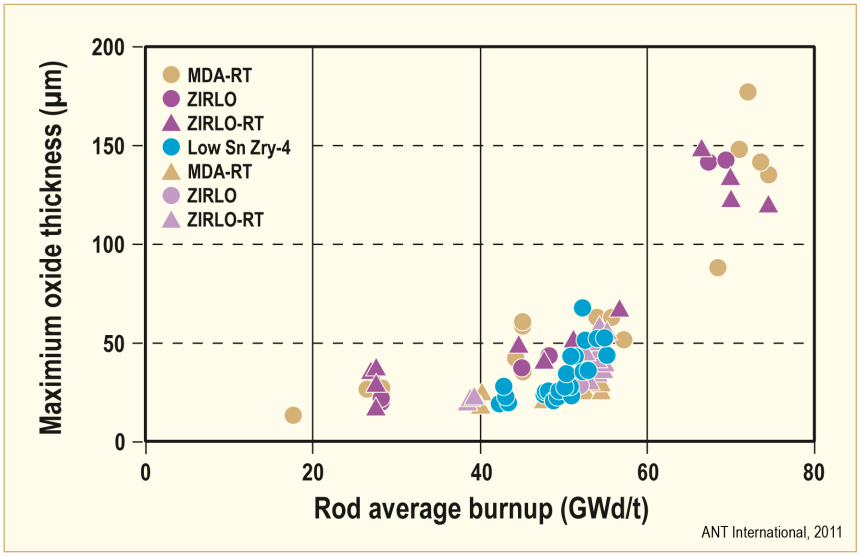

Figure 4-34: Maximum oxide thickness (peak among the circumference) of MDA and ZIRLO versus burnup, after [Watanabe et al, 2005].

Extensive measurements were also reported on the HPUF of the different alloys tested in Vandellos II and Ohi. Figure 4-35 shows that all tested materials (Low-Sn Zry-4, ZIRLO, and MDA) have the same HPUF (of about 15%) in these reactors independent on the material composition and oxide thickness.

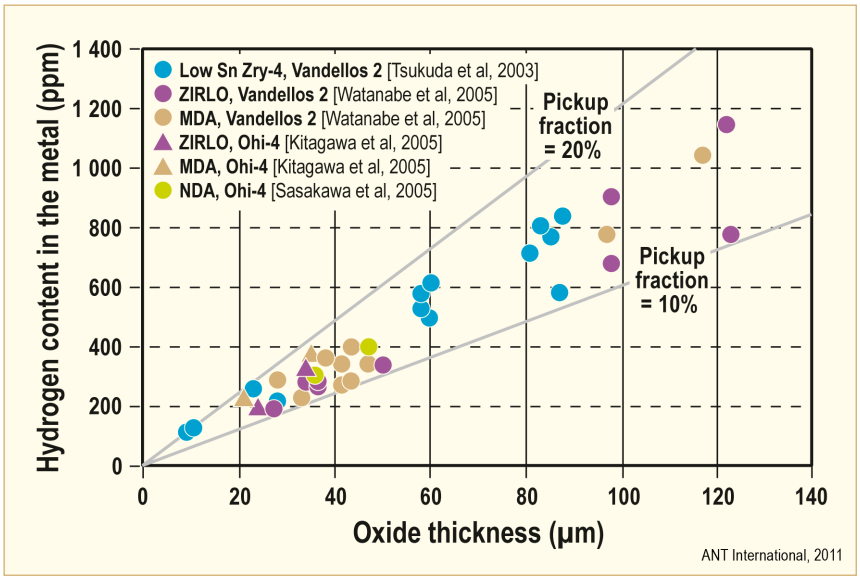

Figure 4-35: Relationship between oxide thickness and hydrogen content for MDA, NDA, ZIRLO, and Low-Sn Zry-4 after irradiation in Ohi and Vanderllos II, after [Tsukuda et al, 2003], [Watanabe et al, 2005], [Kitagawa et al, 2005] and [Sasakawa et al, 2005].

The corrosion behaviour of M5 fuel claddings can be seen from Figure 4-36. The hydrogen content of fuel claddings picked up during corrosion is very low compared to Zry-4 claddings, even for a rod burnup of 78 MWd/kgHM (see Figure 4-37). The hydrogen content in M5 is below the solubility limit at operation temperature (~100 ppm) due the low oxidation rate and also due to the small HPUF (approximately 10%). *Due to the very low hydrogen content, no late in life corrosion acceleration has occurred for the M5 material.*

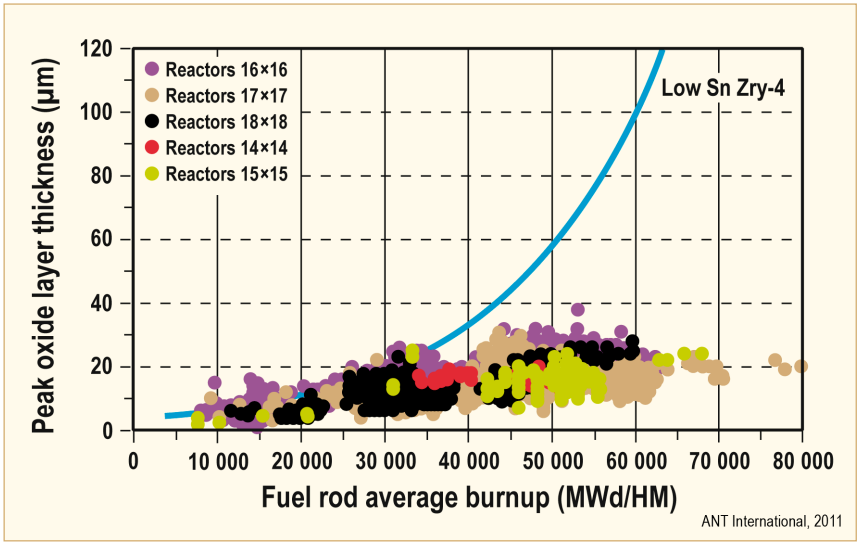

Figure 4-36: In-reactor cladding corrosion experience: comparison between the Zry-4 and the M5, after [Mardon et al, 2010].

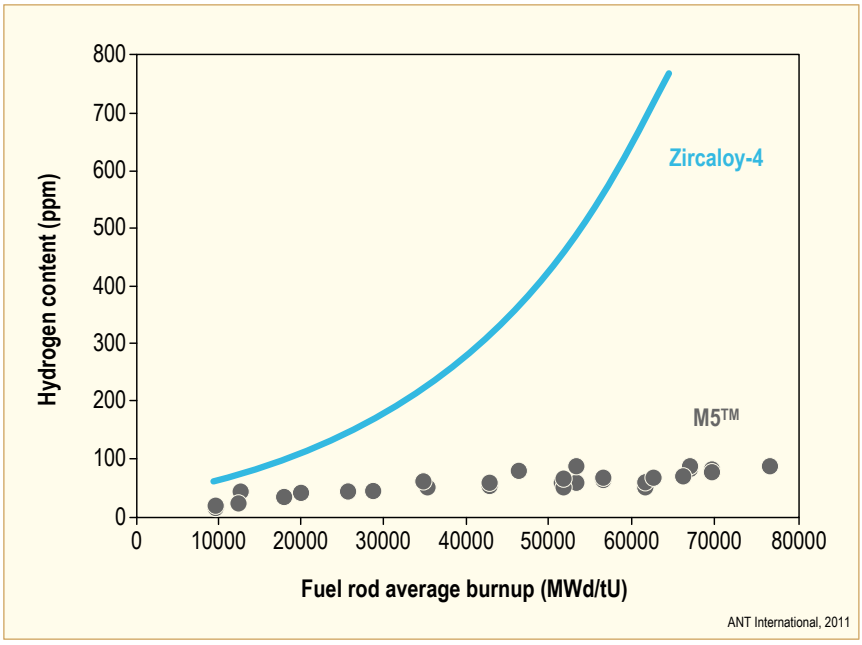

Figure 4-37: Hydrogen content for M5 and Zry-4 vs. burnup, after [Mardon et al, 2010].

VVER alloys – For the claddings of the VVER FRs, E110 is used. The E110 alloy used by the Russians is a Zr alloy with 1%Nb, with a lower O and Fe content than M5 or Zr1Nb (as tested by Westinghouse and Siemens) and is also not alloyed with S such as M5.

E110 has a similar material condition as M5 (processed in the α-range, and RX), but was up 2008 fabricated from electrolytic Zr with some iodide Zr. This contrasts with M5 and Zr1Nb which utilize Zr sponge as their source material. The difference in source material (sponge Zr vs. electrolytic Zr + iodide Zr) results in different results in different impurity levels, e.g. a relatively high F content in electrolytic Zr + iodide Zr. Until 2008, pickling was also used as final surface treatment for the FR claddings.

In the last years an optimization of E110 was ongoing [Novikov et al, 2006]. During the last years the source material has been changed to Zr sponge as is being used for M5 and the surface treatment is being changed to belt polishing. The change was prompted by the need for changes in composition and surface finish to improve the resistance of E110 to breakaway corrosion in simulated LOCA tests.

The oxide layers formed on E110 claddings in VVERs as well as the HPU are very low similar as observed for M5 in PWRs (Figure 4-38), largely independent on surface treatment and Zr source material. The E110 oxide layer thickness values from VVER-440 and VVER-1000 are surprisingly quite similar and below the scatter band of M5 oxide data. The larger oxide layer thickness of M5 and Zr1Nb compared to that of E110 is probably due to:

- The difference in water chemistry between VVERs and PWRs,
- The fact that the thermal hydraulic conditions are more demanding in most PWRs than in the VVERs,
- The EC measurement technique, which is not as accurate as metallography and the former technique, often overpredicts the oxide thickness values.

The oxide layer on E110 claddings was reported to be dense and black with a thickness of 3-7 μm up to a burnup of about 45 MWd/kgU. At higher burnups the film thickens in the in the peak temperature region (between the 13th and 15th spacer grid) reaches values of ≥10 μm, becomes grey-white, and exhibits film cracking and spallations in some areas (Figure 4-39) [Smirnov et al, 2006]. The reasons for the degradation of the corrosion behaviour of E110 at high burnup, which are not seen with M5 or Zr1Nb tested by Siemens, are not known. The relatively high F content (introduced by the electrolytic process) or the very low Fe content of E110 might be the root cause for the increased corrosion rate at high burnups.

Several cases of unusual corrosion (mostly nodular corrosion[7]) were observed with E110 claddings, initiated by [Adamson et al, 2006/2007]:

- Coolant contamination by carbon containing species from ion-exchange resin,
- Increased oxygen contents in the coolant, and
- Galvanic coupling with Ni-base alloys and stainless steel.

[7] A localized corrosion type that is normally only seen in BWRs

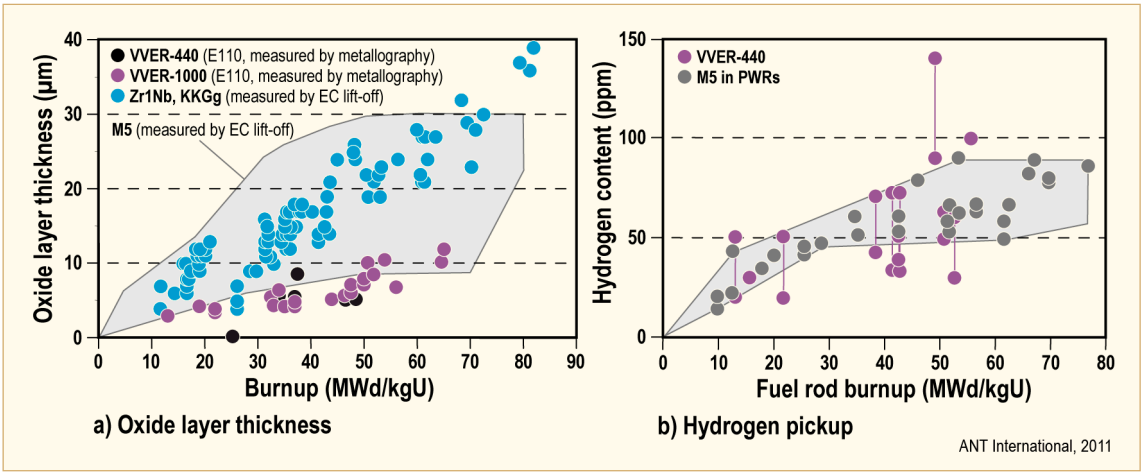

Figure 4-38: Normal corrosion behaviour of E110 FR cladding in VVERs. Data from [Solonin et al, 1997], [Smirnov et al, 2001], [Markov et al, 1999] and [Markov et al, 2005], in comparison with Zr1Nb and M5 in PWRs, after [Thomazet et al, 2005].

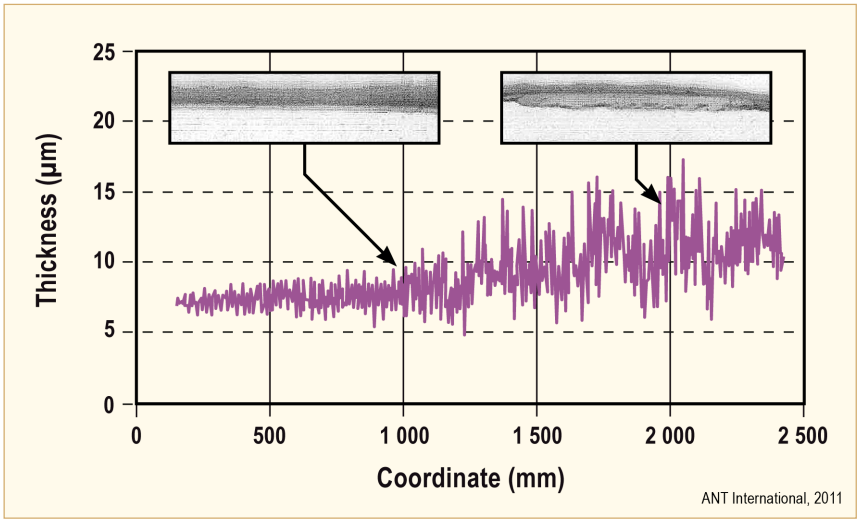

Figure 4-39: Axial oxide profile on FR claddings operated within 6 cycles to 56 MWd/kgU, after [Smirnov et al, 2006].

4.2.4.2 PWR/VVERs structural components

Oxidation and hydrogen pick-up were evaluated on unfuelled tubing of Zircaloy 4 up to an equivalent burnup of 92.9 GWD/MT (21.0×10^{25} n.m^2 fluence) and on M5 up to an equivalent burnup of 79.1 GWD/MT (17.1×10^{25} n.m^2 fluence) [Bossis et al, 2007]. The oxidation at the peak exposure was in µm:

	Inner diameter	Outer diameter
Zircaloy 4	81.8	61.6
M5	6.6	7.5

The corresponding Hydrogen Pick-Up (HPF) was lower for M5 (

Figure 4-40).

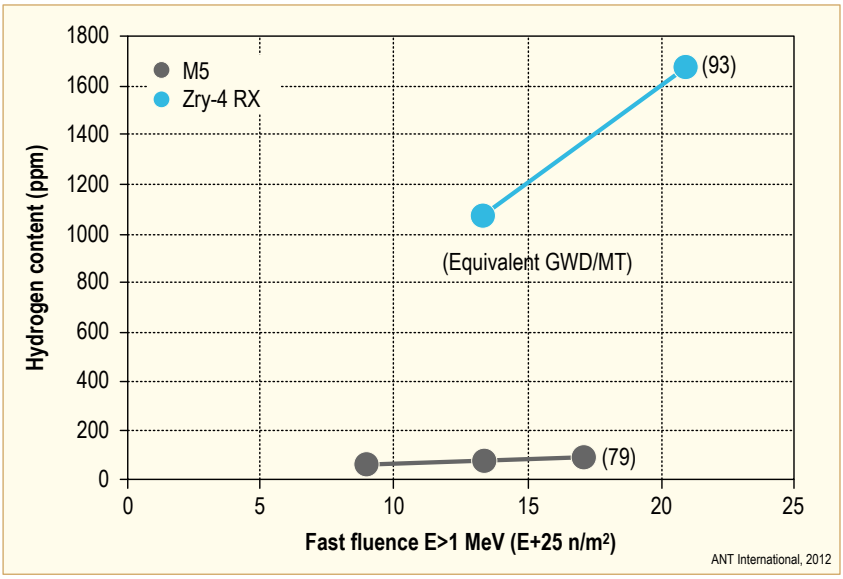

Figure 4-40: Hydrogen content in RXA low tin Zry-4 and M5®, after [Bossis et al, 2007].

4.3 Irradiation

In reactors the zirconium alloys, the oxide film, the CRUD and the coolant are all exposed to neutrons, γ, β, and α radiation and possibly fission fragments. Their collective and interactive effects change the corrosion mechanisms and rates of the materials involved. The major effects of irradiation on the oxidation process are:

- The phase stability of secondary phase particles and the zirconia are changed,
- The local electrical properties that affect the local electrochemistry are changed,
- The water chemistry is modified by radiolysis.

The overall effect is to increase oxidation rates as shown on Figure 4-41 that compares long term irradiation data of Zry-4 with long term ex-reactor corrosion data of the same material.

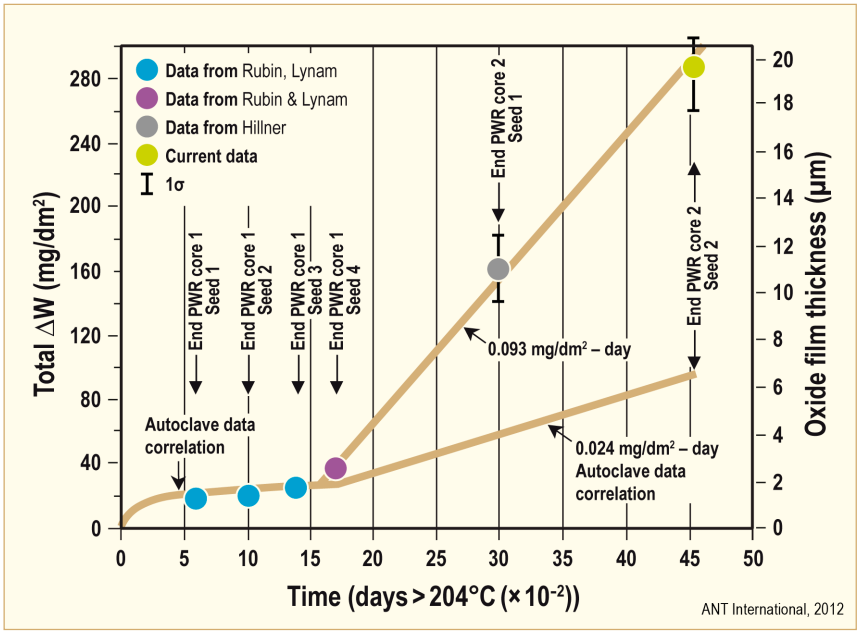

Figure 4-41: Comparison of Zry-4 corrosion in Shippingport reactor and ex-reactor autoclave, after [Hillner, 1982].

To enable a comparison of corrosion data of Zr alloys obtained at different metal/oxide interface temperatures, normalized time, was introduced by [Garzarolli et al, 1991] as follows:

Eq. 4-1: $$\Sigma t_i \bullet \exp(-14200/T_i),$$

where

t_i and T_i are the time and temperature at the metal-oxide interface during the individual time steps i. With this concept, the corrosion time at a certain temperature is modified to a time which would result in the same oxide growth at 350°C out-of-reactor.

Figure 4-42 shows the oxide weight gain versus normalized time in reducing and oxidizing environments. It is clear that in reducing environment (PWR) the uniform growth rate follows the out of pile behaviour up to an oxide thickness of about 5 μm, after which it is enhanced by irradiation (Figure 4-42a and b). However, in oxidising environment (BWR), the corrosion acceleration due to irradiation occurs already at thin oxide thickness, Figure 4-42c.

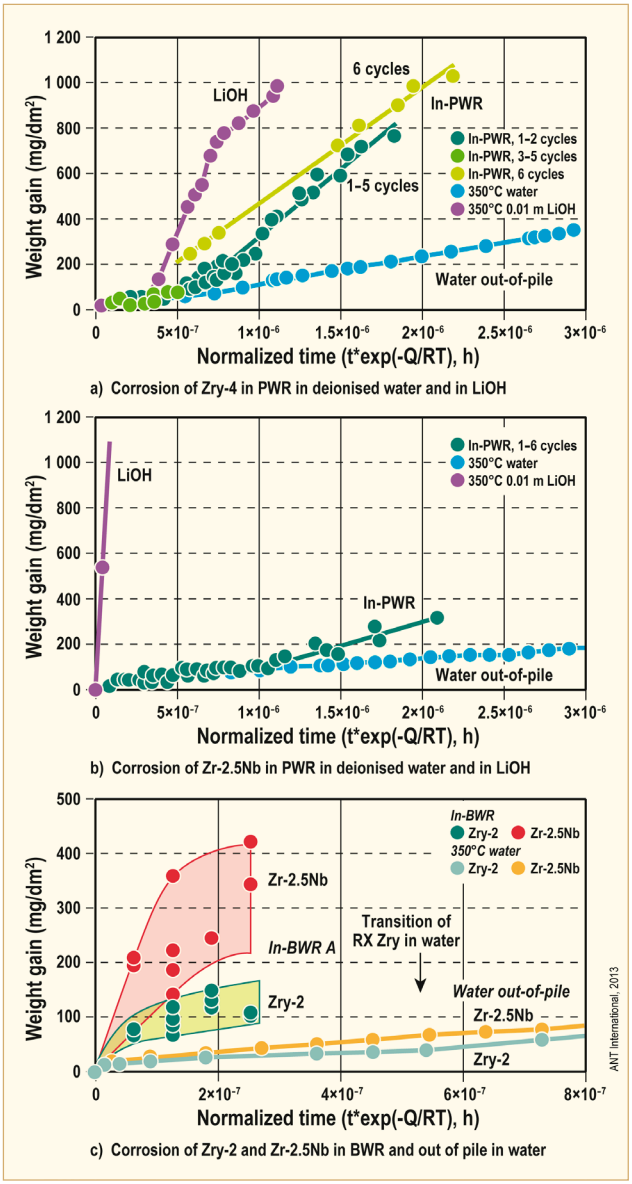

Figure 4-42: Effect of irradiation under hydrogenated conditions (PWR) and oxygenated conditions (BWR) on corrosion of Zry-2/4 and Zr2.5Nb, after [Garzarolli et al, 1991].

4.4 Temperature

The corrosion rate increases with increasing temperature at the zirconium metal/zirconium oxide interface, as follows:

$$\frac{ds}{dt} = C \exp\left(-\frac{Q}{RT}\right)$$

Q/R is reported to be between 11000 and 16000 K and appears to quite independent on Zr-alloy composition and condition. Probably the best Q/R value for Zry-4 corrosion in water is 12880 K, as deduced from long-time experiments at 270-360°C, [Hillner et al 2000].

where

s is the oxide thickness

t is the time

Q is the post-transition activation energy

C is an irradiation corrosion enhancement factor

R is the Gas Constant

T is the temperature at the metal/oxide interface

The pre-exponential constant (C) is very different for different zirconium alloys as well as different in BWRs and PWRs. Experiments (see e.g. [Stehle et al, 1984]) comparing the Zry-4 out-of-pile with the PWR corrosion rates have suggested a value of C= 2 to 5, while similar tests for Zry-2 in BWRs have indicated a C constant that varies with temperature. At temperatures of 200°C, C=1000, while at 400°C the C=1. Thus, the out-of-pile and in-pile corrosion rates for Zircaloy can be schematically shown as in Figure 4-43. *The bottom line is that a temperature increase at the metal/oxide interface (below a maximum temperature of 400°C) results in a larger increase of the corrosion rate in a PWR than in a BWR. This is the reason that there has historically been a licensing limit on the maximum oxide thickness for fuel rods in PWRs but not in BWRs[8]. Since the oxide has a lower thermal conductivity than that of the metal a large oxide thickness increase may increase the metal/oxide temperature and thereby increase the corrosion rate in a PWR leading to a thermal feedback effect.*

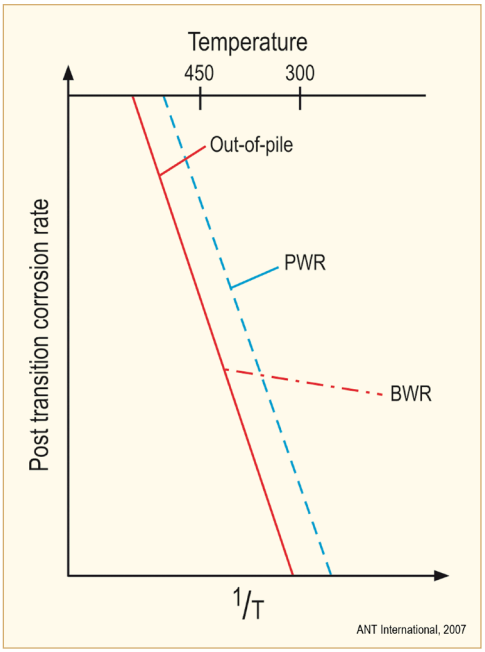

Figure 4-43: Schematic diagram showing the impact of metal/oxide interface temperature on post-transition corrosion rate, after [Garzarolli & Rudling, 2011].

The factors affecting the temperature are (Figure 4-44):

[8] The USNRC has proposed a limit on oxide thickness and uniformity for BWR fuel. The motivations for the proposed limit were closer control of vendor's processes and limitations on hydrogen pickup and localized hydriding as related to RIA failure limits.

- Rod power
- Oxide thickness and its thermal conductivity
- CRUD thickness and its thermal conductivity
- Heat transfer coefficients
- Bulk coolant temperature

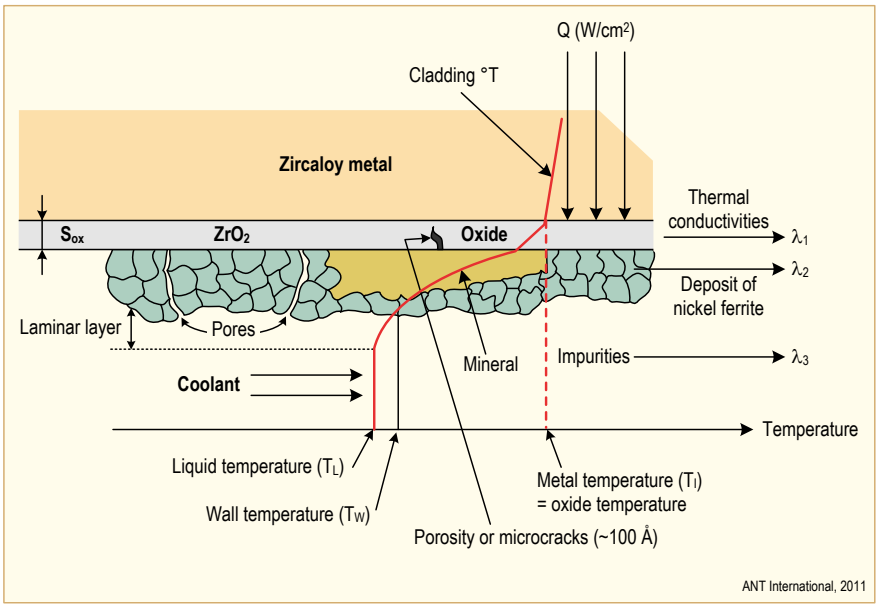

Figure 4-44: Factors that affect cladding temperature, after [IAEA, 1998a].

The temperature effect on corrosion rate is related to the increased transport rate of the corrosion species responsible for the oxide growth (oxygen ions through the barrier layer) with increased temperature.

4.5 Water chemistry

4.5.1 Introduction

The influence of water chemistry on the corrosion of zirconium alloys under nuclear reactor conditions is an important but often not fully acknowledged aspect in the understanding and interpretation of corrosion behaviour. Such influence may derive from chemical additives to the reactor coolant such as boric acid, alkalising species and hydrogen or from impurities such as oxygen, halogenides, sulphates, chromates, nitrates, resin and deposited oxides from the coolant system. In most cases chemical additions or impurities affect:

- The time to corrosion rate transition and
- Post-transition corrosion rate.

Only in some cases (e.g. H_2O_2 additions) is pre-transition corrosion rate is increased.

Gases have very little effect on Zr alloy corrosion out-of- pile. Only Nb-containing alloys are affected by oxygen in the water (probably as a result of a change of the Nb valence in the oxide from +3 to +5 and the associated volume expansion).

In-reactor there is a large effect of oxidation potential on corrosion and hydriding rates [Cox, 1985b] (Figure 4-45). This effect results from the impact of the gases on the radiolysis. There are two effects of radiation on the coolant: 1) radio-activation of water and 2) corrosion products radiolysis of the coolant. Ionizing radiation decomposes water to the following species: H^+, OH^-, H, OH, H_2, O_2, H_2O_2, e^-(aqueous) and HO_2^-. Recombination of the radiolysis products results in stable products, such as H_2, H_2O_2 and O_2. Addition of hydrogen or NH_3 to pressurized water reduces O_2 and H_2O_2 concentrations to undetectable levels. Hydrogen is kept in the coolant of PWRs at levels of 2-4.5 ppm (25-50 cc/kg). In VVER plants the coolant hydrogen concentration is also specified in the same range. However, NH_3 is injected to produce this amount of hydrogen in the coolant by radiolysis. The coolant NH_3 concentration that is needed to produce the specified hydrogen concentration depends on reactor power and is approcimately 10 ppm at 100% power.

Most studies report that irradiation accelerate the corrosion rate of zirconium alloys. This corrosion acceleration effect depends on the hydrogen and oxygen contents in the water. [Cox, 1985a] reviewed the existing information of Zircaloys in this respect and proposed the relations given in Figure 4-45.

- At H/O ratios above 100 (PWR, VVER and CANDU) only uniform corrosion exists, which is increased above a certain oxide thickness and the HPUF is relatively high. Hydrogen is kept in the coolant of PWRs at levels of 2-4.5 ppm (25-50 cc/kg).

- At a H/O ratio below 10, (BWR and RBMK), radiolytic oxygen and hydrogen-peroxide is formed and an early increase of uniform oxidation and nodular corrosion occurs. In addition, accelerated uniform and shadow corrosion may occur in this H/O ratio regime. The HPUF becomes low under irradiation except in case of the accelerated uniform corrosion occurring at higher burnups. Figure 4-46shows that nodular corrosion can form at oxygen contents of >20 ppb in the water and that it is most pronounced for Zr-Nb binary alloys (green and yellow symbols). Significant nodular corrosion has been found in:

  – BWRs and RBMKs,

  – PWRs in early times, when no hydrogen was added to the coolant,

  – Loop tests simulating BWR conditions and,

  – Loop tests simulating VVER-1000 conditions. In this case severe nodular corrosion (up to 250 µm) was found on Zr1Nb fuel rod claddings under heavy surface boiling, [Konkov et al, 1999].

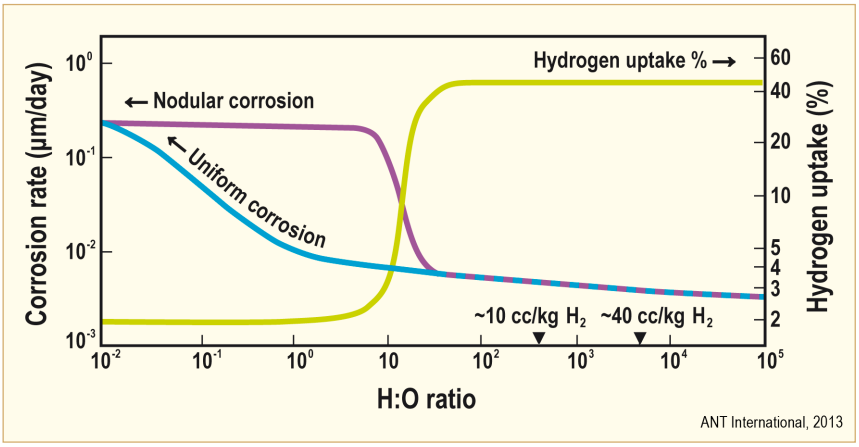

Figure 4-45: Effect of water chemistry on in-reactor oxidation and hydrogen uptake rates, according to [Cox, 1985a].

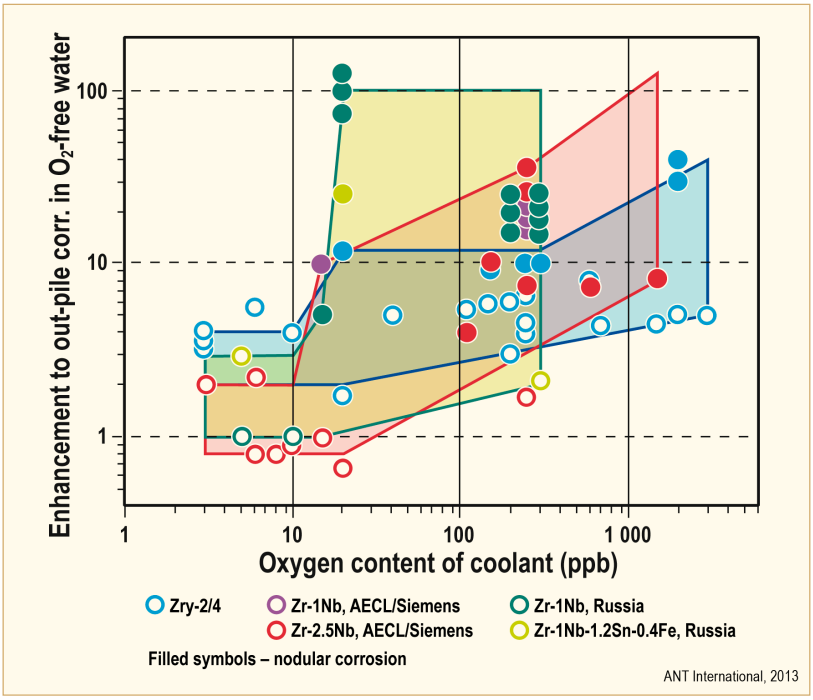

Figure 4-46: Influence of oxygen in water on in-reactor corrosion. The ratio between the in-reactor to out-of-reactor corrosion rate (in oxygen free water) is plotted versus the oxygen coolant content, after [Cox et al, 2004/2005].

According to more recent studies, the minimum hydrogen content necessary to suppress formation of oxidative radicals is at about 0.5 ppm (5 cc/kg) e.g. [Christensen et al, 1996] and [Garbett et al, 1998] as can be seen from Figure 4-47. As pointed out previously, in-reactor and out-of-reactor corrosion rates are similar in a hydrogenated environment up to a certain oxide thickness (~5 μm) after which the in-reactor corrosion rate becomes larger than that out of reactor by a factor depending upon alloy composition (this irradiation enhancement factor is ~4 for Zry-4).

In BWRs, where corrosion rate is affected not only by irradiation but also by oxidative species produced by radiolysis, corrosion rate follows pre-transition time characteristics but is enhanced by irradiation from the early beginning. Furthermore, nodular corrosion and shadow corrosion may arise under in-BWR conditions. N and ammonia additions in the coolant are also affected by radiolysis. In a hydrogenated environment, a certain ratio between N and NH_3 is maintained by radiolysis, whereas in an oxygenated environment N and NH_3 are transformed to NO_3^- to a large extent.

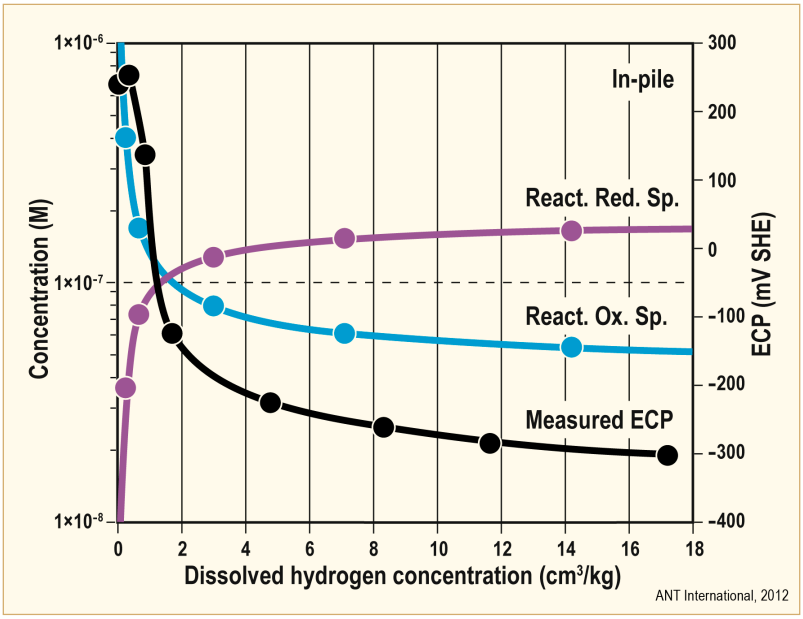

Figure 4-47: Calculated steady-state concentration of oxidative species (O_2 and H_2O_2), of reducing species (e_{aq}^-, H) and the SS electrochemical potential versus H_2 content, after [Christensen et al, 2000].

In PWRs, up to 1800 ppm boric acid and up to 3.5 ppm alkalising additions (as LiOH or KOH) are added for reactivity and pH control. In case of VVERs up to 1500 ppm Boric acid and KOH as alkalizing agent (5-26 ppm K) are added; whereas the coolant contains in addition up to 0.6 ppm of Li produced from B-10 by (n,γ) reaction. Boric acid additions do not affect corrosion performance of Zr alloys other than reducing the corrosion acceleration effect of LiOH. LiOH, more than 4E-3 Mol (30 ppm Li), increases corrosion rate under isothermal out-of-pile conditions. This concentration is higher, by a factor of 10, than the typical concentration used in PWRs (≤3.5 ppm Li). However, Li may concentrate significantly in the outer porous part of thicker oxide layers during sub-cooled boiling conditions.

Grain boundary dissolution and reprecipitation of oxide in basic solutions, such as LiOH, NaOH, NaF, may significantly degrade the barrier layer and increase corrosion rate.

The key factors of the LiOH effects are;

- Pore formation due to preferential cubic or tetragonal ZrO_2 dissolution [Cox & Wu, 1993] and consequently a drastic reduction of the barrier layer thickness at the metal/oxide interface e.g. [Une et al, 2010].
  - SIMS studies of the Li concentration profile have shown that Li penetrates into the innermost part of the oxide layer only in samples exhibiting an increased corrosion rate. If the Li penetration stops at the barrier layer no significant corrosion enhancement is observed, e.g. [Pêcheur et al, 1996]. Thus, it can be considered that the migration characteristic through the outer, porous part of the oxide may be an important aspect for the aggressiveness of a certain species.

- Modified crystal growth of equiaxed grains e.g. [Pêcheur et al, 1996],
  - SEM studies of the metal side of oxide samples from corrosion coupons exposed in LiOH and NaF have shown a relatively coarse structure and a network of large pores with an average spacing similar to the average metal grain size [Garzarolli et al, 1989b]. Furthermore, TEM studies of samples exposed in LiOH and having a very high corrosion rate have shown that the inner part of the oxide is composed mainly of equiaxed grains [Pêcheur et al, 1996]. These observations indicate that modification of the oxide microstructure, possibly by the crystallizing effect of the monovalent elements discussed previously, Section3.2 plays an important role in the corrosion increase.

4.5.2 PWRs and VVERs

According to the present status of knowledge, Li in the PWR coolant up to 7 ppm does very likely not affect in-PWR corrosion at low oxide layer thickness (at <30 µm) and with no subcooled boiling (moderate fuel duties), e.g. [Evans & Polley, 1992] and, [Stevens & Bosma, 2008]. At significant amount of boiling (very high fuel duty) and/or large oxide layer thickness values a Li induced acceleration of the corrosion rate may occur. It should be taken into account that once Li accelerated corrosion has started the corrosion attack will be very likely localized and the probability of fuel failures will be significant.

4.5.2.1 Effects of LiOH and KOH

4.5.2.1.1 No irradiation

Boric acid reduces the harmful effect of LiOH on corrosion rate (Figure 4-48). The out of pile effect of LiOH and KOH was summarised by [Garzarolli et al, 1989b] and is shown in Figure 4-49. As can be seen, the effect of LiOH on corrosion rate is much larger than that of KOH.

The concentration, at which the corrosion rate increases with increasing LiOH content, is under isothermal conditions 4E-3 mol (30 ppm Li). This concentration is higher than the concentration used in PWRs (as low as ≤3.5 ppm Li, ≤6 ppm Li in a few plants) by a factor of 5-10. However, Li may concentrate significantly in the outer porous part of thicker oxide layers on fuel rods due to the surface heat flux, specifically during subcooled boiling [Garzarolli, 2002].

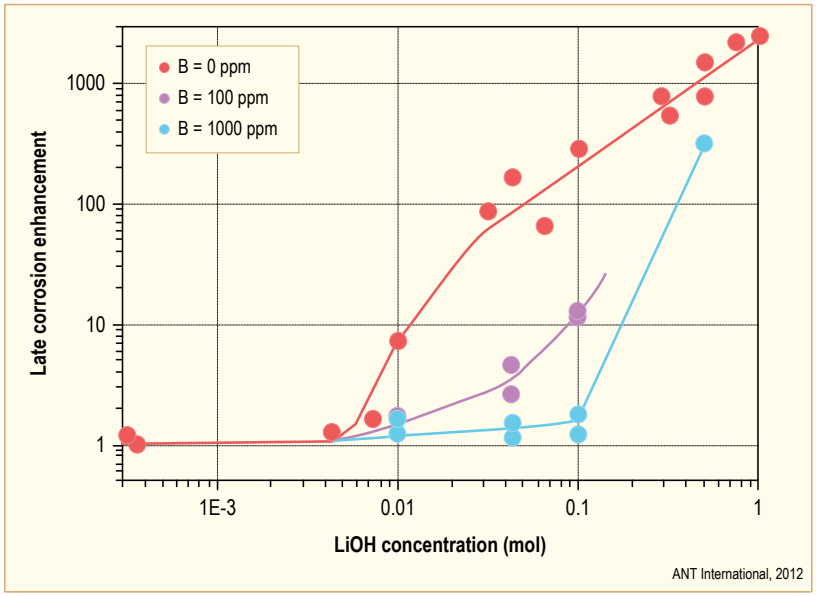

Figure 4-48: Effect of LiOH and boric acid on corrosion rate of Zry-4 in water at 350°C, after [Garzarolli et al, 2002b].

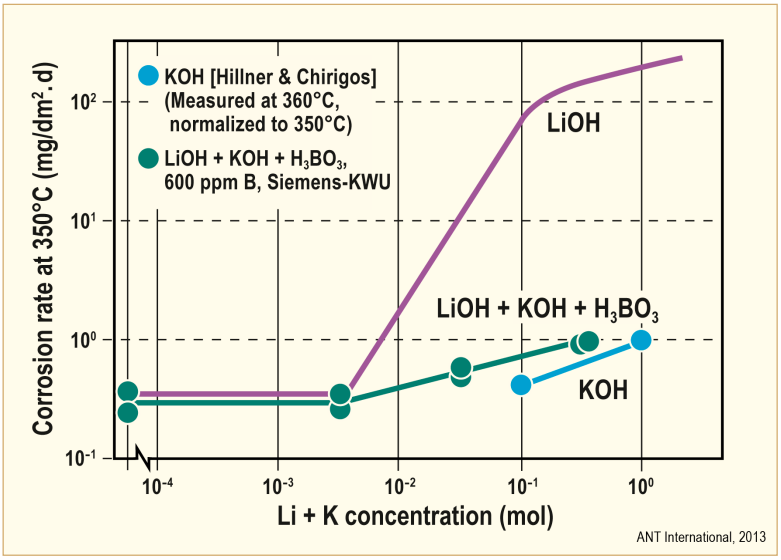

Figure 4-49: Out of pile effect of LiOH, KOH and a mixture of KOH, LiOH, and H_3BO_3 on post-transition corrosion behaviour of Zry-4 at 350°C, after [Garzarolli et al, 1989b].

[Billot et al, 1994] reported on corrosion behaviour of Zry-4 claddings in loop tests under heat flux for a broad range of lithium and boron concentrations. The results show that corrosion enhancement due to Li at concentrations <10 ppm in the water is small when a heated Zry surface has no or low void fraction (<5%). At higher lithium concentrations and higher void fractions, a significant corrosion enhancement was detected. These tests were performed on fresh cladding, thus the total oxide thickness was <10 µm, except in a few cases.

[Garzarolli et al, 1989b] and [Garzarolli et al, 2002b] pointed out that the analysis of the oxide layer for Li incorporation indicates a correlation between the Li content in the oxide lattice and the corrosion enhancement (Figure 4-50). Li increased corrosion rate is correlated with concentrations more than 100 ppm Li in the oxide lattice. Tests under changing Li concentrations in the test solution showed that corrosion changes rapidly with the Li content of the coolant (Figure 4-51). This indicates that no memory effect has to be considered.

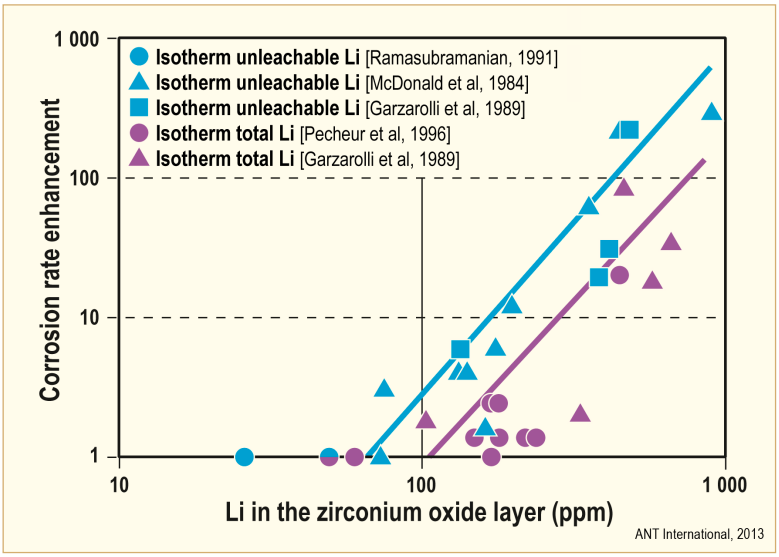

Figure 4-50: Correlation between corrosion rate and Li pickup in the oxide of Zry- samples from isothermal tests with 0.001-0.1 mol LiOH, after [Adamson et al, 2002].

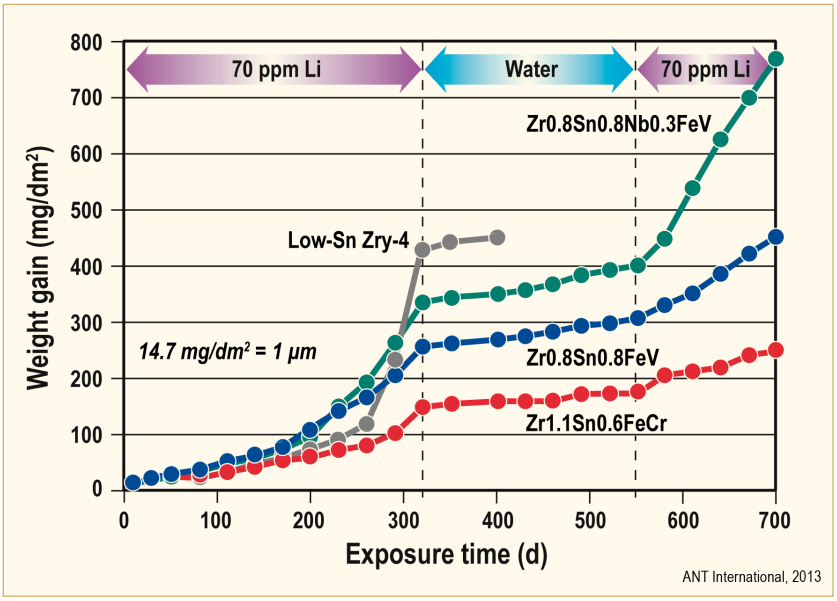

Figure 4-51: Corrosion behaviour of different Zr alloys during a corrosion test in pure and lithiated water at 350°C, after [Garzarolli et al, 2002b].

[Bojinov et al, 2008] studied the effects of KOH in VVER water on the oxidation of E110 and Zry-4 by Electrochemical Impedance Spectroscopy (EIS). KOH contents of 11, 28 and 56 ppm were compared at 310°C over a 5 day period. Results at the highest KOH concentration (56 ppm) for E110 and Zry-4 are presented as microscopic estimates of the oxide film thickness in Figure 4-52. Differences between E110 and Zry-4 appear to be small but both alloys show increasing corrosion rates with increasing KOH content. The authors conclude that the effects of increasing KOH concentration are related to increases in the dissolution rates of the oxide films.

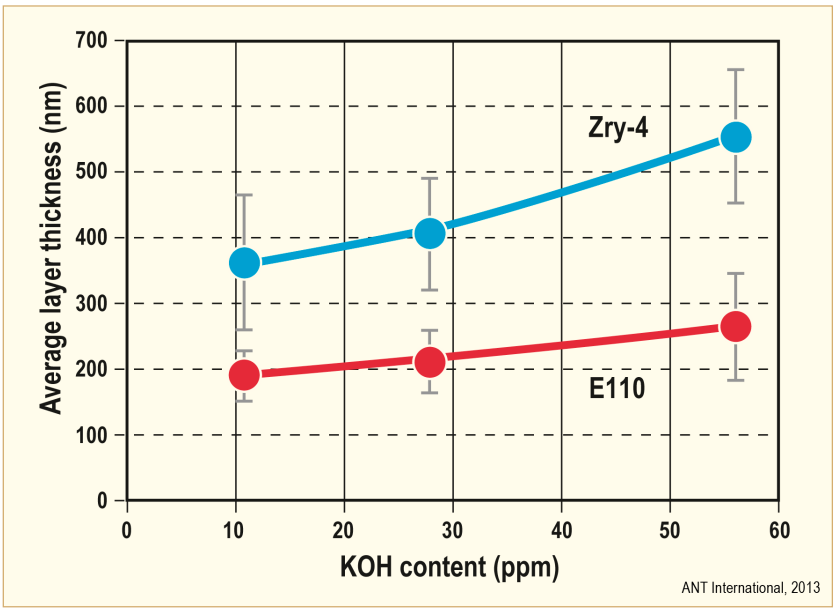

Figure 4-52: Microscopic estimates of the oxide film thickness on E110 and Zircaloy- 4 after 120 h of exposure to simulated VVER water as depending on the KOH content, after [Bojinov et al, 2008].

[Jeong et al, 1993] have studied the effect of the influence of group -1 alkali hydroxides (Li-, Na-, K-, Rb-, and Cs-hydroxides) on the corrosion behaviour of different zirconium alloys. Zirconium alloys corrode significantly faster in LiOH and NaOH environments than in the other alkali hydroxides – a good mechanistic understanding explaining this difference does not exist today. The lowest corrosive aggressiveness has been found for CsOH followed by KOH. Boric acid reduces the deleterious effect of alkali hydroxides. A summary of the mitigating effect of boric acid on the deleterious corrosion influence of LiOH out of pile is shown in Figure 4-53.

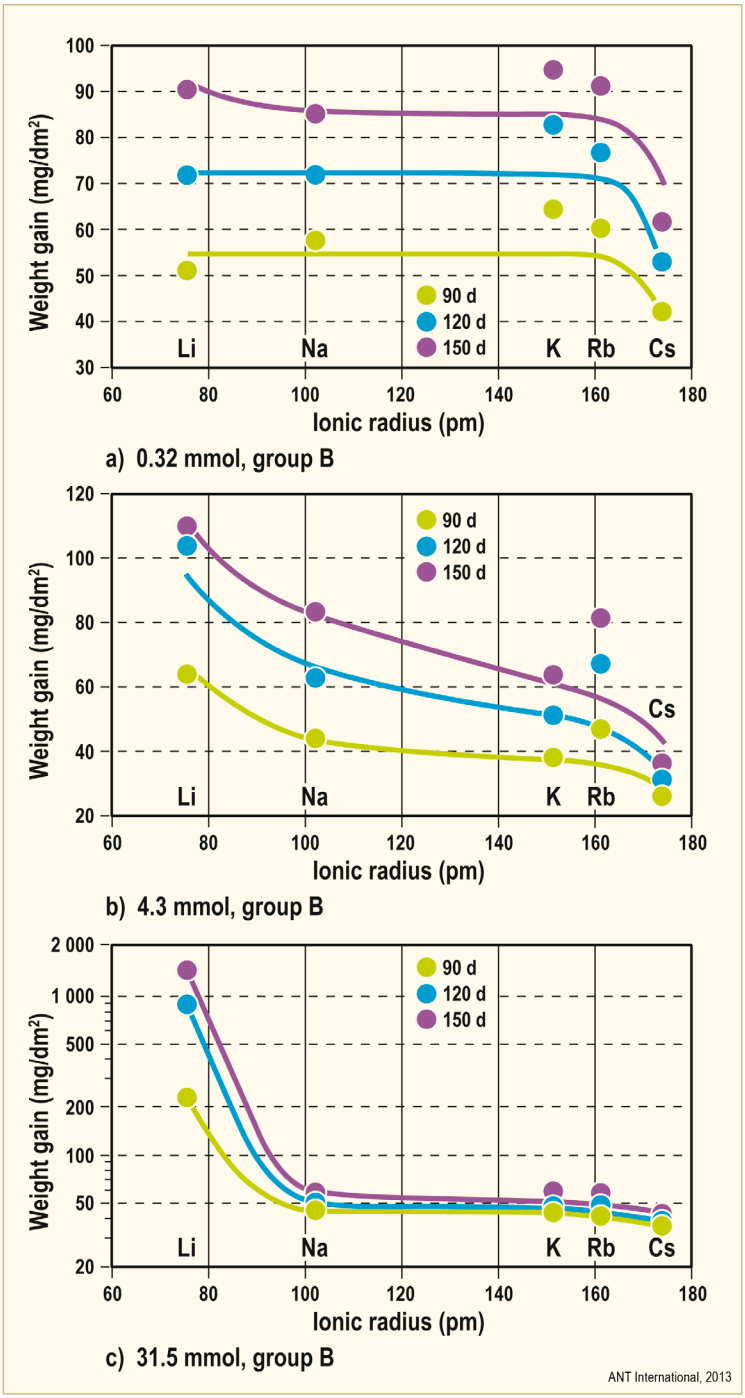

Figure 4-53: Comparison of the corrosion behaviour of a Zr-Sn-Nb-FeCr alloy in different alkali hydroxide environments with consideration of cation ionic radii, after [Jeong et al, 1993].

4.5.2.1.2 Loop tests under irradiation

[Horwath, 2004] reported on a corrosion test program in Halden in the PWR loop (IFA[9]-638) at high heat fluxes in a water chemistry with a constant Li and B content of about 3 ppm and 1000 ppm respectively, resulting in a pH of about 7.1 at 300°C. The hydrogen and oxygen coolant concentration during the test was kept between 2 and 4 ppm and <0.005 ppm, respectively. In this program experimental rods with Low-Sn Zry-4, ZIRLO, M5, and other Zr-alloy-claddings were tested. Some of the claddings were from FRs pre-irradiated in PWR up to a BU of 20-32 MWd/kgU with an initial oxide layer thickness between 9.5 and 31 µm. All materials behaved well during the 4 irradiation cycles in Halden up to the final BU in spite of the high heat fluxes. Only the high Sn Zry-4 with an initial BU of 34 MWd/kgU and an initial oxide layer thickness of 31 µm exhibited heavy spalling after the second cycle after a BU of 44.5 MWd/kgU. The measured oxide thickness values are shown versus the BU in Figure 4-54 for the different materials. The test indicates that the critical Li concentration in the oxide lattice may be even larger than 100 ppm.

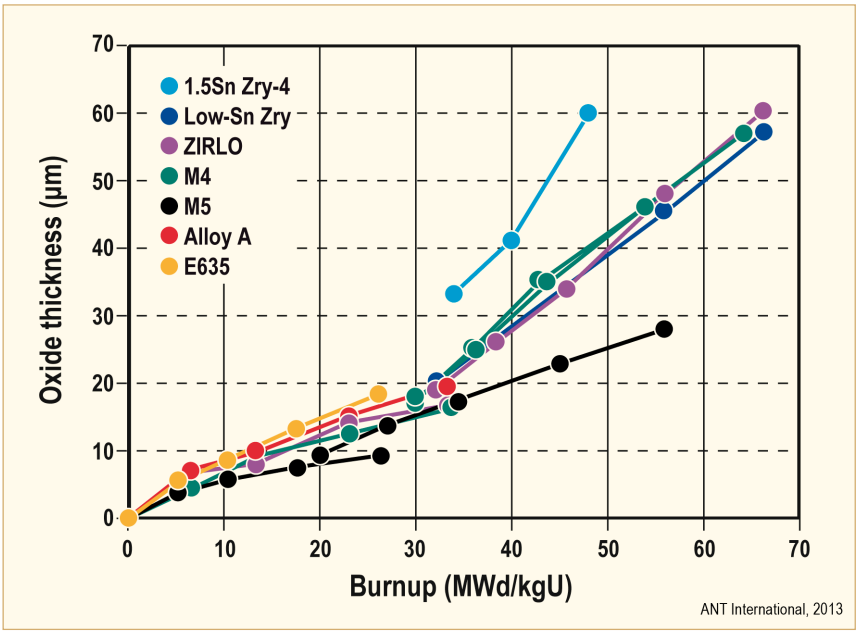

Figure 4-54: Oxide thickness of FR claddings irradiated in the Halden program, IFA-638, under PWR water conditions, after [Horwath, 2004].

In Figure 4-55 the measured oxide layer thickness values are shown in a map versus the heat flux during the irradiation period. In this figure two calculated limit curves are shown. The curves represent Li contents of 100 and 300 ppm in the oxide and were calculated by applying the correlations given by [Garzarolli et al, 2002b]. The figure indicates that the limit for the onset of accelerated corrosion is ≥300 ppm. This is in agreement with the one reported Li induced accelerated PWR corrosion case where several hundreds of ppm Li were found in the oxide layer on the Zry-4 rod close to the position where accelerated corrosion has occurred.

[9] Instrumented Fuel Assembly

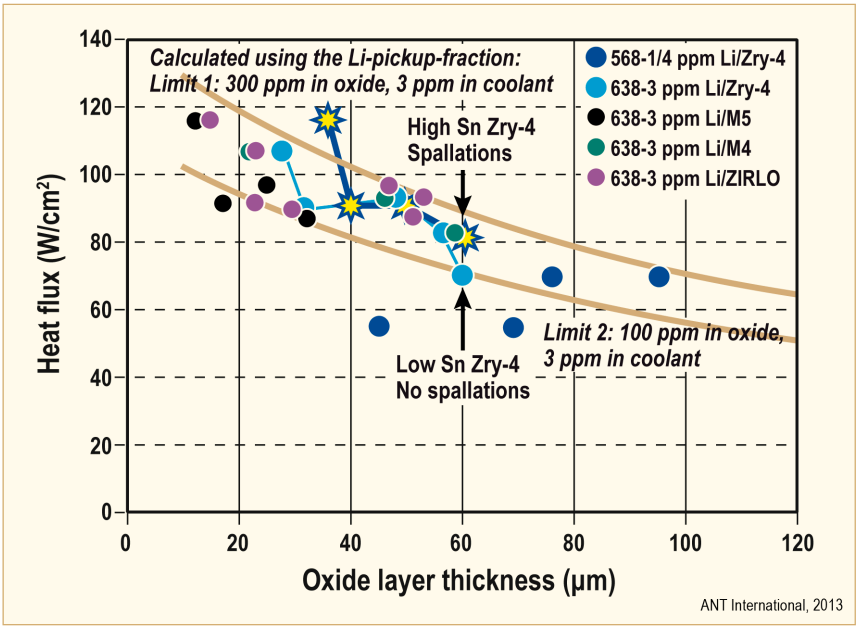

Figure 4-55: Heat flux – oxide layer thickness map for different Halden PWR-tests, after [Karlsen & Vitanza, 1994] and [Horwath, 2004].

4.5.2.1.3 In-reactor data

[Garzarolli et al, 2001b] pointed out that in-PWR increased corrosion rate of FRs under normal water chemistry condition (2 ppm Li) probably occurred only once, during an experimental irradiation, where FRs with rather thick oxide layers were exposed to a very high heat flux. PIE of these rods revealed very localized corrosion and Li contents of several 100 ppm in the oxide lattice.

Careful examinations of the Li content of FR oxide layers grown under demanding operation conditions revealed that the Li concentration in the porous oxide layer depends on oxide layer thickness and local heat flux as key parameters. From an analysis of these data a Li pickup parameter was deduced. This Li-pickup parameter describes the dependence of Li picked up in the oxide lattice on oxide layer thickness s_{ox} and heat flux q" [Garzarolli et al, 2000], as shown below.

Eq. 4-2 $$\text{Li-pickup-parameter} = (160+s_{ox})^{6.8} * (q")^{4.8}$$

where

s_{ox} is the oxide layer thickness in µm and

q" is the heat flux in W/cm².

Figure 4-56 summarizes available data from FR claddings irradiated in different plants operating under different Li strategies and thermal conditions. The figure shows that the Li content in the oxide also depends on the Li content in the coolant (compare the two grey curves). Furthermore, Figure 4-56 suggests that the Li-pickup characteristic is the same for different Zr alloys, such as Zry-4, ELS alloys, and Zr1Nb. For Zr1Nb it is not possible to validate the linear relationship as established for the Zry type alloys, due to the lack of high Li-parameters data.

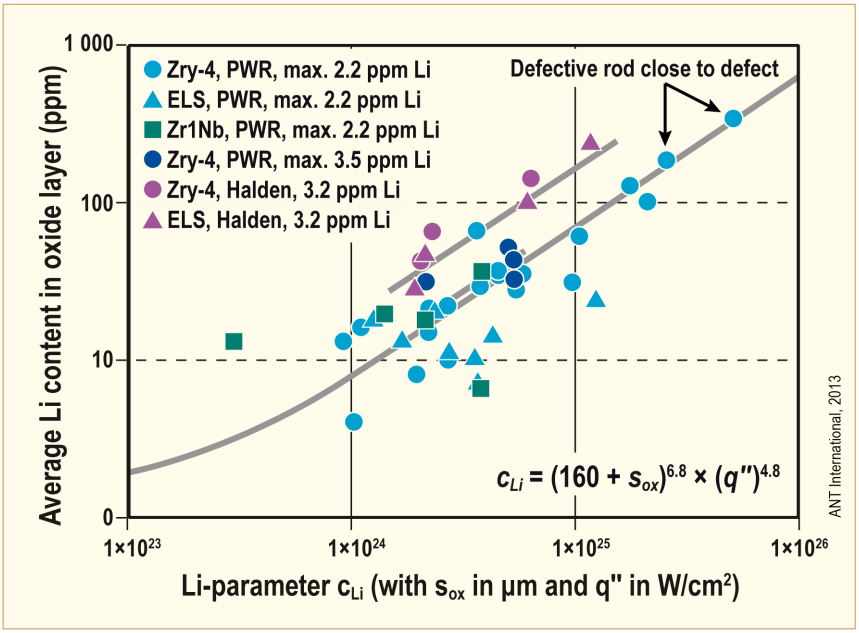

Figure 4-56: Li pick-up in the oxide lattice of PWR FR claddings versus oxide layer thickness and heat flux, after [Garzarolli et al, 2002b].

4.5.2.2 Effect of elevated constant pH 7.3/7.4 on PWR fuel rod corrosion

The constant elevated pH program was implemented on *Comanche Peak (CPNPP) Unit 2* in cycle 7. Cycle 6 was operated with the traditional pH_t 7.1-7.2 regime (Li ≤3,5 ppm) and served as the baseline comparison cycle. Cycle 7 was operated at pH_t 7.3 (Li ≤5 ppm). Cycle 8 was operated for 18 month with a constant reactor coolant pH_t 7.4 regime. The BOC Li started at 6 ppm and was maintained above 3.5 ppm for approximately 12 months for this cycle. CPNPP continued operation at pHt 7.4 in Cycle 9.

The peak values of all ZIRLO fuel oxide measurements during the elevated pH cycles (Cycles 7-9) including the Refuel 9 baseline data from the Unit 1 "M" ZIRLO fuel assemblies are shown as a function of fuel rod burn-up in Figure 4-57. The oxide measurements (lift-off measurements by Eddy Current (EC)) include both a CRUD and oxide component, which are not separated by the measurement technique.

An overall comparison of the measured and predicted oxide thickness data revealed that the measured values were at or below the best estimate predictions at lower spans. However, a large fraction of the measurements exceeded the best estimate predictions at upper spans, where the highest clad temperatures and consequently the highest Sub-Nucleate Boiling (SNB) and CRUD deposition occur. But all of the measurements were below the upper bound predictions and well within the licensing limits. The values of cycle 8 were at the upper bound of the ZIRLO database indicating the influence of the core duty increase in this cycle. Even though the influence of elevated pH and increase in coolant lithium concentration on FR clad oxidation cannot be excluded, it was estimated that this has less effect compared to core duty (for details see Section 5.2.3.3.2.2 in [Riess et al, 2011a].

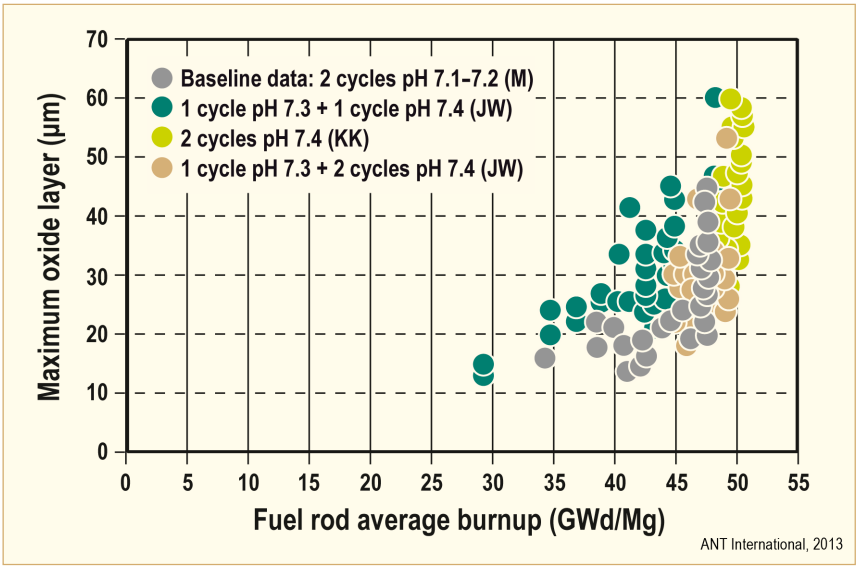

Figure 4-57: Oxide measurement results in CPNPP Unit 2 during elevated pH cycles and base line data from Unit 1, after [Stevens & Bosma, 2008].

4.5.2.3 Effects of Zn in PWRs

For more detailed information please see Section 5.2.3.3.3 in [Riess et al, 2011a].

At Vandellos-2 PWR baseline oxide thickness data were obtained during Refuel 14 (2005), i.e. before Zn-injection was being implemented (EOC14). Oxide thickness measurements performed at EOC15 and EOC16 were made after Ultra-Sonic Fuel Cleaning (UFC) and loose CRUD was removed from spans 8 and 9 by brushing. Figure 4-58 displays the maximum oxide thickness measured at EOC14, EOC15 and EOC16 for each inspected rod. *These results suggest that zinc injection in Vandellos II did not impact corrosion rate.*

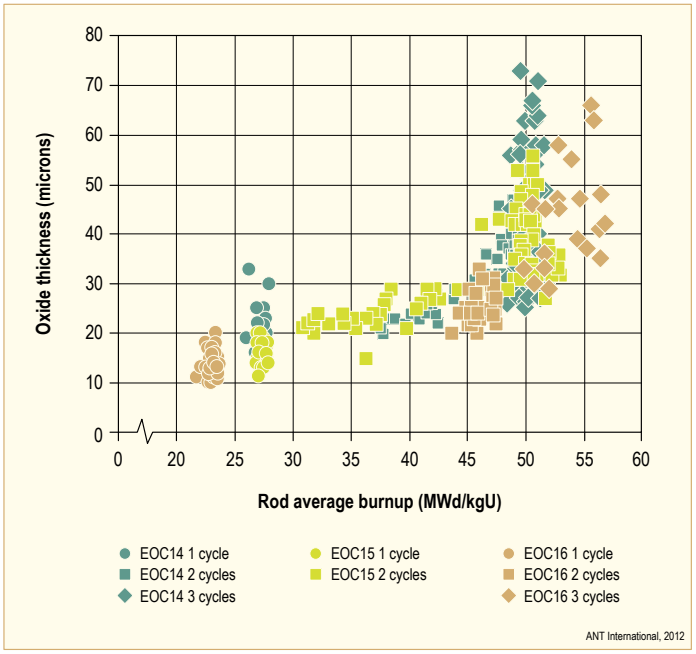

Figure 4-58: Vandellos II maximum oxide thickness. EOC14 (1, 2 and 3 cycles) represent the corrosion baseline data before Zn injection started – green data points. ECO15 (yellow data points) and EOC16 (brown data points) represent corrosion data after various number of cycles of non-Zn injection and Zn-injection, after [Doncel et al, 2011].

Eddy current oxide data after cycles 17 and 18 at Asco II was collected after UFC on three fuel assemblies and compared with data obtained at the end of cycle 16 without zinc (Figure 4-59). *Comparing the maximum oxide thickness measurements to pre-zinc measurements no significant differences were noted.*

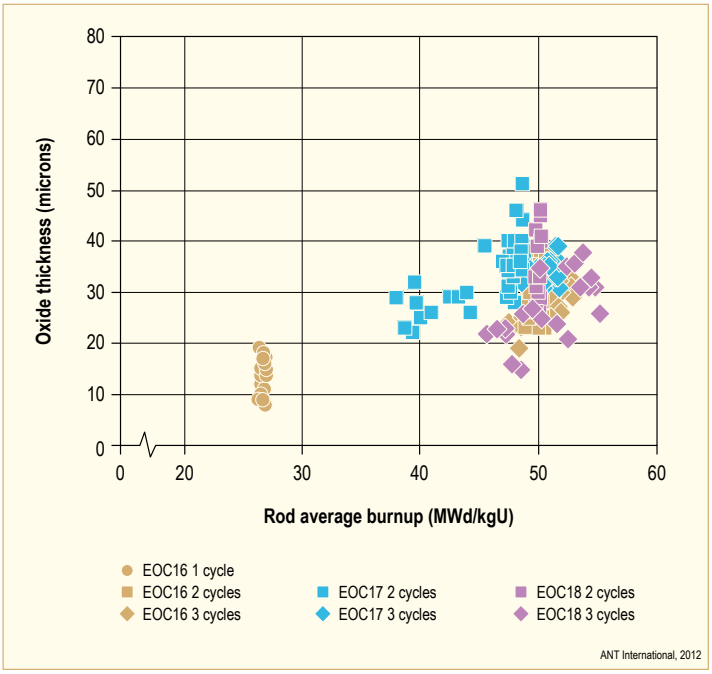

Figure 4-59: Asco II maximum oxide thickness. EOC16 (1, 2 and 3 cycles) represent the corrosion baseline data before Zn injection started – brown data points. ECO17 (blue data points) and EOC18 (purple data points) represent corrosion data after various number of cycles of non-Zn injection and Zn-injection, after [Doncel et al, 2011].

Various cladding materials have been exposed to zinc and operated successfully since the initial Farley 2 experience. In US most experience has been gained with ZIRLO cladding and less with Low-Sn-Zry-4 and M5 claddings. Additional cladding materials were used in the Siemens plants adding 5-10 ppb Zn. *No adverse effect on the fuel performance has been observed [Perkins et al, 2008].*

[Guillermier et al, 2008] presented the feedback regarding the behaviour of M5 cladding material with zinc injection in the primary coolant at Sequoyah-2. Sequoah-2 has a rather moderate fuel duty. At Sequoyah-2, a coordinated chemistry is implemented with lithium content limited at 3.5 ppm at the beginning of the cycle. The pH target is 7.15 at the core average temperature of 303.4°C. The zinc content is targeted at 5 ppb using depleted zinc acetate. Zinc injection was implemented on September 2002 for approximately 13.5 months during Cycle 12. Figure 4-60 shows the Zn concentration during the cycles 11 to 15. Two Alliance Fuel Assembly (FAs) and 4 Mark-BW FAs were examined for visual appearance and oxide layer thickness.

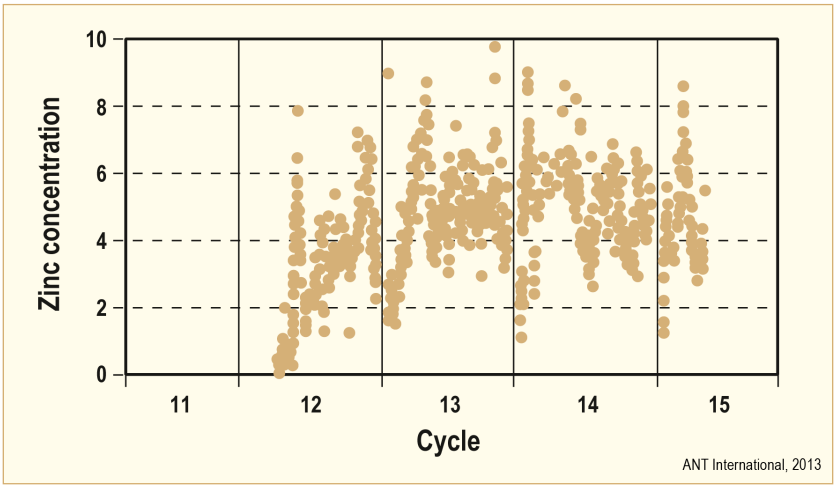

Figure 4-60: Zinc concentration in the primary coolant of SQN-2 in ppb during Cycle 11 to 15, after [Guillermier et al, 2008].

Figure 4-61 shows no difference in the expected trend for SQN-2 results plotted in the graph of fuel rod average burnup vs. peak oxide layer thickness for M5 FA cladding without zinc injection chemistry.

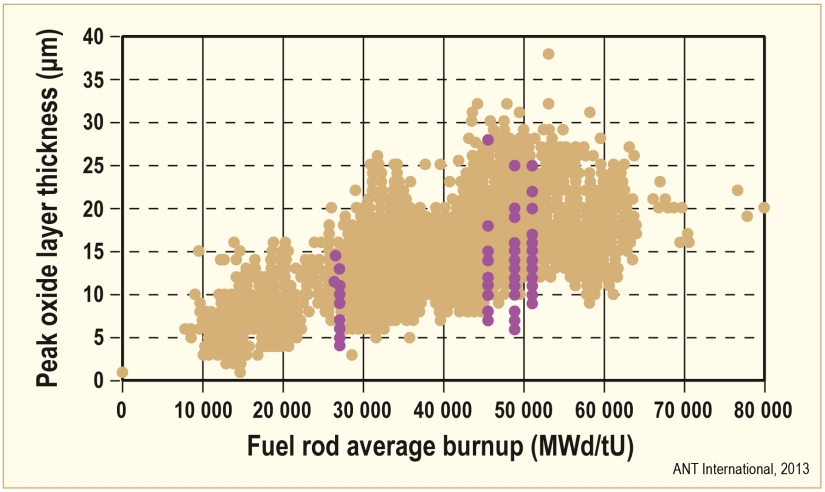

Figure 4-61: SQN-2 results plotted (in black) on the graph of fuel rod average burnup vs. peak oxide layer thickness (in µm) for M5 FA cladding without zinc injection chemistry (in grey) , after [Guillermier et al, 2008].

4.5.3 BWRs

4.5.3.1 Zn and Noble Metals (NMCA and OLNC)

The addition of additives to control corrosion may increase the risk of CRUD buildup on the fuel. For example, the combination of feedwater hydrogen and zinc addition combined with noble metal treatment in BWRs tends to increase the adherence of CRUD deposits on the fuel, which can result in undesirable oxide spalling in higher-rated cores. (This effect is also seen in moderate HWC plants using Zn addition).

Concern about the possibility of adverse effects of NMCA and OLNC on fuel has prompted imposition of a strict limit on the amount of noble metal that can end up on the fuel, and guidance on the injection of zinc. Plant data indicates that spalling of the corrosion layer from fuel cladding, which is often regarded as a precursor to cladding failure, is prevented if the cycle average feedwater zinc is maintained below 0.4 ppb in NMCA plants (0.6 ppb for non-NMCA plants). More recent data indicates that quarterly averages may be as high as 0.5 ppb for NMCA plants, without occurrence of spalling, as shown in Figure 4-62 [Garcia & Wood, 2008].

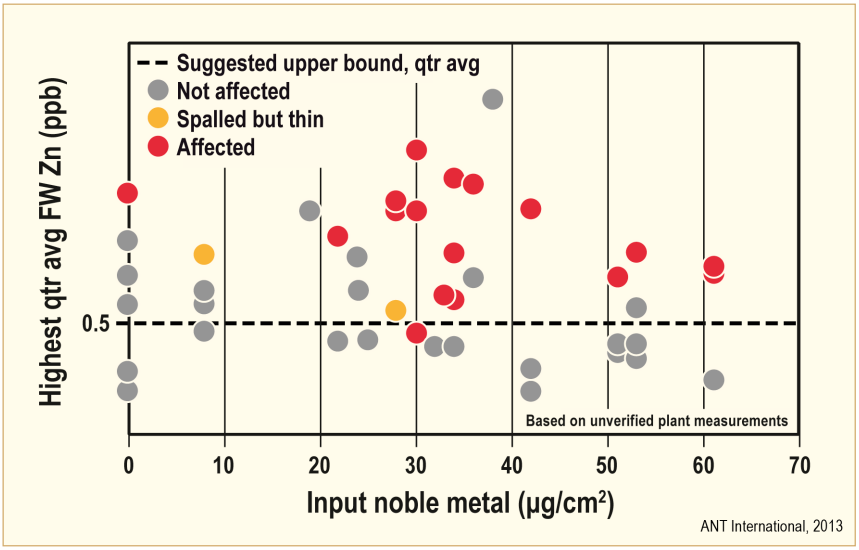

Figure 4-62: Quarterly average feedwater zinc fuel spalling vs. noble metal input and spalling experience, after [Garcia & Wood, 2008].

Typically, spalling is observed at relatively high bundle exposures, as shown in Figure 4-63, which indicates that a cycle average feedwater zinc of 0.4 ppb or less does not result in spalling.

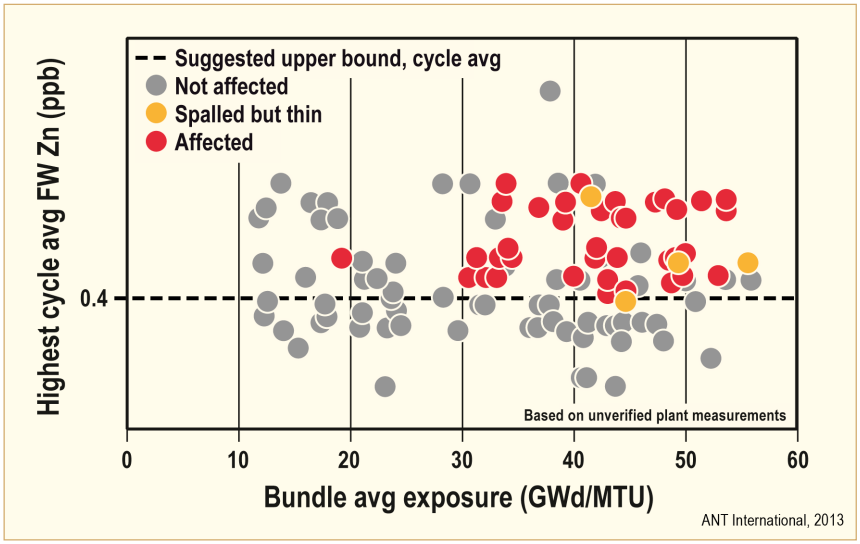

Figure 4-63: Cycle average feedwater zinc vs. bundle exposure and spalling experience, after [Garcia & Wood, 2008].

These feedwater zinc data are the basis for limits in the water chemistry guidelines. The 2008 chemistry guidelines [EPRI, 2008] retain the cycle average feedwater zinc limit of 0.4 ppb (0.6 ppb for non-NMCA plants) but enable a slight increase in the quarterly average to 0.5 ppb for one quarter of each fuel cycle, which may allow flexibility in controlling radiation buildup in parts of the cycle.

4.5.3.2 Unknown water chemistry effects in BWRs

The accelerated HPUF at high burnups is the BWR water chemistry appears to be dependent on water chemistry.

Both in Kernkraftwerk Leibstadt, KKL [Blaser, 1999] - with a low Room Temperature (RT) electrical conductivity (<0.1 µS/cm), low Fe and Cu and Zn injection and in, Swedish BWRs - also with low electrical coolant conductivities, low Fe and Cu contents without Zn injection a certain ranking of the corrosion and HPUF performance was obtained for fuel claddings with different SPP sizes, as follows:

- The lowest corrosion rate, scatter in the corrosion data (which indicates less sensitivity to different water chemistry conditions on corrosion performance) (Figure 4-64), and HPU (Figure 4-65), was recorded for LK3 fuel claddings (with largest SPPs) while the highest corrosion rate, scatter in corrosion data at high burnups (suggest large sensitivity of water chemistry on corrosion performance) and high hydrogen pick up, was obtained for LK2 (with smallest SPPs) [Limbäck et al, 2003].

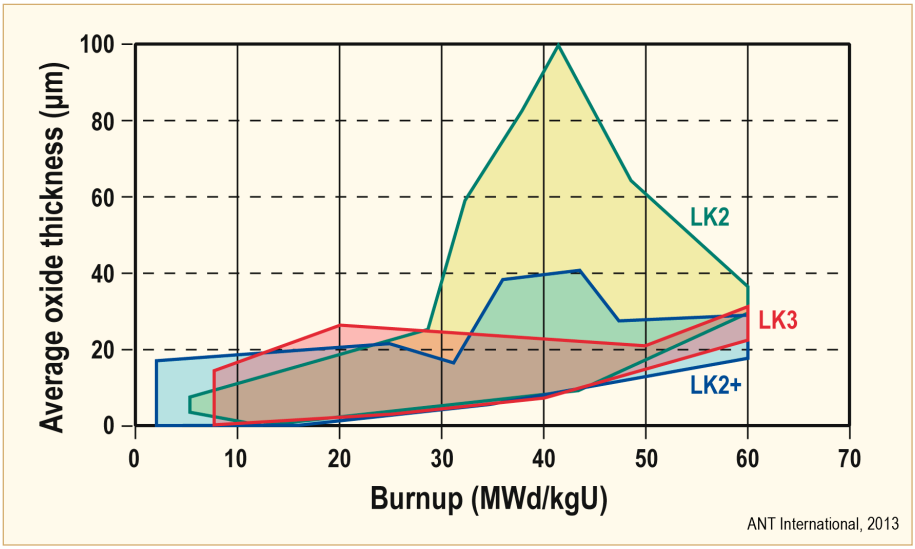

Figure 4-64: Corrosion behaviour of Westinghouse Atom BWR cladding. The SPP size varied as follows: LK3 (largest)>LK2+ (intermediate)>LK2 (smallest), modified after [Limbäck et al, 2003].

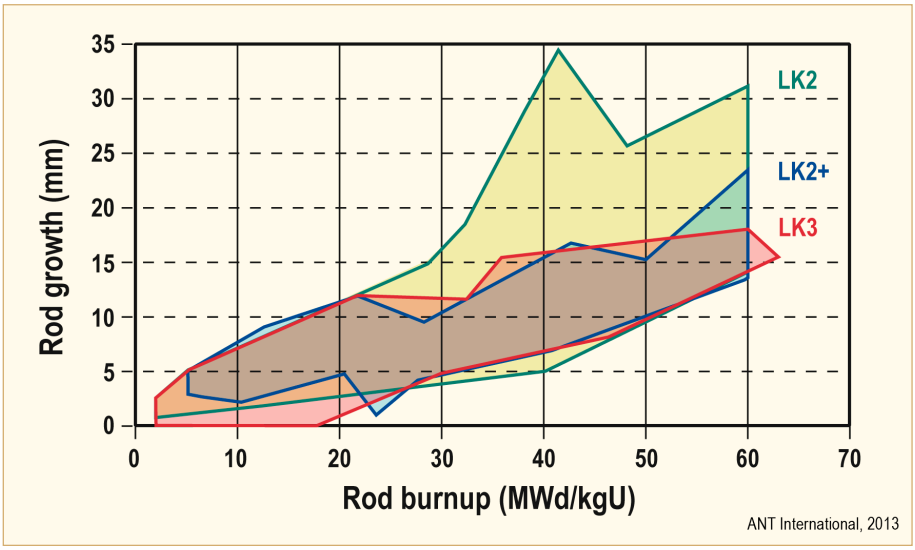

Figure 4-65: Rod growth behaviour of Westinghouse Atom BWR cladding. The rod growth is related to HPU with larger growth for larger HPU, modified after [Limbäck et al, 2003].

Contrary to the above conclusions a different ranking was observed for the various LK variants in Kernkraftwerk Brunsbuttel, KKB [Ketteler et al, 2003], a reactor characterised by medium Cu content (due to admiralty brass condensers). According to [Roßkamp, 1998], the conductivity in KKB was 0.11-0.16 µS/cm, the Cu content 5-20 ppb, and the Zn content 2 to 10 ppb. In KKB, LK3 (with largest SPPs) showed thicker oxide than LK2+ (with intermediate size SPPs) (Figure 4-66). Also, the LK2 rod elongation in KKB is much smaller than in other reactors (not containing Cu) (Figure 4-67). The low rod elongation values indicate that hydrogen pick up rate of LK2 cladding at high burnups is low in KKB, much lower than in the other reactors analyzed by [Ketteler et al, 2003]. *The different behaviour suggests that the coolant chemistry may impact HPU. As discussed in Section 4.2.3.3, the authors of this report [Garzarolli et al, 2010] believes that Cu, reducing the efficiency of radiolysis, may not reduce the oxidation potential enough in the thick porous ZrO_2 oxide to such an extent to keep the nickel – from the irradiation induced SPP dissolution – in metal state in the oxide barrier layer. This means that metallic nickel bands in the barrier oxide will not be available for rapid hydrogen ingress – in Cu containing coolants.*

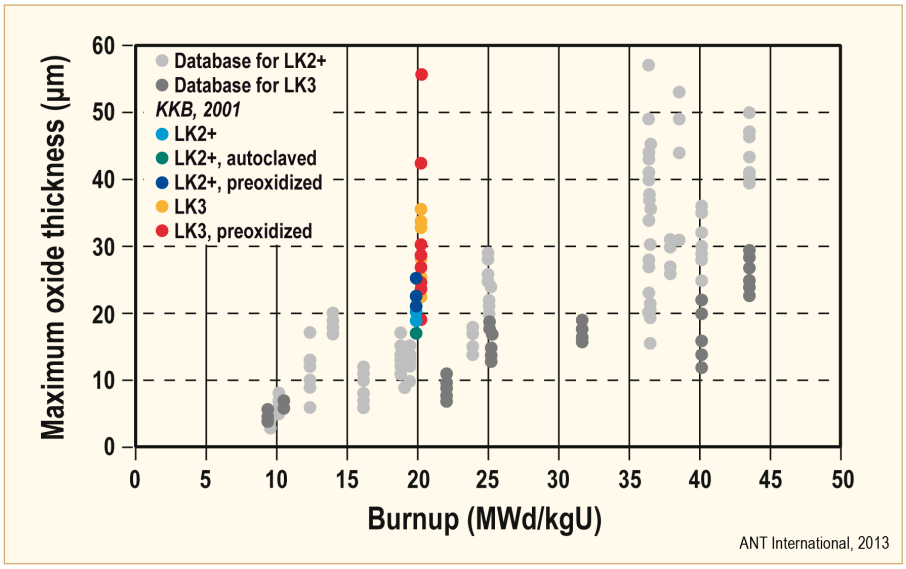

Figure 4-66: Corrosion behaviour of different Westinghouse Atom BWR cladding variants in KKB, after [Ketteler et al, 2003].

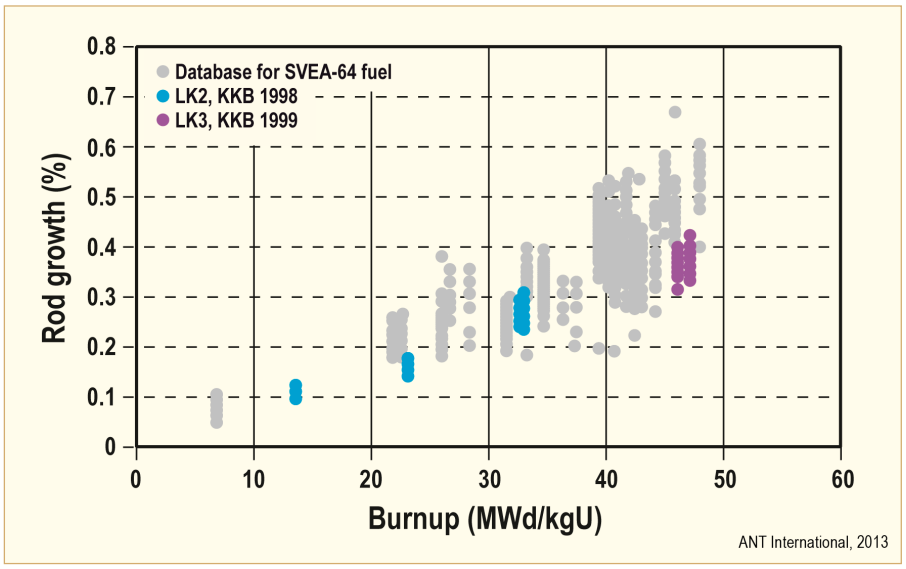

Figure 4-67: Rod growth behaviour of LK2 cladding in KKB, after [Ketteler et al, 2003].

It is noteworthy that BWRs, operating with admiralty brass condensers and consequently some Cu in the reactor water all show lower tendency for HPU also in Zry-2 structural components. The black data points in Figure 4-68 "Zry-2, BWR-B" and "Zry-4, BWR-B" [Garzarolli et al, 2002a] showing very low HPUF (6-16%) in spite of the rather high burnup (1372-1693 EFPD ≈ 7.6-9.3E21 n/cm² ≈ 38-46 MWd/kgU). The data represents Zry-2 coupon irradiated in German BWRs, with medium Cu and low to medium Fe content and low to medium RT electrical conductivity.

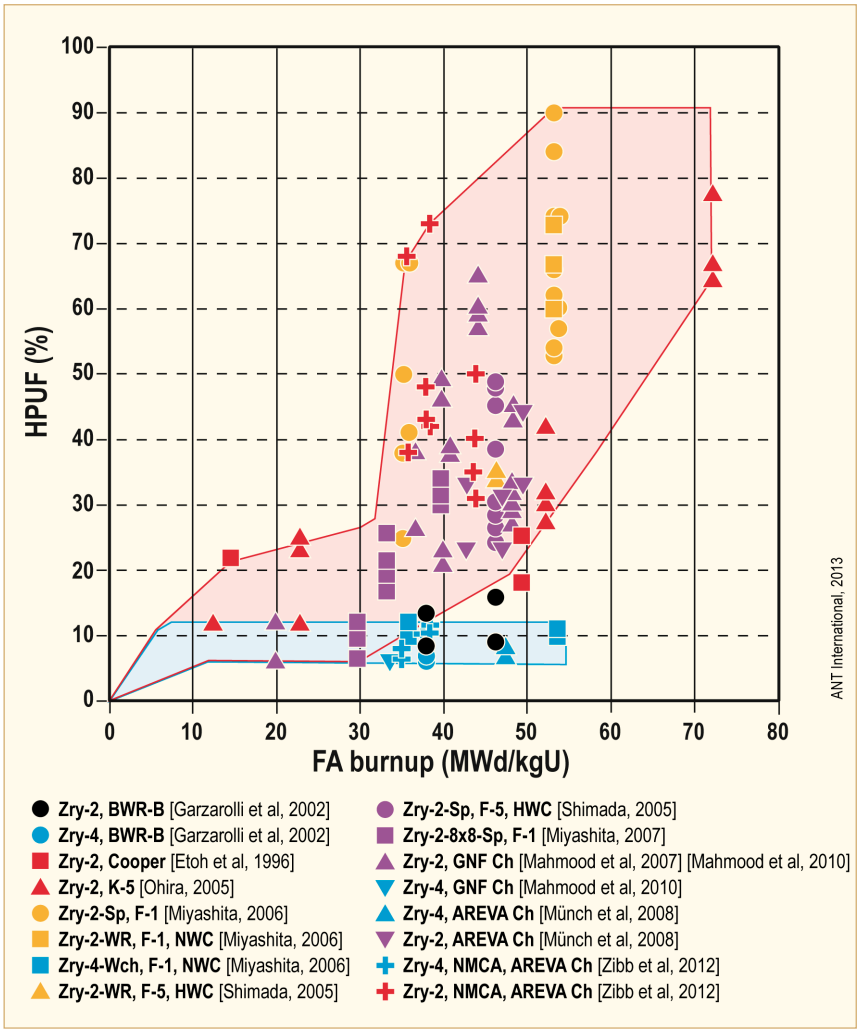

Figure 4-68: Hydrogen pickup fraction (HPUF) of Zry-2 and -4 structural components in BWR, after [Rudling et al, 2012].

5 References

Adamson R and Cox B., Impact of Irradiation on Material Performance, ZIRAT-10 Special Topics Report, ANT International, Sweden, 2005/2006.

Adamson R. B., Cox B., Garzarolli F., Riess R., Sabol G., Strasser A. and Rudling P., ZIRAT11/IZNA6 Annual Report, ANT International, Mölnlycke, Sweden, 2006/2007.

Adamson R. B., Cox B., Garzarolli F., Strasser A., Rudling P. and Wikmark G., Corrosion of Zirconium Alloys, ZIRAT-7 Special Topics Report, ANT International, Mölnlycke, Sweden, 2002/2003.

Adamson R., Cox B., Garzarolli F., Massih A., Riess R., Strasser A. and Rudling P., ZIRAT-10 Annual Report, ANT International, Mölnlycke, Sweden, 2005/2006.

Adamson R., Cox B., Rudling P., Strasser A. and Wikmark, The Annual Review of Zirconium Alloy Technology for 2000, ZIRAT5/IZNA1 Annual Report, ANT International, Mölnlycke, Sweden, 2000/2001.

Adamson R., Garzarolli F., Cox B., Strasser A. and Rudling P., Corrosion Mechanisms in Zirconium Alloys, ZIRAT12/IZNA7 Special Topics Report, ANT International, Mölnlycke, Sweden, 2007/2008.

Adamson R., Garzarolli F., Patterson C., Rudling P., Strasser A., Coleman K. and Lemaignan C., ZIRAT16/IZNA11 Annual Report, ANT International, Mölnlycke, Sweden, 2011/2012.

Amaev A. D., Anisomova J. A., Nikulina A. V., Saenko G. P., Sedova A. V and Fiveiskii M. B., Corrosion of Zr alloys in boiling water under irradiation, Proc. 4th U.N. Int. Conf. on Peaceful Uses of Atomic Energy, Geneva, CH, A/Conf.49/P/428, 1971.

Anada H. and Takeda K., Microstructure of oxides on Zry-4, 1.0Nb Zry-4, and Zry-2 formed in 10.3-MPa steam at 673°C, ASTM STP 1295, pp. 34-54, 1996.

Aomi M. et al., Evaluation of Hydride Reorientation Behavior and Mechanical Properties for High-Burnup Fuel-Cladding Tubes in Interim Dry Storage, Journal of ASTM International, Vol. 5, Issue 9, Paper ID JAI101262, 2009.

Asher R. C. and Trowse F. W., The Distribution of Hydrogen in Zirconium Alloy Fuel Cladding: The Effects of Heat Flux, J. Nucl. Mat. 35, p. 115-121, 1970.

Beie H. J. et al., Examination of the corrosion mechanism of Zr alloys, ASTM STP 1245, pp. 615-643, 1994.

Berry E. B. et al., Hydrogen pickup during aqueous corrosion of Zr alloys, Corrosion Vol. 17, pp. 109t-117t, 1961.

Billot P., Robin J- C., Giordano A., Peybernès J., Thomazet J. and Amanrich H. Experimental and Theoretical Studies of Parameters that Influence Corrosion of Zircaloy-4, Zirconium in the Nuclear Industry: Tenth International Symposium, ASTM STP 1245, pp 351-377, Philadelphia, 1994.

Blaser W., Chemie im Siedewasserreaktor, SVA-Vertiefungskurs “Wasserchemie und Materialverhaten”, April 1999.

Blat M. and Noel D., Detrimental Role of Hydrogen on the Corrosion Rate of Zirconium Alloys, 11th Int. Symposium on Zirconium in the Nuclear Industry, Garmisch-Partenkirchen, Germany, p. 319, ASTM STP 1295, 1995.

Blat M., Legras L., Noel, D. and Amanrich H., Contribution to a Better Understanding of the Detrimental Role of Hydrogen on the corrosion Rate of Zry-4 Cladding Materials, 12th Int. Symposium on Zirconium in the Nuclear Industry, Toronto, Canada, p. 563, ASTM STP 1354, 1998.

Bojinov et al., Kinetic Parameters of the oxidation of zirconium alloys in simulated VVER water – Effect of KOH content, Journal of Nuclear Materials, 372, pp. 152-159, 2008.

Bossis P. Lelievre G., Barberis P., Iltis X. and LeFebvre F., Multi-Scale Characterisation of the Metal-Oxide Interface of Zirconium Alloys, Proc. 12th Int. Symp. on Zr in the Nucl. Ind., ASTM-STP-1354, pp. 918-940, 2000.

Bossis P., Thomazet J. and Lefebvre F., Study of the Mechanisms Controlling the Oxide Growth Under Irradiation: Characterization of Irradiated Zry-4 and Zr-1Nb-O Oxide Scales, Zirconium in the Nuclear Industry: Thirteenth International Symposium: ASTM STP 1423, G. D. Moan and P. Rudling, Eds., ASTM International, pp. 190-221, West Conshohocken, PA, 2002.

Bossis P., Verhaeghe B., Doriot S., Gilbon D., Chabretou V., Dalmais A., Mardon J. P., Blat M. and Miquet A., In PWR Comprehensive Study of High Burn-up Corrosion and Growth Behaviour of M5 and Recrystallized Low-Tin Zircaloy-4, 15th ASTM International Symposium: Zirconium in the Nuclear Industry – Sunriver, OR, June 25-27, 2007.

Bouineau V., Ambard A., Bénier G., Pêcheur D., Godlewski J., Fayette L. and Duvernix T. A new model to prodict the oxidation kinetics of Zirconium Alloys in a Pressurized Water Reactor, Symposium Zirconium in the Nuclear Industry: 15th International, Sunriver Oregon, USA, June 24-28, 2007.

Broy Y., Garzarolli F., Seibold A. and Van Swam L. F., Influence of Transition Elements Fe, Cr, and V on Long-Time Corrosion in PWRs, Zirconium in the Nuclear Industry: 12th Int'l Symposium, ASTM STP 1354, G. P. Sabol and G. D. Moan, Eds., ASTM, West Conshohocken, PA, 609-622, 2000.

Charquet D. et al., Hydrogen absorption kinetics during Zircaloy oxidation in steam, ASTM STP 1245, pp. 80-97, 1994.

Chen J. S. F. and Adamson R. B., Observations of Shadow Phenomena on Zirconium Alloys, Proceedings of the International Topical Meeting on LWR Fuel Performance, ANS, West Palm Beach, Florida, 309-317, 1994.

Cheng B. and Adamson R. B., Mechanistic Studies of Zircaloy Nodular Corrosion, Zirconium in the Nuclear Industry: 7th Int'l Symposium, ASTM STP 393, Adamson R. B. and Van Swam L. F. P., Eds., ASTM, Philadelphia, 387-416, 1987.

Cheng B., Smith F. and Lemons J., BWR Fuel Reliability under Challenging Water Chemistry Conditions, Proceedings of Top Fuel 2009, Paris, France, September 6-10, 2009.

Cheng B-C., Krüger R. M. and Adamson R. B., Corrosion Behaviour of Irradiated Zircaloy, Proc. 10th Int. Symp. in the Nucl. Ind., ASTM-STP-1245, pp. 400-418, 1994.

Christensen H. et al., Experimental studies of radiolysis in an in-core loop in the Studsvik R2 reactor, Proc. BNES conference on Water Chemistry of Nuclear Reactors Systems, pp. 483-485, 1996.

Christensen H. et al., Radiolysis Modelling and Corrosion Potential Measurements in Nuclear Power Environment, BNES 3rd Workshop on LWR coolant water radiolysis and electrochemistry, Dorset, UK, Oct. 2000.

Cox B. and Johnston T., Corrosion V. 18, p.33, 1962.

Cox B. and Pemsler J. P., J. Diffusion of oxygen in growing zirconia films, Nuclear Mater., 28, 73-78, 1968.

Cox B. and Roy C., Transport of oxygen in oxide films on zirconium determined by the nuclear reaction 17O (3He, a) 16O, Electrochem. Tech., 4, 121-127, 1966.

Cox B. and Wong Y. M., A hydrogen uptake micro-mechanism for Zr alloys, J. Nucl. Mat. Vol. 270, pp. 134-146, 1999.

Cox B. and Wu C., Dissolution of Zirconium oxide film in 300°C LiOH, J. Nucl. Mat. 199, pp. 272-284, 1993.

Cox B., Assessment of in-reactor corrosion models and data for Zircaloys in water, Proc. 2nd Int. Symp. on Environmental Degradation of Materials in Nuclear Power Systems-Water Reactors, pp. 219-226, Monterey, Ca., USA, 1985b.

Cox B., Garzarolli F., and, Rudling R., Corrosion of Zr-Nb Alloys, ZIRAT9/IZNA4 Special Topics Report, ANT International, Mölnlycke, Sweden, 2004/2005.

Cox B., Mechanisms of Zirconium Alloy Corrosion in Nuclear Reactors, Proc. Int. Symp. on Corrosion Science in the 21st, Century, Manchester, UK, July 6-10th, J. Corr. Sci. and Eng., Vol. 6, pp. 14, 2003.

Cox B., Oxidation of Zirconium and Its Alloys, Advances in Corrosion Science and Technology, Vol. 5, Edited by Mars G. Fontana and Roger W. Staehle, pp. 173-391, Plenum, N. Y., 1976.

Cox B., Some Thoughts on the Mechanisms of In-Reactor Corrosion of Zirconium Alloys, Journal of Nuclear Materials, 336, pp. 331-368, 2005.

Cox B., Ungurelu M., Wong Y-M., and Wu C., Mechanisms of LiOH Degradation and H3BO3 Repair of ZrO2 Films, Proc. 11th Int. Symp. on Zr in the Nuclear Ind., Garmisch-Partenkirchen, Ger., ASTM - STP – 1295, 114-136, 1996.

Cox, B., Mechanisms of hydrogen absorption by zirconium alloys, Atomic Energy of Canada Ltd., Chalk River Labs., Report AECL-8702, 1985a.

Doncel et al., Zinc Addition Experience at Spanish PWR Plants, 2011 Water Reactor Fuel Performance Meeting Chengdu, China, Sept. 11-14, 2011.

Elmoselhi M. et al., A study of the hydrogen uptake mechanism in zirconium alloys, Proc. 10th Int. Symp. On Zr in the Nucl. Ind., Baltimore, MD., ASTM-STP-1245, pp 62-79, 1994.

EPRI Guidelines: Fuel Surveillance and Inspection, Product 1015032, 2008.

Etoh Y., Shimada S, Yasuda T., Ikeda T., Adamson R.B, Chen J-S F., Ishii Y. and Takei K., Development of new zirconium alloys for a BWR, ASTM STP 1295, pp. 825-849, 1996.

Evans E. and Polley V., A review of the effect of Li on PWR fuel rod corrosion, 6th Int. Conf. on Water chem. of Nucl, Rector Systems, BNES, Windermere, 1992.

Fuketa T., Sasajima H. and Sugiyama T., Behaviour of high-burnup PWR fuels with low-tin Zircaloy-4 cladding under reactivity-initiated-accident conditions, Nucl. Technology, 133, pp. 50-62, 2001.

Fukuya K., Echigoya H., Hattori Y., Kobayashi K., Kobayashi K., and Sasaki T., BWR Fuel Channel Performance and Localized Corrosion at High Burnups, Proceedings of the International Topical Meeting on LWR Fuel Performance, ANS, West Palm Beach, Florida, 580-586, 1994.

Garbett K., Henshaw J., Polley M. V. and Sims H. E., Oxygen and Hydrogen Behaviour in PWR Primary Circuits, Proc. JAIF Int'l Conf. Water. Chem. Nucl. Power Plants, Oct. 13-16, 1998, Kashiwasaki City, Japan, 902-909, 1998.

Garcia S. E. and Wood C. J., Recent Advances in BWR Water Chemistry, International Conference on Water Chemistry of Nuclear Reactor Systems, NPC'08, Paper L4-1, Berlin, Germany, September 14-18, 2008.

Garde A. M. Smith G. P. and Pirek R. C., In-PWR Irradiation Performance of Dilute Tin-Zirconium Advanced Alloys, Zirconium in the Nuclear Industry: Thirteenth International Symposium, ASTM STP 1423, pp. 490-506, 2002.

Garde A. M., Enhancement of Aqueous Corrosion of Zry-4 Due to Hydride Precipitation at the Metal-Oxide Interface, ASTM STP 1132, pp. 566-594, 1991.

Garde A. M., Patti S. R., Krammen M. A., Smith G. P. and Endter R. K., Corrosion Behaviour of Zry-4 Cladding with Varying Tin Content in High-Temperature Pressurized Water Reactors, Zirconium in the Nuclear Industry: 10th Int'l Symposium, ASTM STP 1245, pp. 760-778, A. M. Garde and E. R. Bradley, Eds., ASTM, Philadelphia, 1994.

Garzarolli F. and Rudling P., Performance Evaluation of New Advanced Zr Alloys for PWRs/VVERs, ZIRAT16/IZNA11 Special Topics Report, ANT International, Mölnlycke, Sweden, 2011.

Garzarolli F. and Sabol G.P., EPRI Report 10135522, Assessment oft he effect of elevated reactor coolant hydrogen on the performance of PWR Zr-based alloys, 2006.

Garzarolli F. and Sell H. J., Effect of Cathodic Polarization on Zircaloy Oxidation and Hydriding, EPRI meeting on "BWR Shadow Corrosion/Hydriding on Zircaloy Components: Impact, Mechanism, Testing and Mitigation", Paolo Alto, July 2006.

Garzarolli F. and Stehle H., Behaviour of structural materials for fuel and control elements in light water cooled power reactors, Proc IAEA International Symposium on Improvement in water reactor fuel technology and Utilization, Stockholm, pp. 387-407, 1987.

Garzarolli F. et al, Corrosion phenomena at high burnup, 10th Environmental Degradation Conference, Lake Tahoe, Nevada, 2001b.

Garzarolli F. et al, Effect of In-PWR irradiation on size structure and composition of intermetallic precipitates of Zr alloys, ASTM STP 1295, pp 541-566, 1996b.

Garzarolli F. et al., Oxide growth mechanism on Zr alloys, ASTM STP 1132, pp. 394-415, 1991.

Garzarolli F. et al., Review of corrosion and dimensional behaviour of Zircaloy under water reactor conditions, ASTM STP 681, pp. 91-106, 1979.

Garzarolli F., Cox B. and Rudling P., Optimization of Zry-2 for high burnups, 16th International Symposium on Zirconium in the Nuclear Industry, Chengdu, China, 2010.

Garzarolli F., Dewes P., Maussner G. and Basso H-H., Effects of high neutron fluences on microstructure and growth of Zircaloy-4, Zirconium in the Nuclear Industry: Eighth International Symposium, ASTM STP 1023, pp. 641-657, ASTM, 1989a.

Garzarolli F., et al., Influence of various additions to water on Zry-4 corrosion in autoclave tests at 350°C, Proc. IAEA Techn. Committee Meeting on Fundamental Aspects of Corrosion of Zr-Alloys in Water Reactor Environments, Portland Or., pp.65-72, Sept. 1989b.

Garzarolli F., Hoffmann P. B. and Seibold A., Shadow Corrosion or Crevice Corrosion, J. Nucl. Mat. 289, pp. 338-341, 2001a.

Garzarolli F., Manzel R. and Reynolds R. S., A Decade Irradiation Experience and Duplex Cladding, Proceedings: Int'l Topical Meeting on Light Water Reactor Fuel Performance, American Nuclear Society, pp. 81-88, Park City, UT, April 10-13, 2000.

Garzarolli F., Pohlmeyer I, and Steinberg E., Long term out-of-pile corrosion of Zry-4 in 350°C water, IAEA TC Meeting on External Corrosion in Water Power Reactors, Caderache, France, 1985.

Garzarolli F., PWR Li Coolant Chemistry and Fuel Cladding Performance, Proc. Jahrestagung Kerntechnik, pp. 285-288, Stuttgart, Germany, 2002.

Garzarolli F., Ruhmann H. and Van Swam L., Alternative Zr alloys with irradiation resistant precipitates for High Burnup BWR Application; Zirconium in the Nuclear Industry: Thirteenth International Symposium, ASTM STP 1423, G. Moan and P. Rudling, Eds., ASTM International, pp. 119-132, West Conshohocken, PA, 2002a.

Garzarolli F., Sell H.-J., and Thomazet J., PWR Li coolant chemistry and fuel cladding performance, Jahrestagung Kerntechnik, 2002b.

Garzarolli F., Stehle H., Steinberg, E., Behaviour and Properties of Zircaloys in Power Reactors: A Short Review of Pertinent Aspects in LWR Fuel, Zirconium in the Nuclear Industry: 11th Int'l Symposium, ASTM STP 1295, Bradley E. R. and Sabol G. P., Eds., American Society for Testing and Materials, 12-32, 1996a.

Godlewski J., Gros J. P., Lambertin M., Wadier J. F. and Weidinger H. Raman spectroscopy study on the tetragonal to monoclinic transition in Zr oxide scales and determination of overall oxygen diffusion by nuclear microanalysis of 18O, ASTM-STP 1132, pp. 416-436, 1991.

Guillermier P. et al., M5® Cladding Behaviour with Zinc Injection: Results obtained at Sequoyah 2, International Conference on Water Chemistry of Nuclear Reactor Systems, NPC'08, Paper L13-2, Berlin, Germany, September 15-18, 2008.

Göhr H., Schaller J., Ruhmann H., and Garzarolli F., Long-Term In Situ Corrosion Investigation of Zr Alloys in Simulated PWR Environment by Electrochemical Measurements, ASATM STP 1295, pp. 191-202, 1996.

Harada M. et al., Effect of alloying elements on uniform corrosion resistance of Zr-based alloys in 360°C water and 400°C steam, ASTM STP 1132, pp. 368-391, 1991.

Hayashi H., Shimada S. and Sakurai H., Outside-in Failure of High Burnup BWR Segment Rods Caused by Power Ramp Test, International conference Top Fuel-2003, Würzburg, Germany, March 16-19, 2003.

Heck C., BWR Control Rod Drop Accident (CRDA), NRC RIA Workshop, Bethesda, MD, November 9, 2006.

Hillner E., Corrosion of zirconium base alloys, an overview, ASTM STP 633, pp. 211-235, 1977.

Hillner E., Franklin D. and Smee J. D., Long Term Corrosion of Zircaloy Before and After Irradiation, p. 334-345, J. of Nuclear Materials, V. 278, 2000.

Hillner E., Hydrogen Absorption in Zircaloy During Aqueous Corrosion, Effect of Environment, WAPD.TM-411, 1964.

Hillner E., Hydrogen Absorption in Zircaloy During Aqueous Corrosion, Effect of Environment, WAPD.TM-411, 1964.

Hillner E., Long term in reactor corrosion and hydriding of Zry-2 tubing, ASTM STP 754, pp. 450-478, 1982.

Hirano Y., Mozumi Y., Kamimura K. and Tsukuda Y., Irradiation Characteristics of BWR High Burnup 9×9 Lead Use Assemblies, Proc. Water Reactor Fuel Performance Meeting, pp. 403-420, Kyoto, Japan, October 2-6, 2005.

Hoffmann P. B., Sell H-J., Private information, 2011.

Hoffmann P.B. and Manzel R., Shadow Corrosion. Schönheitsfehler oder Gefahr, Proc. Jahrestagung Kerntechnik 99, pp. 395-398, Karlsruhe, Germany, 1999.

Horwath A., Results From the 1st-4th Interim Inspections of Coupons and Fuel Rods from the PWR Corrosion and Hydriding Test IFA-638, Enlarged Halden Programme Group Meeting, 2004.

Huang P. Y., Mahmood S. T. and Adamson R. B., Effects of Thermomechanical Processing on In-Reactor Corrosion and Post-Irradiation Mechanical Properties of Zry-2, Zirconium in the Nuclear Industry: Eleventh International Symposium, ASTM STP 1295, American Society for Testing Materials, E. R. Bradley and G. P. Sabol, Eds., ASTM, pp. 726-757, 1996.

Ishimoto S, Jubo T. and Kubota O., Development of New Zirconium Alloys for Higher Burnup Fuel, Proceedings of the ENS TopFuel 2003, March 16-19, Würzburg, Germany, 2003.

Ishimoto S, Kubo T, Adamson R.B., Etoh Y., Kunio T.I. and Suzaswa Y., Development of new zirconium alloys for ultra-high burnup fuel; ANS Topical Meeting on Light Water Reactor Fuel Performance, Park City, 2000.

Ishimoto S., Etoh Y., Matsumoto T., Lutz D. and Takagi A., Improved Zr Alloy for High Burnup BWR Fuel, TopFuel-2006, Salamanca, Spain, 2006.

Itagaki N. Kakiuchi K., Yasuhiro M., Furuya T., Development of New High Corrosion Resistance Zr Alloy "HiFi" for High Burnup BWR Fuel, Topfuel-2003, Würzburg Germany, 2003.

Jeong Y.H. et al., Influence of alkali metal hydroxides on corrosion of Zr alloys, IAEA TECDOC 927, pp. 161-192, 1993.

Johnson A. B., Jr., LeSurf J. E. and Proebstle R. A., Study of Zr Alloy Corrosion Parameters in the ATR, Zirconium in Nuclear Application, ASTM STP 551, 495-513, 1974.

Karlsen T. and Vitanza C., Effects of Pressurized Water Reactor (PWR) Coolant Chemistry on Zircaloy Corrosion Behaviour ASTM STP 1245, pp. 779-789, 1994.

Kass S., The development of the Zircaloys, Proc. of the USAEC symposium on zirconium alloy development – Castlewood, GEAP 4089, pp. 1-1-1.44, Pleasanton, California, November 12-14, 1962.

Ketteler M., Skusa J., and Limbäck M., Operating experience of Westinghouse fuel rod cladding in KKB, Jahrestagung Kerntechnik, Berlin, Deutschland, 2003.

Kido T., A Study on Enhanced Uniform Corrosion of Zry-4 Cladding During High Burnup Operation in PWRs, Sixth Symposium on Environmental Degradation of Materials in Nuclear Power Systems - Water Reactors, pp. 449-454, 1993.

Kim Y-J. et al., Photoelectrochemical Investigation of Radiation-Enhanced Shadow Corrosion Phenomenon, 16th International Symposium on Zirconium in the Nuclear Industry, Chengdu, China, 2010.

Kiselev A. A., Myshkin V. A., Kozhevnikov A. V., Korolev S. I. and Shorina, E. G., Research on the Corrosion of Zirconium Alloys in Water and Steam at High Temperature and Pressure, Corrosion of Reactor Materials, Vol. 2, Proceedings of the Conference on Corrosion of Reactor Materials, p. 67, IAEA, Vienna, 1962.

Kitagawa T. et al, Post irradiation examination of fuel rods in 55 GWd/t Lead Use Assembly, Proc. Water Reactor fuel Performance Meeting, Kyoto, Japan, October 2-6, 2005.

Konkov V. F., Nikulina A. V. et al, Factors affecting out-of-and in-reactor corrosion of Zr claddings of fuel rods, IAEA-TECDOC-1128, pp. 103-113, 1999.

Ledergerber G., Limbäck M. and Abolhassani S., Characterisation of high burnup fuel irradiated in KKL, Proc. Water Reactor Fuel Performance Meeting, Kyoto, Japan, October 2-6, 2005.

Limbäck M., Dahlbäck M., Tägtström P, Jourdain P, Massih A., Sihver L, Andersson T and Witt P., Westinghouse Optimised BWR Cladding and Channel Materials, Proc: ENS, Top Fuel, Stockholm, Sweden, May, 2001.

Limbäck M., Kesterson R.L. and Hallstadius L.G., Development of Alloys for High Duty LWR Operation, Jahrestagung Kerntechnik, Berlin, Deutschland, 2003.

Limbäck M., Krammen M., Rudling P., Pati S. and Garde A., Corrosion and Hydriding Performance of Zry-2 and Zry-4 Cladding Materials in PWRs, Proceedings of the International Topical Meeting on LWR Fuel Performance, West Palm Beach, FL, ANS, p 286, 1994.

Lysell G., Nystrand A-C. and Ullberg M., On the Shadow Corrosion Mechanism for Zirconium Alloys, TopFuel 2001, P2-13, Stockholm, Sweden, 2001.

Markov D. et al., PIE results of the WWER FA elements made of E-110 and E-635 alloys, 6th International Conference on WWER Fuel Performance, Modelling and Experimental Support, Albena, Bulgaria Sept. 19 – 23, 2005.

Markov D. et al., Validation of WWER-1000 Fuel Rod efficiency at operation during four cycles, Proc. 3rd International Seminar VVER Reactor Fuel Performance, pp. 147-152, Pamporova, Bulgaria, 1999.

Mitchell D., Garde A. and Davis D., Optimized ZIRLOTM Fuel Performance in Westinghouse PWRs, LWR Fuel Performance Meeting/TopFuel/WRFPM, Orlando, Florida, USA, September 26-29, 2010.

Miyashita T. et al, Corrosion and hydrogen pick-up behaviour of Zircaloy component of BWR high burnup 9x9 Lead Use Assemblies, IAEA Technical Meeting on High Burnup fuel Experience and Economics, Sofia, Bulgaria, 2006.

Miyashita T. et al., Corrosion and hydrogen pick-up behaviours of cladding and structural components in BWR high burnup 9x9 lead use assemblies, Proc. 2007 Intern. LWR Fuel Performance Meeting, San Francisco, CA, 2007.

Motta A. T. et al, Synchrotron radiation study of second phase particles and alloying elements in zirconium alloys, ASTM STP 1423, pp. 59-79, 2002.

Motta A. T., Yilmazbayhan A. Comstock R. J., Partezana J. and Sabol G. P., Microstructure and growth mechanism of oxide layers formed on Zr alloys studied with micro-Beam synchrotron radiation, ASTM STP 1467, pp. 205-232, 2005.

Novikov V. V., Markelov V. A., Tselishchev A. V., Kon'Kov V. F., Sinelnikov L. P. and Panchenko V. L., Structure-Phase Changes and Corrosion Behaviour of E110 and E635 Claddings of Fuels in Water Cooled Reactors, Journal of Nuclear Science and Technology, 43, p. 991-997, 2006.

Pêcheur D. et al., Microstructure of oxide films formed during the waterside corrosion of the Zry-4 cladding in lithiated environment, ASTM STP1295, pp. 94-113, 1996.

Pêcheur D., Lefebvre F., Motta A., Lemaignan C., Charquet D., Oxidation of intermetallic precipitates in Zry-4: impact of irradiation, ASTM STP 1245, pp. 687-708, 1994.

Perkins D., Ahluwalia A., Fruzzetti K., Kucuk A., Libby C. and Marks C., PWR Operation with Elevated Hydrogen, VGB NPC '08 Water Chemistry Conference, Berlin, September 14-18, 2008.

Pettersson H., Bengtson B., Andersson T., Sell H-J, Hoffmann P-B and Garzarolli F., Investigation of increased hydriding of guide tubes in Ringhals 2 during cycle start-up, International LWR Fuel Performance Meeting, Paper 1082, San Francisco, California, 2007.

Ploc R. A., Hydrogen Uptake Mechanism for Zr 2.5Nb, Proc. 4th Int. Conf. on Microscopy of Oxidation, Trinity Hall, Cambridge, U.K., 29-33, 1999.

Ploc R. A., Physical Changes in thin Zr O2 Films with Thickening, Proc. 7th Int. Conf. on Electron Microscopie. Grenoble. Fr., p 313-374, 1970.

Potts G. A., GE Fuel Performance, Proceedings of the International Topical Meeting on Light Water Reactor Fuel Performance, American Nuclear Society, Park City, Utah, April 2000a.

Preuss M., Frankel P., Lozano-Perez S. et al., Towards a mechanistic understanding of corrosion mechanisms in zirconium alloys, 16th Int. Symposium on Zirconium in the Nuclear Industry, Chengdu, China, May 10-13, 2010.

Ramasubramanian N., Billot P., and Yagnik S., Hydrogen evolution and pickup during the corrosion of Zr alloys: A critical evaluation of the solid state and porous oxide electrochemistry, ASTM STP 1423, pp. 222-244, 2002.

Ramasubramanian N., Lithium and boron effects in the corrosion mechanism of zirconium alloys under coolant chemistry conditions, Proc. 7th Int. Conf. On Water Chemistry of Nuclear Reactor Systems, Bournemouth, UK, Vol. 1, pp 91-93, 1996.

Ramasubramanian N., Perovic V. and Leger M., Hydrogen Transport in the Oxide and Hydrogen Pickup in the Metal during Out- and In-Reactor Corrosion of Zr-2.5Nb Pressure Tube Material, Proc. 12th Int. Symp. on Zr in the Nuclear Ind., Toronto, ON, CAN, ASTM - STP – 1354, 853-876, 2000.

Richter H. and Tverberg J.C., Development of Zr-Nb-Sn alloys for reactor application, Proc. USAEC Symposium on Zirconium Alloy Development, Castlewood, CA, 1962.

Riess R., Odar S., Kysela J. and Normann F., PWR/VVER Primary Side Coolant Chemistry, Volume I – Technical Basis and Recent Discussions, LCC7 Special Topic Report, ANT International, Mölnlycke, Sweden, 2011.

Rishel D.M., Eklund K.L. and Kammenzind B.F., In situ EIS measurements of irradiated Zr-4 post transition corrosion kinetic behaviour, 15th International Symposium on Zirconium in the Nuclear Industry, Sunriver Oregon, 2007.

Roßkamp M., Kupfer-Reduzierung im Wasser-Dampf-Kreislauf einer SWR Anlage durch Anwendung von Chitin, VGB Konferenz "Chemie im Kraftwerk", 1998.

Rudling P. and Patterson C., Fuel Material Technology Report, Vol. IV, ANT International, Mölnlycke, Sweden, 2009.

Rudling P. and Vesterlund G., ABB Atom Zircaloy Material Cladding Development for BWR and PWR Applications, Proc. KTG Fachtagung Brennelemente, 20-30, 11, pp. 79-98, Karlsruhe, Germany, 1993.

Rudling P., Patterson C., Adamson R., Garzarolli F. Strasser A. and Turnbull T., High Burnup Fuel Design Issues and Consequences, ZIRAT17/IZNA12 Special Topical Report, ANT International, Mölnlycke, Sweden, 2012.

Sabol G. P., Kilp G. R., Balfour M. G. and Roberts E., Development of a Cladding Alloy for High Burnup, Zirconium in the Nuclear Industry: Eighth International Symposium, ASTM STP 1023, L. F. P. Van Swam and C. M. Eucken, Eds., ASTM, pp. 227-244, Philadelphia, 1989.

Sabol G. P., Kilp G. R., Balfour M. G. and Roberts E., Development of a Cladding Alloy for High Burnup, Zirconium in the Nuclear Industry: Eighth International Symposium, ASTM STP 1023, L. F. P. Van Swam and C. M. Eucken, Eds., ASTM, pp. 227-244, Philadelphia, 1989.

Sasakawa T., Taniguchi Y., Murata T. and Sendo T., Post-Irradiation Examination of Lead Use Assemblies for 55 GWD/T, Proc. Water Reactor Fuel Performance Meeting, Kyoto, Japan, October, 2005

Seibold A. and Garzarolli F., Influence of composition and condition on behaviour of Zr-Sn-FeCrV alloys, Zirconium in the Nuclear Industry: 13th Int'l Symposium, June 10-14, 2001, Annecy, France, ASTM STP 1423, Eds, American Society for Testing and Materials, pp. 743-757, West Conshohocken, PA, 2002.

Seibold A., Garzarolli F. and Manzel R., Optimized Zry-4 with enhanced Fe and Cr and DUPLEX cladding – the answer to corrosion in PWR, Proc. TopFuel-1995, Vol. 2, pp.117-120, Würzburg, Germany, 1995.

Sell H., Trapp-Pritsching S. and Garzarolli F., Effect of Alloying Elements and Impurities on In-BWR Corrosion of Zirconium Alloys, 14th Int. Symposium on Zirconium in the Nuclear Industry, ASTM STP 1467, p. 404-417, Stockholm, Sweden, 2005.

Shewmon P. G., The Redistribution of a Second Phase During Annealing in a Temperature Gradient, Transactions of the Metallurgical Society of AIME, pp. 642 - 647, October 1958.

Sihver L. and Hallstadius L., Zero-failure fuel, Proc, ENS TOPFUEL 99, Topical Meeting on Nuclear Fuel, Avignon, France, pp. 396-406, September 1999.

Smirnov A. et al, Results of post irradiation examination to validate WWER-440 and WWER-1000 fuel efficiency at high burnups, Proc. 4th International Seminar VVER Reactor Fuel Performance, pp. 63-82, Varna, Bulgaria, 2001.

Smirnov V. P., Markov D. V., Polenok V. S., Ivashchenko A. A. and Maershina G. I., PIE Results of High-Burnup VVER FA, IAEA Technical Co-ordination Meeting High Burnup Experience and Economics, Sofia, Bulgaria, 26-28 September, 2006.

Solonin M. et al, WWER Fuel performance and material development for extended burnup in Russia, Proc. 2nd International Seminar VVER Reactor Fuel Performance, pp. 48-57, Sandalinski, Bulgaria, 21-25 Apr. 1997.

Stehle et al., ASTM STP 824, pp. 483-506, 1984.

Stevens J. and Bosma J., Elevated RCS pH Program at Comanche Peak, International Conference on Water Chemistry of Nuclear Reactor Systems, "NPC'08", Paper L2-3, Berlin, Germany, 2008.

Takeda K., Harada M., Ishii Y and Miyazaki A., Effect of Metallographic Factor on Hydrogen Pick-up Properties of Zry-2, Journal of Nuclear Sscience and Technology, Vol. 43, No. 9, p. 984–990, 2006.

Thomazet J. et al, The corrosion of the alloy M5TM: an overview, IAEA Technical Committee Meeting on behaviour of high corrosion Zr-based alloys, Buenos Aires, Argentina, October 24-28, 2005.

Trowse F. W., Sumerling R. and Garlick A., Nodular Corrosion of Zry-2 and Some Other Zirconium Alloys in Steam Generating Heavy Water Reactors and Related Environments, Zirconium in the Nuclear Industry, ASTM STP 633; A. L. Lowe, Jr., and G. W. Parry, Eds., ASTM STP 633, 236-257, 1977

Tsukuda Y., Kosaka Y., Kido T., Doi S., Sendo T., Gonzáles P. and Alonso J. M., Performance of advanced fuel materials for high burnup, ENS TopFuel, Nuclear Fuel for Today and Tomorrow: Experience and Outlook, Würzburg, Germany, 16 19 March 2003.

Tyzack C., Hurst P., Slattery G. F., Trowse F. W., Garlick A., Sumerling R., Stuttard A., Videm K., Lunde L., Warren M., Tolksdorf E., Tarkpea P. and Forsten J., SCANUK: A Collaborative Programme to Develop New Zirconium Cladding Alloys, J. Nucl. Mater., Vol. 66, pp. 163-186, 1977.

Tägtström P., Andersson T., Bergström O., Dahlbäck M. and Limbäck M., The effect of secondary phase particle distribution on the in-reactor performance of BWR cladding, Enlarged Halden Progr. Meeting, Loen, 1999.

Une K., Sakamoto K., Aomi M., Matsunaga J., Etoh Y. et al., Hydrogen Absorption Mechanism of Zirconium Alloys Based on Characterization of Oxide Layer, 16th ASTM Zr Symposium, Chengdu, China, May 9-13, 2010.

Urbanic V. F, Gray R., and Lister D. H., Review of in-reactor Zircaloy corrosion and CRUD deposition experience at AECL, EPRI Report NP1254, 1979.

Urbanic V.F., Cox. B., Field G.J., Long term corrosion and deuterium uptake in CANDU-PHW pressure tubes, ASTM STP-939, pp. 189-205, 1987.

Watanabe S., Abeta S., Serna J., Alonso J. and Sendo T., Gonzalez, P., Post irradiation examinations on 67-75 GWd/t rods for confirmation of the integrity and appropriate performance of the claddings for future, Proc. Water Reactor Fuel Performance Meeting, Kyoto, Japan, October 2-6, 2005.

Yilmazbayhan A. et al, Transmission Electron Microscopy Examination of Oxide Layers Formed on Zr Alloys, J. Nucl. Mater, 349, 265-281, 2006.

Yilmazbayhan A., Motta A. T., Comstock R. J., Sabol G. P., Lai B. and Cai Z., Structure of zirconium alloy oxides formed in pure water studied with synchrotron radiation and optical microscopy: relation to corrosion rate, J. Nucl. Mater. 324, pp. 6-22, 2004.

Zhou C. H., Ma H. T. and Wang L. Effect of compressive loads on the oxide-scale morphology formed on Ni-12Cr alloy at 1173 K. NACE ICC 2009 17th International Congress, Las Vegas, Nevada, USA, October 6-10, 2009.

Zwicky H–U., Loner H., Andersson B., Wiktor C–G. and Harbottle J., Enhanced Spacer Shadow Corrosion on SVEA Fuel Assemblies in the Leibstadt Nuclear Power Plant, ANS Int'l Topical Meeting LWR Fuel Perform., Park City, UT., USA, April 10-14, 2000.